CHARACTERIZATION OF DISLOCATION STRUCTURES AND THEIR INFLUENCE ON PROCESSING OF Al ALLOYS

By

PANKAJ TRIVEDI

A dissertation submitted in partial fulfillment of
the requirements for the degree of

DOCTOR OF PHILOSHOPY

WASHINGTON STATE UNIVERSITY
School of Mechanical & Materials Engineering

MAY 2005

To the Faculty of Washington State University:

The members of the Committee appointed to examine the dissertation of PANKAJ TRIVEDI find it satisfactory and recommend that it be accepted.

David Fields
Chair

GARY S. COLLINS

ACKNOWLEDGMENTS

First of all, I would like to express my sincere gratitude, deepest respect and special thanks to my major professor, Dr. David Field, for providing me an opportunity to conduct research work under his supervision and without whose vision, guidance, help, and patience this project wouldn't have been possible. I would also like to thank Dr. Hasso Weiland, Dr. Ben Li, Dr. Sinisa Mesarovic, and Dr. Gary Collins for their time and service as my PhD committee members.

I would like to reserve my deepest thanks to Dr. Grant Norton for his help and support towards completion of my PhD work. I would like to acknowledge Dr. Richard Alldredge for his help with the statistical analysis. I am also grateful to Department of Energy for financial support and Alcoa Technical Center for helping us with conducting necessary characterization and experimental works. I would also like to thank all my friends, especially Tejodher, Pablo, Reza, Rajesh, Daniel, Aziz, Firas, Ashis, Kakoli, and Samar, for their help and making my stay at WSU very pleasant. I would like to convey my special thanks to all staffs of the department for their help. In particular I would like to than Mary Simonsen, Janet Danforth, Carmello Delgado and Jon Grimes for their assistance with various matters.

I am thankful and grateful to my parents, my brother and sister for their moral support. I would like to express special thanks to my wife for her sacrifices, help with programming and providing me constant encouragement. Finally I would like to thank my loving daughter 'Radha' for beginning my each day with a great smile.

CHARACTERIZATION OF DISLOCATION STRUCTURES AND

THEIR INFLUENCE ON PROCESSING OF Al ALLOYS

Abstract

by Pankaj Trivedi, Ph.D.
Washington State University
May 2005

Chair: David Field

A proper understanding of the relationships that connect processing conditions, microstructural evolution and mechanical properties is required to optimize the processing parameters, reduce alloy content and improve product quality. This requires significant effort in performing accurate analysis of deformed microstructure, identifying important microstructural parameters influencing stress response and developing a physically based model that incorporates these microstructural parameters. Most models are based on observed phenomenology of the process and therefore fail to predict stress-strain behavior beyond a given set of observations. Current research is aimed towards making contribution in the areas of (i) microstructural characterization, (ii) understanding the influence of various microstructural parameters on the evolution of dislocation structures and (iii) on relating the physically measurable microstructural parameters to stress response.

New strategies to analyze the local orientation gradient in deformed single crystals are introduced. Interrogation of the dislocation substructure is accomplished by extracting information gleaned from small point to point misorientations as measured by

electron back-scatter diffraction (EBSD). Microstructural evolution during small strain deformation of 3003, 5005, and 6022 Al alloys was investigated using EBSD and transmission electron microscopy (TEM) techniques. The variables observed to influence the deformation behavior include alloy chemistry, crystallite lattice orientation, character and morphology of neighboring grains and precipitate morphologies. The difference in the evolution of dislocation structures of the 3 alloys is attributed to their alloy content. Quantitative parameters obtained from microstructural characterization of 5005 and 6022 Al alloys were analyzed by a multiple regression analysis technique to determine the relative influence of various microstructural parameters on the observed stress response. The GND density was determined to be the most important measured parameter affecting the yield stress. Experimental and statistical analysis showed a linear relationship between yield stress and average GND density. The yield strength model was developed for 6022 alloy connecting the observed stress response with experimentally determined microstructural parameters.

TABLE OF CONTENTS

Page

LIST OF TABLES

LIST OF FIGURES

Dedication

This dissertation is dedicated to my family

CHAPTER – 1

INTRODUCTION

Over the years there has been a significant increase in demand for new products with unique or improved performance or for extended life of existing products, all with minimum cost requirements. Transportation, aerospace and energy related industries have a need for lighter and stronger materials, which lead to a significant growth in the development and use of advanced structural materials. Also during the last few decades, new analytical tools for examining microstructures, new sensing devices for process control, and improved modeling capability have increased our knowledge base and ability to tailor materials to specific applications.

Automakers are turning more and more to light weight materials such as aluminum alloys to achieve significant weight-savings and achieve greater fuel economy. Aluminum is an essential material for modern manufacturing because of its excellent combination of properties such as lightweight, high-strength, corrosion-resistance and high electrical and thermal conductivity. The United States aluminum industry is the world's largest, processing over 10.7 million metric tons of metal and producing about $39 billion in products and exports [1]. Top markets for the aluminum industry are transportation, beverage cans and other packaging, and building construction. Energy represents about one third of the total production cost of primary aluminum. Currently most Al alloys used in structural applications possess microstructure with much higher load bearing

capacity than required to ensure a higher factor of safety. Such over-engineering, which leads to a significant increase in energy consumption and cost of manufacturing, is done because of lack of proper understanding of how details of the starting microstructure affect mechanical properties. Therefore, a proper understanding of the relationships that connect processing conditions, microstructural evolution and mechanical properties is required to optimize the processing parameters, reduce alloy content and improve product quality. Most microstructural based research is aimed towards developing a process that produces material with a microstructure just good enough for the desired application. There are three challenging tasks that must be overcome to achieve a good degree of success in this field. One is to perform accurate microstructural analysis of the deformed material and to develop quantitative parameters that are representative of the microstructural heterogeneity. Second is to identify major microstructural parameters affecting the desired properties. Third is to develop a physically based model that incorporates these microstructural parameters.

Modeling the microstructure evolution and the macroscopic stress response during deformation has been a focus of research for many years. Many attempts on microstructural modeling in processing of Al alloys have used an internal state variable approach, which consists of evolution equations for the microstructural elements considered and a kinetic equation of state that connects the microstructure, temperature and strain rate with the necessary flow stress [2-6]. This state variable formalism has been used to describe non-isothermal transformation behavior in a variety of systems ranging from steels to cast iron to aluminum alloys. So far, the problems explored have

been chosen selectively, often involving the microstructure from a well-characterized starting condition, e.g., particle and grain coarsening behavior, particle dissolution, and diffusion controlled growth. The generalized constitutive equation for the flow stress response during thermomechanical processing of Al alloys can be written in the form:

$$\sigma = (\dot{\varepsilon}, T, S_i) \qquad \ldots\ldots\ldots\ldots\ldots\ldots (1.1)$$

where $\dot{\varepsilon}$ is strain rate, T is temperature and S_i includes a number of parameters describing chemistry, dislocation structure, particle morphology etc. Some of these microstructural parameters evolve with strain at a rate which is governed by the characteristics of the starting microstructure and externally imposed deformation conditions. Various yield strength models have been developed for Al alloys, which often include the evolution equations for precipitate or dislocation structures as a function of processing parameters [6-9]. Parameters that were used to describe S_i in Equation 1.1 often contained phenomenological description of microstructures. The phenomenological models of material response ignore the details of the material structure, but postulate the material response to be within a mathematical structure. Constitutive models used in process modeling and optimization are usually empirically or phenomenologically developed using data from large strain experiments any may not incorporate phenomena at small strains. Physically based models more realistically describe material properties, yield more meaningful results, and can be reliably extended beyond the scope of experimental data. Thus physics based models that incorporate physically measurable microstructural parameters, has potential to be used for alloy and process designs, assuming evolution equations are sufficiently based upon physical principles.

1.1 Importance of Microstructure

During industrial thermomechanical processing of Al alloys, materials are subjected to a wide range of strain, strain rate and temperature. Since deformation induced during such processing is quite heterogeneous, materials possess a variety of microstructures. Microstructure of material plays a critical role in deriving mechanical response of material during deformation and in the evolution of final microstructure after deformation. Parameters that influence the evolution of microstructure during deformation can be divided into two broad categories: processing parameters (such as strain, strain rate and temperature) and microstructural parameters (such as dislocation structures, precipitate morphologies, grain orientation, neighboring grains, and grain size and shape). For example Winther systematically studied the evolution of dislocation boundaries in Al using TEM and showed that there is a strong correlation between evolving dislocation boundaries and the grain orientation [10]. Figure 1.1 shows that different types of dislocation structures are formed for grains with different orientation. The difference between these five regions (marked A – E) lies in the slip planes to which the boundaries are related; the axis around which the boundaries are rotated away from the slip plane; the magnitude and sign of the angle between the boundary plane and the slip plane.

The microstructures and consequent properties of a metal are not static in behavior for they may be altered by various external forces such as (i) mechanical forces, (ii) thermal changes, and (iii) chemical environments. Therefore, a microstructure may be varied by processing factors and service conditions. Various microstructural parameters such as

grain size, dispersoids, solid solution morphology, precipitate morphology, dislocation structures etc., can be altered to achieve required strength. The ability of a metal to deform depends on the ability of dislocations to move, so restricting dislocation motion makes the material stronger. Below is a brief review on some general strengthening mechanisms achieved by altering microstructure:

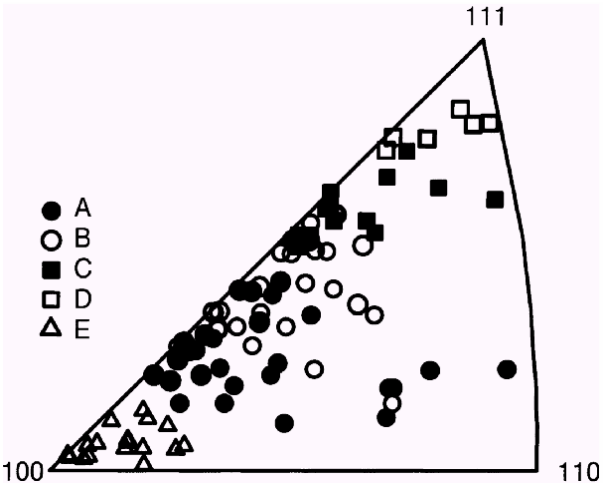

Figure 1.1: Stereographic unit triangle showing five different types of dislocation boundaries (labeled A – E) formed in tensile deformed polycrystalline aluminum [10].

1.1.1 Grain Size Effect

The yield strength of most crystalline solids increases with decreasing grain size. Quantitatively it is described by the Hall-Petch equation:

$$\sigma_y = \sigma_0 + kD^{-1/2} \qquad \text{..... (1.2)}$$

where σ_0 is the yield strength of single crystal, k is constant determining the effectiveness of grain boundary in increasing strength and D is average grain size of the material [11,12]. Figure 1.2 shows the schematic of a dislocation moving along a slip plane

approaching grain boundary [13]. In order for yielding of the polycrystal to occur throughout the sample it is necessary for the plastic strain to propagate from one grain to next. This means that the stress concentrations that are built up at the ends of the first slip band must be sufficient to start yielding in the second grain. The intensity of the stress at the tip of the slip band is dependent on the applied stress and less dependent on the length of slip band. Thus materials with large grain size usually have lower yield strengths. However beyond a certain range of grain size, the mechanical properties of Al alloys are not very sensitive to grain size.

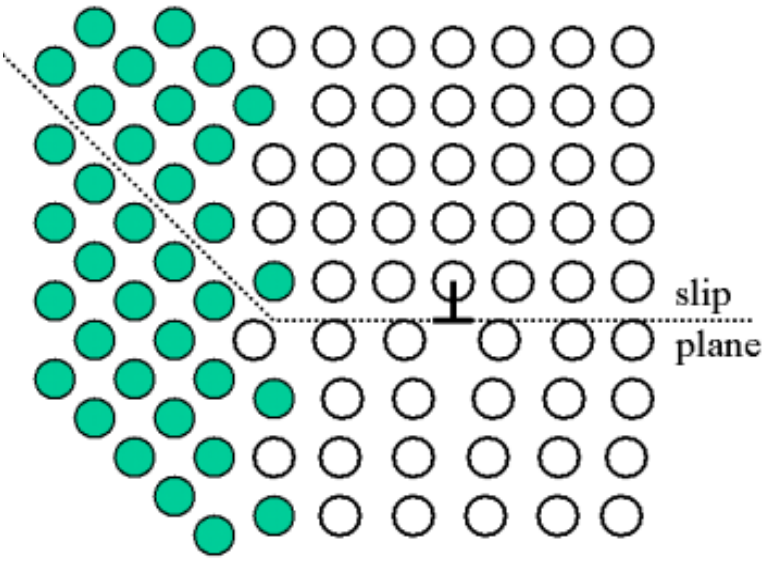

Figure 1.2: Schematic showing a dislocation approaching a grain boundary [13].

1.1.2 Solid Solution Strengthening

The introduction of solute atoms into solid solution in the solvent-atom lattice invariably produces an alloy which is stronger than pure metal. There are various ways solute atoms can interact with dislocations: elastic interaction, modulus interaction, stacking-fault

interaction, electrical interaction, short-range order interaction, long-range order interaction. The resistance to dislocation motion that constitutes solid-solution strengthening can come from one or more of these factors. In solid solutions of FCC metals the hardening is often linearly proportional to the concentration of solute atoms.

1.1.3 Strain Hardening

Strain hardening or cold working is an important industrial process that is used to harden metals or alloys by increasing the dislocation density. A high rate of strain hardening implies mutual obstruction of dislocations gliding on intersecting systems. This can come (1) through interaction of stress fields of the dislocation (2) through interactions which produce sessile locks, (3) through the interpenetration of one slip system by another which results in the formation of dislocation jogs. The strength contribution of dislocation structures to the macroscopic flow stress is often represented by an Orowan type equation [14]:

$$\sigma = \sigma_0 + \alpha G b \rho^{1/2} \qquad \text{..... (1.3)}$$

where, $\boldsymbol{\sigma}$ is macroscopic flow stress, $\boldsymbol{\sigma_0}$ is friction stress, α is constant, $\boldsymbol{G}$ is shear modulus, $\boldsymbol{b}$ is Burger's vector and ρ is total dislocation density. Figure 1.3 is the schematic showing the influence of cold working on yield stress and ductility of material. It can be seen that with increase in amount of cold work yield stress increases but ductility decreases.

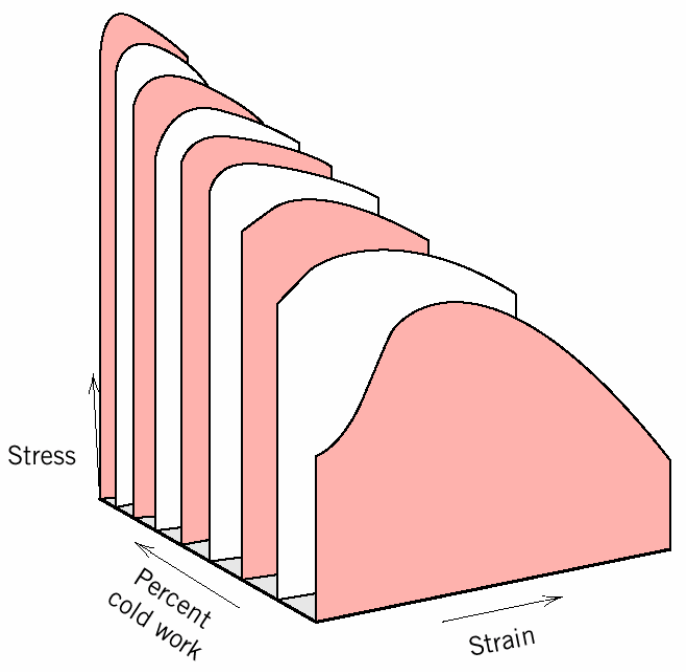

Figure 1.3: Schematic showing the influence of cold work on strength and ductility of material [13].

1.1.4 Strengthening from Fine Particles

Precipitation hardening or age hardening is produced by solution treating and quenching an alloy in which a second phase is in solid solution at the elevated temperature but precipitates upon quenching and aging at a lower temperature. There are several ways in which fine particles can act as barrier to dislocations. Figure 1.4 shows the schematic of various modes of interaction between precipitates and dislocations [15]. They can act as strong impenetrable particles through which the dislocations can move only by sharp changes in curvature of the dislocation line. On the other hand, they can act as coherent particles through which dislocations can pass, but only at stress levels much greater than those required to move dislocations through the matrix phase. The degree of strengthening from second phase particles depends on the morphology of particles in the

matrix such as size distribution, inter-particle spacing, size and shape of particles and volume fraction. Various other mechanisms of strengthening such as texture, dispersion strengthening, fiber strengthening and martensitic strengthening are not discussed here.

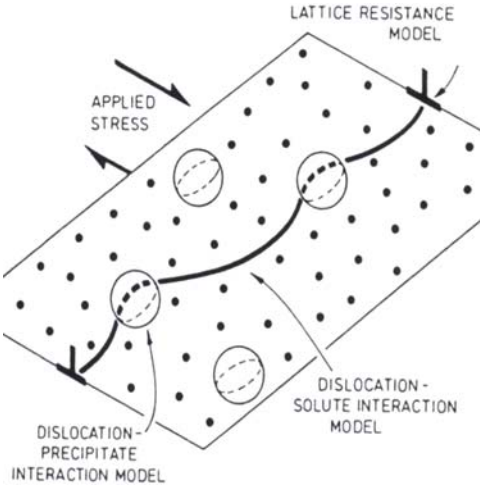

Figure 1.4: Schematic showing interaction of dislocation line with precipitates [15].

Knowledge of the relation between structure and mechanical properties will allow us to describe the microstructures that must be produced to achieve a given mechanical property. Microstructures of materials can be described by various structural parameters and each variable can potentially have a dominating effect on certain properties exhibited by the material. Therefore the selection of a microstructural variable of importance should depend on the desired property. At the highest microstructural level, grain size is a common parameter, or the volume fraction of grains of different types, or the fraction of solid in solidification. Below this level are characteristics of deformation substructures, i.e., subgrain size, dislocation density, or sub-boundary misorientation (which effectively characteristics the dislocation density of the boundary), second phase particles including

primary intermetallic particles, dispersoids and precipitates. Particles may variously be described by their number density, size or volume fraction and the matrix surrounding them may be described by its solute content. It is questionable whether any property is wholly insensitive to the materials microstructure, rather, it may be a matter of accuracy of measurement. It is believed that almost all mechanical properties are sensitive to microstructure; however the degree of dependence upon microstructure varies from property to property, ranging from essentially insensitive to extremely sensitive. Accurate analysis of microstructure is therefore important to understand the correlation between microstructure and properties.

1.2 Characterization of Microstructure

The geometric variations of microstructure include difference in (i) size, (ii) shape, and (iii) orientation of the constituent grains/cells. Compositional differences in microstructure include (iv) variations in the relative number of grains of the several phases which may be present, and (v) local segregation within specific grains. A complete analysis of deformed microstructure require statistically reliable information about the quantitative parameters that describes the distribution of dislocation content and the local orientation gradient as a function of crystal lattice orientation and position within a sample. Often orientation distribution functions (ODFs) are used to characterize the macroscopic texture of polycrystalline material without any information about their spatial distribution [16]. Attempt was made to characterize textured materials using deviation in average orientation as a function of thickness of sample to develop scalar parameters that describes the severity of texture gradients and degree of texture banding

[17]. Most frequently the image (pattern) quality of the EBSD pattern is used by the researchers to define the level of stored energy or the distribution of the plastic strain in the material [18]. However there are various factors that govern the image quality, apart from the local dislocation content, such as the spot size, magnification, surface preparation etc. Characterization of local misorientation could be made by using frequency distribution of the misorientation angle as a function of data point distance (Vorhauer et al. 2003) or a point to point misorientation profile (Delannay et al. 2001) to analyze the cell structure and determine the type of subdivision occurring within a grain [19,20]. However such analysis lacks the complete quantitative description of microstructure heterogeneity and spatial information about the local orientation gradient. Attempts have been made to characterize the degree of subdivision as a function of crystal lattice orientation using the parameter of in grain orientation spread (algebraic average of misorientation between all the points within a grain) (Trivedi et al. 2003) [21]. Barton and Dawson described orientation gradients using a correlation tensor where a vector describing the deviation from the average orientation in a crystallite, $\boldsymbol{\omega}$, is combined with the spatial position relative to the grain centroid, $\boldsymbol{x}$, in a dyadic product [22]. The correlation tensor is given as the sum of the dyadic products of $\boldsymbol{\omega}_i$ by $\boldsymbol{x}_i$ as follows:

$$X = \sum_i \omega_i \otimes x_i \,. \qquad \text{..... (1.4)}$$

The summation is performed over all orientation measurements, and it is assumed that these lie on a regular grid so as to represent equivalent regions on the specimen surface. An elegant property of $\boldsymbol{X}$ is obtained by singular value decomposition of $X = U \cdot S \cdot V^T$, where $\boldsymbol{S}$ is a diagonal matrix from which can be obtained the singular values s_k. The

tensors $\boldsymbol{U}$ and $\boldsymbol{V}$ are orthonormal and each singular value s_k has a corresponding left singular vector from $\boldsymbol{U}$ and a right singular vector from $\boldsymbol{V}$. If all vectors are normalized, s_k will give a value from 0 to 1 corresponding to the degree to which misorientations about an axis defined by the left singular vector are correlated along the spatial direction defined by the right singular vector.

Quantitative analysis of sub-grain size and orientation spread within a grain was also discussed by Glez and Driver [23]. Similar to Barton and Dawson [22], they defined a mean orientation and analyzed substructure as a deviation from the average grain orientation. They plotted the frequency distribution of the minimum misorientation angle with respect to the mean orientation and determined the angular orientation spread. Also to get an accurate estimate of subgrain size, the angular resolution of EBSD maps was improved by applying the Kuwahara filtering and sub-grain reconstruction method to EBSD maps (as suggested by Humphreys et al. [24]). This produced a mapping technique where the spatial variation in misorientation from the grain average orientation could be viewed by the investigator. Lehockey et al. [25] define an integrated misorientation density, *IMD*, as

$$IMD_{\varpi} = \frac{1}{N}\sum_{\varpi} \varpi \bullet MD(\varpi) \qquad \text{..... (1.5)}$$

where ω is the angular deviation from a reference orientation in the crystallite, N is the total number of EBSD measurements in the grain, and $MD(\omega)$ gives the number distribution of misorientations for a particular misorientation angle, ω. The measure of misorientation density is useful in locating positions within the material where a high content of geometrically necessary dislocations accumulate, causing a large curvature in

the lattice. To differentiate between a continuously bending lattice and one that oscillates about a mean, smoothing masks are constructed as is done in conventional image analysis. As the size of the smoothing mask is increased, the smoothed misorientation density will be increasingly lower for a structure that oscillates about a mean, while it will remain relatively constant for a continuously bending lattice.

Most of these studies done in the past either failed to provide the scalar measures that describe the microstructure heterogeneity completely or failed to include the spatial distribution of orientation gradient. The current research is an effort towards improving characterization procedures for quantifying dislocation structures and local orientation gradient. Effect of alloy chemistry, grain orientation, neighboring grains and precipitate morphologies on the evolution of dislocation structures during small to medium strain deformation of 5005 and 6022 Al alloys is discussed. A statistical formulation is used to determine major microstructural parameters affecting stress response and a relation between yield stress and microstructural parameters is developed for 6022 Al alloy.

1.3 Outline & Objectives of the Current Research

To improve the final forming characteristics of aluminum alloy automotive sheet, intermediate annealing of the alloy is typically required subsequent to hot rolling and prior to cold rolling. During annealing, the alloy is heated to sufficiently high temperature to promote recrystallization and transform crystallographic texture. A typical manufacturing cost associated with this process is about $0.01/lb with the addition of 2 days of flow time to the product as it must be cooled back to room temperature before

further processing. In addition, there is handling damages associated with loading and unloading of the coils. In 2000, nearly 2,749,000 metric tons of hot-rolled products were produced in United States and thus a slight improvement in processing parameters could potentially result in significant reduction in energy consumption and cost of manufacturing [1]. The ultimate goal of the project is to minimize annealing time used during processing. The current research is focused on development of tools for quantitative understanding of microstructure-property relationship.

Following are the outline and general objectives of the current research:

a. Chapter 2 introduces new strategies to define and image local orientation gradients in deformed crystalline materials. Information about the local lattice curvature obtained from EBSD data is used to generate maps showing spatial distribution of scalar parameters that represent local orientation gradient.

b. Chapter 3 contains a comparison of dislocation structure evolution during small strain room temperature deformation of 3003, 5005 and 6022 Al alloys. The effect of alloy chemistry, grain orientation and neighboring grains on the evolution of dislocation structures is studied. Also the influence of different precipitate morphologies on the evolution of dislocation structures in 6022 Al alloy is discussed.

c. Chapter 4 deals with high temperature deformation behavior of 5005 and 6022 Al alloys at varying strain rates. A statistical formulation was used to identify important microstructural parameters that influence the yield stress of 6022 alloy

and yield strength model was developed as a function of microstructural parameters.

d. Chapter 5 discusses the overall contribution of the current research and its significance.

e. Chapter 6 summarizes conclusions of the current research.

f. Chapter 7 contains suggestions for future work.

1.4 References

[1]. www.aluminum.org

[2]. Sellars, C. M. and Zhu, Q., *Mat. Sci. Engg*. A 280, (2000) 1.

[3]. Nes, E. *Prog. Mater. Sci*. 41, (1997) 129.

[4]. Grong, O. and Shercliff, H. R., *Prog. Mater. Sci* 47, (2002) 163.

[5]. Richmond, O., *J. Met*. 38, (1986) 16.

[6]. Esmaeili, S., Lloyd, D. J., Poole, W. J., *Acta Mater*. 51, (2003) 2243.

[7]. Barlat, F., Glazov, M.V., Brem, J.C., Lege, D.J., *Int. J. Plasticity* 18, (2002) 919.

[8]. Kocks, U.F., *Phil. Mag.* 13, (1966) 541.

[9]. Gil Sevillano, J., VanHoutte, P., Aernould, E., *Prog. Mater. Sci.* 25, (1981) 69.

[10]. Winther, G., *Mat. Sci. Engg*. A309–310, (2001) 486.

[11]. Hall, E.O., *Proc. Phys. Soc. London* 643, (1951) 747.

[12]. Petch, N.J., *J. Iron. Steel Inst. London* 173, (1953) 25.

[13]. Callister, W. D. Jr., *Materials Science and Engineering: An Introduction* (John Wiley 1999, 5th Edition).

[14]. Mecking, H. and Kocks, U.F., *Acta Metall*. 29, (1981) 1865.

[15]. Ashby, M.F., *Mat. Sci. Tech* 8, (1992) 102.

[16]. Bunge, H.J., *Texture Analysis in Materials Science*, Butterworth-Heinemann (1981).

[17]. Wright, S.I., Field, D.P., Witt, R., Michaulk, C.A., *Mat. Sci. Forum* 408-412, (2002) 107.

[18]. Wilkinson, A.J., *Electron back scatter diffraction in materials science* ed. Schwartz, AJ, Kumar, M and Adams, B.L., (Kluwer Academic/Plenum Publishers, New York) (2000) 231.

[19]. Vorhauer, T., Hebesberger, T., Pippan, R., *Acta Mater*. 51, (2003) 677.

[20]. Delannay, L., Mishin, O.V., Juul Jensen, D., Van Houtte, P., *Acta Mater*. 49, (2001) 2441.

[21]. Trivedi, P.B., Field, D.P., Weiland, H., *Int. J. Plasticity* 20, (2004) 459.

[22]. Barton, N.R. and Dawson, P.R., *Modelling and Simulation in Mat. Sci. and Engg.* 9, (2001) 433.

[23]. Glez, J.C. and Driver J., *J. of App. Cryst*. 34, (2001) 280.

[24]. Humphreys, F.J. and Hurley, P.S., *J. Microscopy* 201, (2001) 50.

[25]. Lehockey, E.M., Lin, Y.P., Lepik, O.E., in *Electron Backscatter Diffraction in Materials Science*, ed. A.J. Schwartz, M. Kumar, and B.L. Adams (Kluwer Academic/Plenum Publishers, New York 2000) 247.

CHAPTER – 2

CHARACTERIZATION METHODOLOGIES

This chapter begins with a brief overview on crystal defects; specifically describing geometric properties of dislocations and various techniques used to observe dislocations. A significant portion of this chapter deals with the improved characterization methodologies developed using EBSD data to characterize dislocation structures and local orientation gradient. Two high purity Al single crystals deformed at widely different strain rates are chosen for this study. Interrogation of the dislocation substructure is accomplished by extracting information gleaned from small point to point misorientations as measured by EBSD. Along with an estimate of the geometrically necessary dislocation (GND) content, the point to point deviation from an average grain orientation is described by an orientation difference vector defined in Rodrigues space. Mapping of parameters such as GND, and divergence and gradient fields created from analysis of the difference vectors provide an alternative approach to obtain quantitative information and images from EBSD data.

2.1 Crystalline Defects

Crystalline materials exhibit long-range order in the position and stacking sequence of atoms or molecules. Crystalline structure consists of a three dimensional arrangement of points in space (lattice points), where each lattice point has identical surroundings. Associated with each of these lattice points is a single atom or identical group of atoms,

depending on the solid under consideration. Real crystals deviate from perfect periodicity with regard to atomic configuration. The term ‘defect’ or ‘imperfection’ is generally used to describe any deviation from an orderly array of lattice points. For a better understanding of structure-sensitive properties it is important to consider these lattice defects. These defects can be classified into the following groups:

(a) Point Defects (Zero dimensional): When deviation from the periodic arrangement of a lattice is localized to the vicinity of only few atoms it is called a point defect. This includes the presence of an impurity atom (substitutional or interstitial) or the absence of an atom (vacancy).

(b) Line Defects (One Dimensional): Line defects are defective regions of the crystal that extend through the crystal along a line. The most important line defect is the dislocation. The dislocation is the defect responsible for the phenomena of slip, by which most metals deform plastically.

(c) Planar Defects (Two Dimensional): Planar defects occupy higher spatial volume than point or line defects. These include grain boundaries, interfaces, stacking faults and twin boundaries.

(d) Bulk Defects (Three Dimensional): Such volume defects are formed by excessive concentration of point or line defects and occupy significant spatial volume in all 3 dimensions. These include precipitates, voids and cracks and are usually controlled during processing of materials.

2.2 Dislocations

The concept of a dislocation was first introduced independently by Orowan [1], Polanyi [2] and Taylor [3] to explain the discrepancy between observed and theoretical shear strength of metals. They showed that the motion of dislocations through a crystal lattice requires less stress than the theoretical stress and the movement of the dislocations produces a step or slip band at the free surface. Figure 2.1 is the schematic of the movement of dislocations through a lattice such that one atomic bond is broken at a time thereby reducing the stress required for deformation [4].

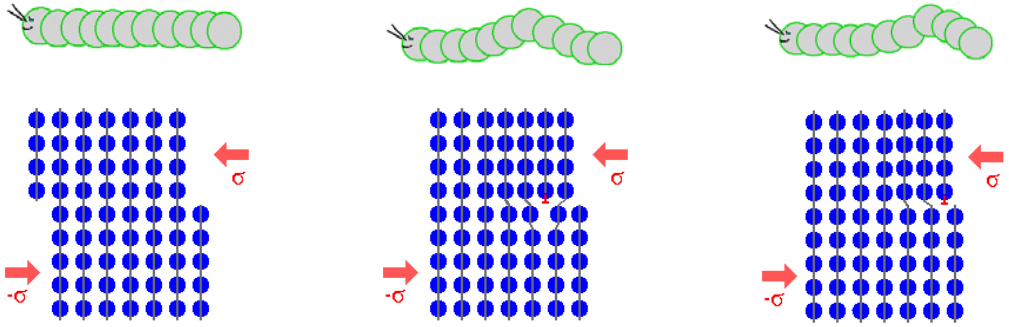

Figure 2.1: Schematic showing progressive movements of a dislocation through crystal lattice [4].

A dislocation is characterized principally by its Burger's vector ***(b)***, the scalar magnitude of which is also called the strength of the dislocation. This is the difference in slip, i.e. in relative atomic positions, produced by crossing the dislocation line from one region to another. Usually, we expect ***b*** to be equal to the interatomic vector in the glide plane, or at least to a small lattice vector. Dislocations of this kind are called perfect or lattice dislocations. In certain cases, it is also possible to have ***b*** equal to a fraction of a lattice repeat vector. The discontinuity is then an imperfect or partial dislocation, and the

original lattice structure is not preserved when the dislocation line is crossed. For example in FCC metals, perfect dislocations of type a/2<110> can decompose into two partial dislocations to minimize the energy e.g. $\frac{a}{2}[10\bar{1}] \rightarrow \frac{a}{6}[2\bar{1}\,\bar{1}] + \frac{a}{6}[11\bar{2}]$. The two basic types of dislocations are the edge dislocation and the screw dislocation. To visualize a dislocation, slice a simple cubic crystal lattice (Figure 2.2) along the plane ABCD and displace the atoms across the plane by a distance equal to the lattice parameter. If we then stick the crystal back together again, we find that we have a distorted crystal where the center of the distortion is along the line CD [5]. Correspondingly, this line CD is a dislocation line. If the atoms are displaced perpendicular to CD we call the resulting defect an edge dislocation, since the defect resembles the edge of an extra half plane of atoms (Figure 2.2 (a)). If the atom displacement is parallel to CD we have a screw dislocation (Figure 2.2 (b)) and if the atoms are displaced at some other angle to CD we have a mixed dislocation or a dislocation with mixed edge and screw components. The shear displacements associated with plastic deformation occur primarily by the movement of dislocations. Planes on which dislocations move is called slip plane and the direction is called slip direction. The slip planes and directions are those of highest packing density. The only prerequisite for a plane to be a slip plane is that it contains both the Burger's vector and line direction. For edge dislocations, since the Burger's vector is normal to the line vector, there exists a unique slip plane in which they are able to move. For screw dislocations however, there exist multiple feasible slip planes, as the Burger's vector and line direction are parallel to each other. And it is for this reason that screw dislocations move between slip planes significantly easier than edge dislocations do.

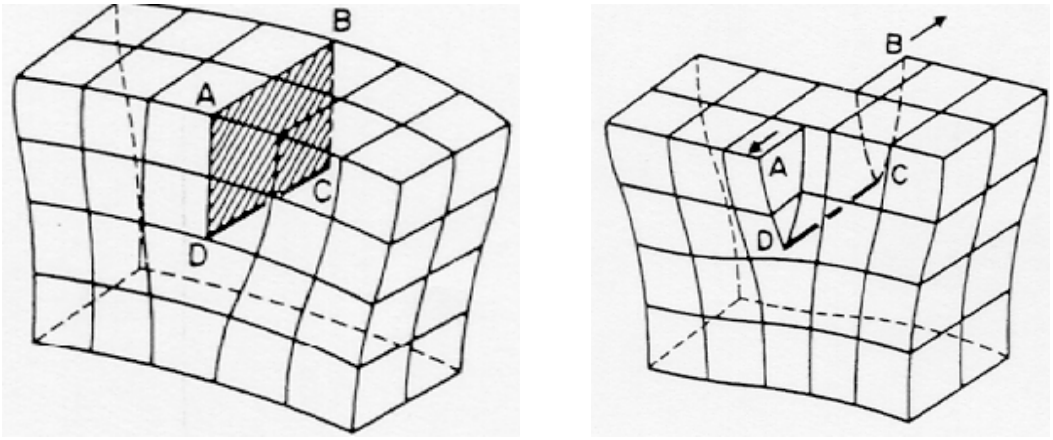

Figure 2.2: Schematics showing (a) edge dislocation and (b) screw dislocation in simple cubic lattice [5].

Plastic deformation in crystalline solids is inhomogeneous and usually occurs by sliding of blocks of the crystal over one another along definite slip planes and in definite slip directions. Every dislocation then produces slip in a specific direction (parallel to the Burger's vector) and moves on a specific slip plane. Each crystal structure thus has a definite set of slip planes and directions (also known as slip systems). Slip planes in FCC metals are {111} and slip directions are <110> (shown in Figure 2.3 and Table 2.1) [5]. To produce an arbitrary change in shape, a crystal must slip on a number of slip systems. Macroscopic slip is observed on a given system when the resolved shear stress reaches the critical value for the onset of dislocation motion, i.e., a stress high enough to overcome the lattice resistance to dislocation motion. This value of the resolved shear stress is called the critical resolved shear stress and is the same for all similar slip systems in a crystal. A single crystal subjected to a shear stress can deform extensively with slip

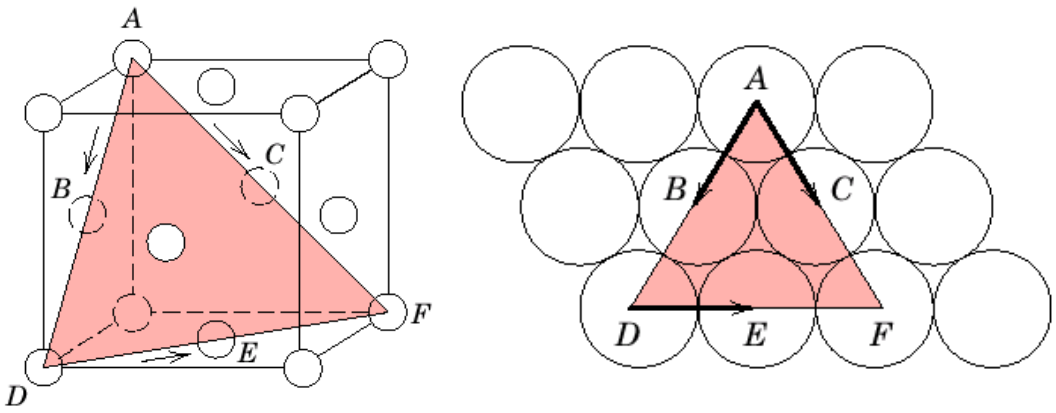

Figure 2.3: Schematic showing slip systems in FCC crystal [4].

Table 2.1: Slip systems for FCC crystals [5].

Slip System	Slip Plane	Slip Direction
A2 – Critical system	(1 1 1)	[1 -1 0]
A6 – Critical system	(1 1 1)	[0 1 -1]
A3 – Critical system	(1 1 1)	[1 0 -1]
D1 – Cross-slip system	(-1 1 1)	[1 1 0]
D6 – Cross-slip system	(-1 1 1)	[0 1 -1]
D4 – Cross-slip system	(-1 1 1)	[1 0 1]
B2 – Coplanar system	(1 1 -1)	[1 -1 0]
B5 – Coplanar system	(1 1 -1)	[0 1 1]
B4 – Primary system	(1 1 -1)	[1 0 1]
C1 – Conjugate system	(1 -1 1)	[1 1 0]
C5 – Conjugate system	(1 -1 1)	[0 1 1]
C3 – Conjugate system	(1 -1 1)	[1 0 -1]

on only a single slip system. However in polycrystals, since all grains are oriented differently, each will respond differently when subjected to a shear stress. And if each grain deforms differently, then the region around grain boundaries is subject to complex shape change if we demand coherency to be maintained between grains. According to Taylor, to achieve arbitrary shape change it is necessary to have five independent slip systems operative [6].

2.3 Observations of Dislocations

Various techniques have been used over the years to observe dislocations. Practically all the experimental techniques for detecting dislocations utilize the strain field around a dislocation to increase its effective size. These experimental techniques can roughly be divided into two categories: those involving chemical reactions with the dislocation and those utilizing physical changes at the site of dislocations. Chemical methods include etch pit techniques and precipitation techniques. Methods based on the physical structure at a dislocation site include electron microscopy and X-ray diffraction.

The etch pit technique employs the use of an etchant, which forms a pit around dislocation sites because of the strain field surrounding the dislocation. Sometimes it is possible to distinguish between edge and screw dislocations using this technique. Advantage of this technique is its relative ease of use and that it can be applied to bulk samples. However this technique cannot be employed for sample with high dislocation density and also care should be taken that the pits are formed only at the dislocation sites. A similar method of detecting dislocations is to form a visible precipitates along the

dislocation line. This technique is called “decoration” of dislocations and involves adding a small amount of impurity to form the precipitate after suitable heat treatment. Even though it is possible to see the internal structure of dislocation lines, this technique is not used extensively with metals. X-ray microscopy can also be used for detecting dislocations but they are not widely used because of low resolution of about 10^5 dislocations/cm^2. Transmission electron microscopy is the most powerful and universally applicable technique for studying dislocations in solids. Thin samples (usually 1000A^o) are electro-polished to make it electron transparent. Individual dislocations can be observed because the intensity of the diffracted beam is altered by the strain field of the dislocation. However since the information is obtained only from the small volume of sample, this technique does not provide statistically reliable information. Also it is possible to alter the defect structure during sectioning and polishing of thin films. A relatively new technique that provides indirect information about dislocation structure is electron back scatter diffraction [7].

2.4 Electron-Backscatter Diffraction Technique

Electron-backscatter diffraction (EBSD) is one of various SEM-based techniques used to obtain local information on the crystallographic character of bulk crystalline or polycrystalline material. EBSD is a convergent beam technique whereby an electron diffraction pattern is formed by coherently backscattered electrons diffracted by planes matching the Bragg condition

$$\lambda = 2d \sin\theta \qquad \ldots\ldots\ldots\ldots\ldots\ldots\ldots\ldots\ldots\ldots \quad (2.1)$$

where λ is the wavelength of the electron beam, d is the interplanar spacing for a given set of lattice planes and θ is the Bragg angle. The collection of an electron backscatter diffraction pattern (EBSP) in the SEM is relatively straightforward. A polished sample must be tilted to a relatively high angle (typically 70°) inside the SEM. When an electron beam encounters a solid material, it is inelastically scattered in all directions beneath the surface of the material. As a result there are always some electrons that satisfy the Bragg angle of every plane in the crystallite. These electrons are elastically scattered as they exit the specimen surface, to form the contrast observed in EBSD patterns. Because the electrons travel from the source in all directions, for each set planes for which the Bragg condition is satisfied, the diffracted beams lie on the surface of a cone whose axis is normal to the diffracted plane. Those cones intersect with a phosphor screen placed in front of the specimen and give rise to the pattern (Figure 2.4). Each pair of cones, whose intersection with the phosphor screen produces a nearly parallel set of lines, is termed a Kikuchi band. An image analysis technique, called Hough transform (modified Radon transform) is used to detect Kikuchi bands. The Hough transform is given by $\rho = x\cos\varpi + y\sin\varpi$, which integrates intensity along all possible straight lines, reducing all lines in real space to a single point defined by (ρ, ϖ) in Hough space. Usually automated indexing of EBSD patterns is done using sophisticated software algorithms. The whole process from start to finish can take less than 0.05 seconds. One major advantage of the EBSD technique is that measurements can be performed on a large area of the sample and thus statistically reliable orientation information can be obtained. Resolution of the technique is dependent upon the SEM type and atomic number of the

metal. Typically under best conditions, an angular resolution in modern FEG-SEM instruments is about 0.5^{o} and spatial resolution is 20 nm.

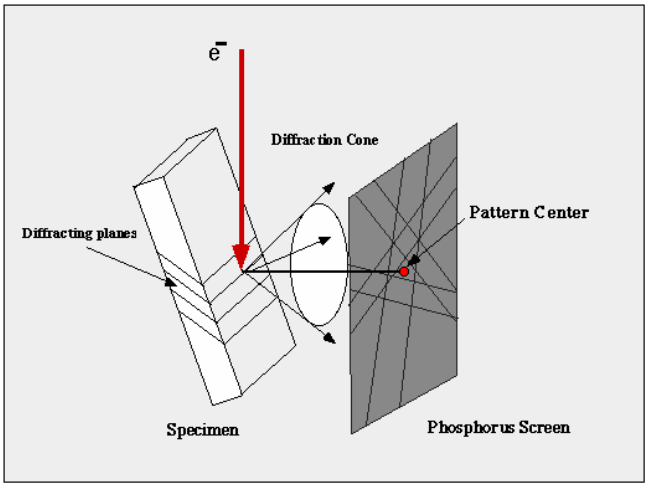

Figure 2.4: Schematic showing the formation of Kikuchi pattern using EBSD in SEM [8].

The following sections of this chapter contain a new approach to analyze the local orientation gradient in deformed single crystals. The density of geometrically necessary dislocations from lattice curvature measurements, and an orientation difference vector defined in Rodrigues space is discussed and calculated for sample crystallites. Also a mapping procedure based on divergence and gradient of an orientation difference vector field is introduced for quantitative characterization of local orientation gradients.

2.5 Experimental Procedures

Two single crystal samples of high purity (99.999%Al) were deformed and characterized using EBSD. One crystal was deformed at room temperature using channel die

compression to 15 percent height reduction. The second crystallite suffered deformation in uniaxial compression at a high strain rate. Characterization of the deformed samples was done using a Camscan series IV scanning electron microscope (SEM) operated with Tungsten filament at 20KeV. EBSD analysis was performed in beam scanning mode using TSL OIM Data Collection 3.0 system with a probe size of 200 nm and a working distance of 25mm. A total of 130000 and 45000 orientation measurements were taken in a hexagonal grid pattern with a step size of 0.5 μm and 1 μm for the channel die deformed and high strain rate deformed samples respectively. Standard orientation images of both samples are shown in Figure 2.5 and color coding indicates pole aligned with the specimen surface normal direction as shown in the orientation key. The average orientations of channel die deformed and high strain rate deformed crystals are $(13\,4\,10)[14\,\overline{13}\,\overline{13}]$ and $(12\,13\,20)[25\,\overline{20}\,\overline{2}]$ respectively. This means that $(13\,4\,10)$ crystallographic plane of channel die deformed sample is parallel to normal direction of the sample and $[14\,\overline{13}\,\overline{13}]$ crystallographic direction is parallel to transverse direction of the sample. The deformation is applied such that compression direction is normal to the images for both specimens, constrained direction is aligned with TD (transverse direction) and direction of the materials flow is parallel to RD (rolling direction) of the sample as shown in the Figure 2.5.

2.6 Results and Discussion

2.6.1 Misorientation Profile

One of the simplest analyses of local orientation gradient can be done by scanning the sample along a line and determining variation of misorientation as a function of distance.

Figure 2.6 contains the misorientation profile plotted along a line shown in Figure 2.5 for both the samples.

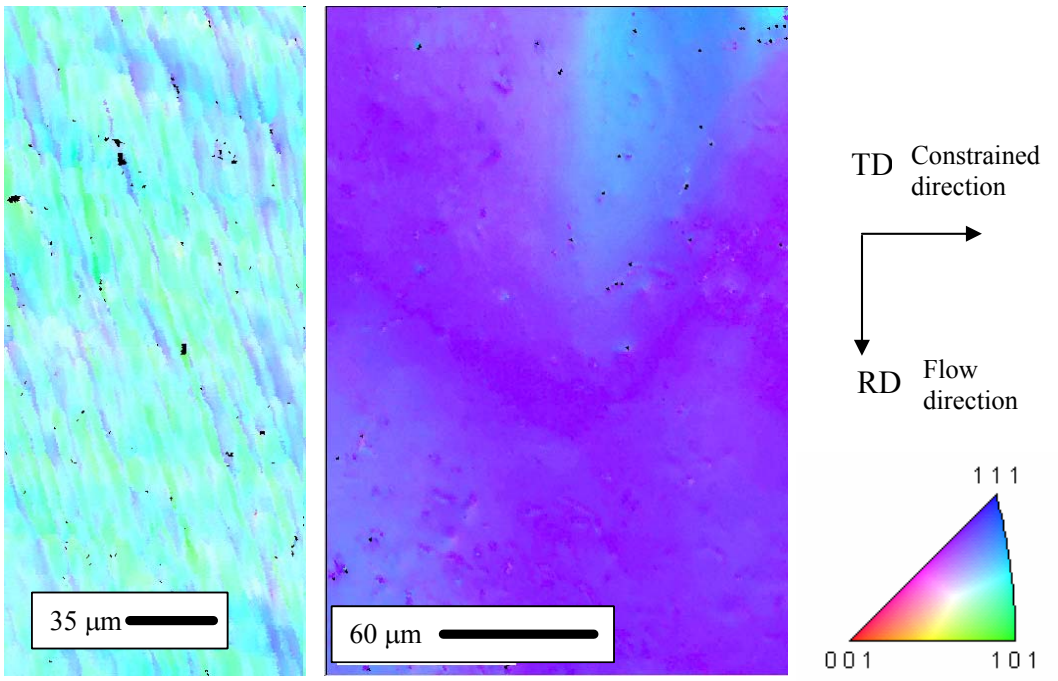

Figure 2.5: Orientation images of pure Al single crystals for (a) the specimen deformed in a channel die at 15% strain and (b) the specimen deformed at high strain rate. The orientation shading key is shown at right.

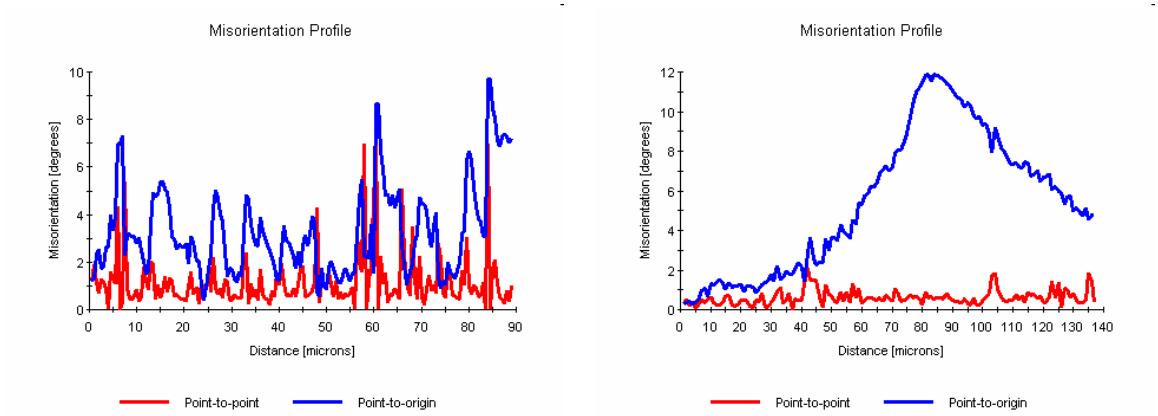

Figure 2.6: Point to Point and Point to Origin misorientation profile for (a) sample deformed in channel die compression and (b) sample deformed at high strain rate.

It can be seen that for samples deformed under channel die compression both point to point and point to origin misorientation profile follow a similar trend. This would be an indication of cell type structure and therefore whenever a point is reached at cell boundaries a peak is observed in the misorientation profile. Such analysis is used to obtain measures of average cell size or average misorientation angle that can be included in the model. In contrast point to origin misorientation continuously increases where as point to point profile is constant for the sample deformed at a high strain rate. This would imply that there is a long range orientation gradient and the crystal lattice is continuously deviating away from the starting orientation until it reaches a misorientation value of 12^{o}.

2.6.2 Geometrically Necessary Dislocation Density

During plastic deformation of polycrystalline materials, individual grains do not rotate as a unit but are sometimes subdivided into crystallites rotating independently of one another to accommodate the imposed strain. The reason for grain fragmentation is that the number and selection of simultaneously acting slip systems differs between neighboring volume elements within a grain. This leads to differences in lattice rotations between neighboring elements within a grain when the material is strained. Depending upon the crystal lattice orientation of the grain and its interaction with near neighbors, grains could develop a well defined cell-block structure of similar lattice orientation but rotating at differing rates and sometimes in differing directions. In some instances the lattice rotation rate within a grain changes in a continuous fashion, thus developing long range orientation gradients. Irrespective of the type of grain subdivision, geometrically necessary dislocations (GNDs) accommodate small lattice rotations.

The concept of geometrically necessary dislocations was first introduced by Nye [9] and further developed by Ashby [10]. Figure 2.7 shows the schematic for the formation of geometrically necessary dislocation during deformation. It can be seen that since individual grains do not deform independently of one another, geometrically necessary dislocations are produced at the grain boundaries to maintain lattice continuity. Nye's tensor, α_{ij}, is a representation of dislocations with Burger's vector ***i*** and line vector ***j***. In Nye's original formulation of the dislocation tensor, dislocation density was described as a number density of lines piercing a plane. He defined the tensor in the following manner:

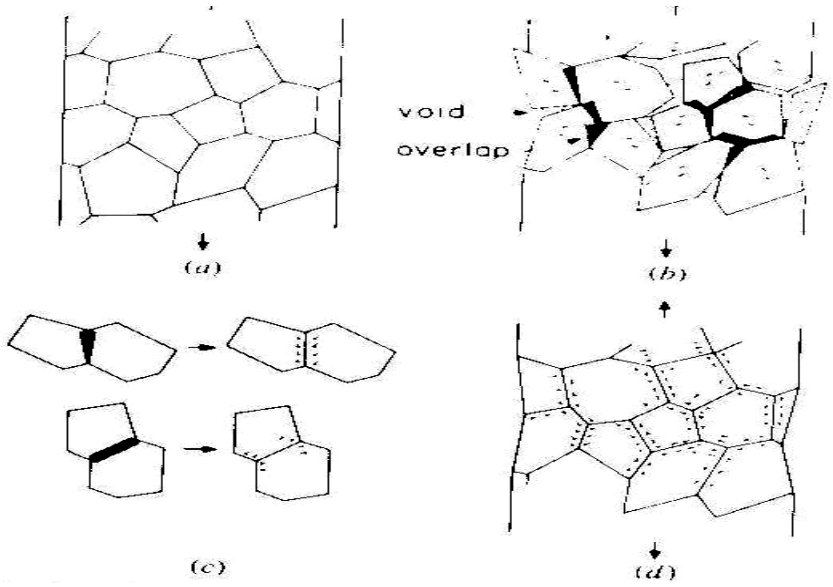

Figure 2.7: Schematic showing the formation of geometrically necessary dislocations during deformation [10].

$$\alpha_{ij} = nb_i t_j \qquad \text{..... (2.2)}$$

where *n* was the number density of dislocation lines with Burger's vector, ***b***, crossing a unit area normal to their unit tangent line vector, ***t***. The discretized Burger's vector, ***b***,

and tangent line vectors, $\boldsymbol{t}$, form n-pairs of geometric dislocation properties. We can extend Equation 2.2 suggested by Nye [9], to relate the dislocation density tensor, $\boldsymbol{\alpha}$, to the dislocations present in the neighborhood for any crystal structure with the relation,

$$\alpha = \sum_{i=1}^{K} \rho^i (b^i \otimes z^i) \quad \ldots\ldots\ldots\ldots\ldots\ldots\ldots\ldots\ldots\ldots (2.3)$$

where, the dislocation dyadic represents a geometrical definition of dislocation i having Burger's vector $\boldsymbol{b^i}$ and slip plane normal direction $\boldsymbol{z^i}$. The sum is over all the dislocations present and ρ^i is the scalar dislocation density of dislocation i. Considering continuously-distributed dislocations, Nye's tensor quantifies a special set of dislocations whose geometric properties are not canceled by other dislocations in the crystal. Any dislocation structure that makes no contribution to the dislocation density tensor, such as a dislocation dipole, is termed statistically stored dislocations. Statistically stored dislocations (SSDs) are formed by statistical mutual trapping of dislocations such as dislocation dipoles. A more detailed description of GNDs and SSDs is given by Arsenlis and Parks [11]. Assuming a minimal effect from elastic strain gradients, any crystallite containing non-zero dislocation density tensor components necessarily contains lattice curvature that can be quantified by spatially specific orientation measurements. Such measurements are inherent to automated EBSD scans of crystalline materials. Thus we can relate the difference in orientation (or misorientation) between two neighboring data points to the Nye dislocation density tensor by the equation:

$$\alpha_{ij} = e_{ikl} g_{jl,k} \quad \ldots\ldots\ldots\ldots\ldots\ldots\ldots\ldots\ldots\ldots (2.4)$$

Since the dislocation density tensor has 9 components it is possible, using a linear simplex method, to determine a set of densities of 9 dislocation types which minimizes

the total dislocation content. One disadvantage of using this technique is that it does not take into account all the types of dislocations that could contribute to lattice curvature. This limitation could be overcome by using a normal equation lower bound method (as shown by El-Dasher et al. [12]) where Equation 2.3 for FCC materials could be reduced to:

$$\alpha_l = A_{lk}\rho_k \qquad \text{……………………………… (2.5)}$$

where, k = 1, 18 and l = 1, 9 and matrix ***A*** represents a component of the dislocation dyadic. We can apply L^2 minimization method to Equation 2.5 and compute the densities of all 18 dislocations using the following equation:

$$\rho_{GN} = A^T\left(AA^T\right)^{-1}\alpha \qquad \text{………………………… (2.6)}$$

There exist 36 distinct dislocations that can be used to account for slip in face centered cubic crystals, but natural choice is to limit the choice to 18 geometrically distinct dislocations: 6 screw and 12 edge. In the current analysis we have limited the dislocation types to pure edge and pure screw and hence code was developed to determine the densities of 18 total dislocation types (12 pure edge and 6 pure screw dislocations). Aluminum alloys possess cubic crystal symmetry with any orientation ***'g'*** having 24 geometrically equivalent orientations. Thus to obtain consistent orientation measurements all measured crystal orientations are reduced to symmetrically equivalent orientations such that the point to point misorientation angle is minimized. Also the orientation measurements are done on the two dimensional structure of material and we do not have any information about orientation gradient in the third dimension. Thus it is assumed that the orientation gradient in the third direction is assumed to be zero (i.e. $g_{jl,3}$ = 0), however accurate determination of dislocation density tensor α requires the information about

orientation gradient in all the three directions. To determine an accurate estimate of GND density when analyzing polycrystalline materials, it is important to ignore the high angle grain boundaries from the calculation of GND. In the current analysis this is accomplished by assigning GND density a value of zero, wherever the point to point misorientation exceeds 14º. Figure 2.8 contains plots showing the distribution of total GND density for the 2 crystals used in the present investigation. The average values of GND densities for the channel die and high strain rate deformed crystals were $51x10^{14}/m^2$, and $61x10^{14}/m^2$ respectively. It is noted that the banded structure apparent in the orientation image of Figure 2.5a is again observed as regions of high GND content (Figure 2.8a). The boundaries of these banded structures contain a high GND density and regions within the bands are relatively free of dislocations that contribute to lattice curvature.

2.6.3 Deviation from an Average Orientation

Microtexture analysis can alternatively be performed by measuring the deviation of orientation from the grain average orientation at any point of the sample [13]. It is possible to plot the deviation from an average orientation in terms of $\Delta\omega(\boldsymbol{x})$ (showing the scalar angle of rotation in degrees) and $\boldsymbol{n}(\boldsymbol{x})$ (showing the axis of rotation). Figure 2.9 contains plots showing the deviation angle ($\Delta\omega(\boldsymbol{x})$) from an average orientation for the crystals analyzed in this investigation. In the current analysis, an average orientation given by Equation 2.7 was determined such that the angle of misorientation between all points in the sample is minimized.

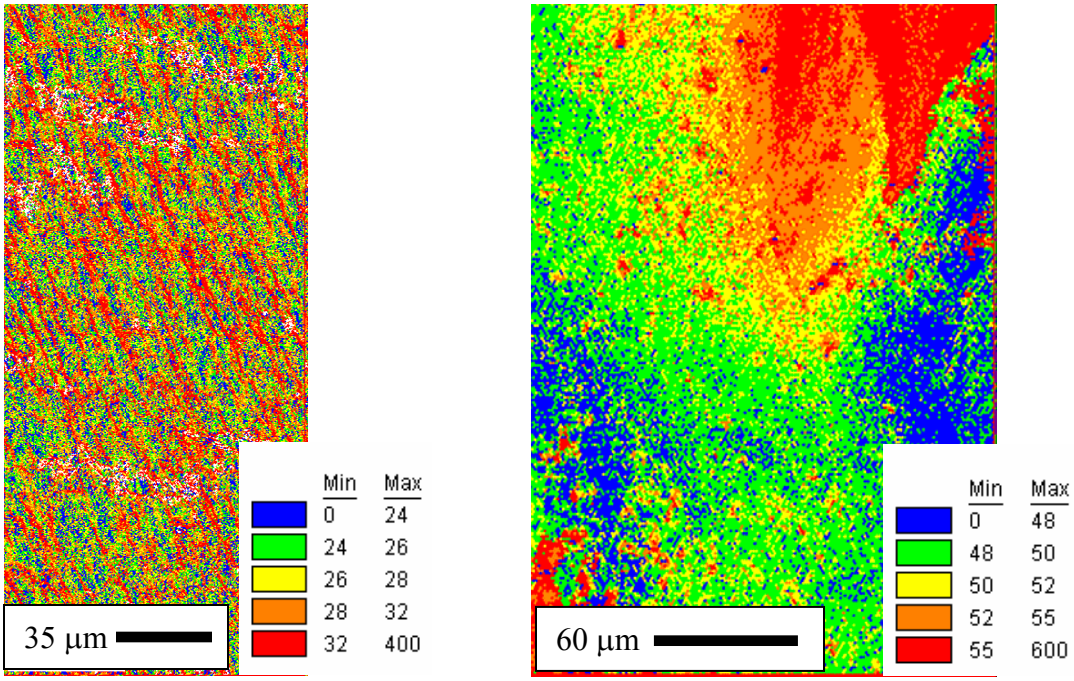

Figure 2.8: Plots showing the distribution of GND density (units are x $10^{14}/m^2$) for high purity single crystal Al samples deformed at (a) 15% strain in channel die deformation, and (b) high strain rate.

$$g_{avg} = \min \sum_i \frac{1}{2} \cos^{-1} tr\left(g_{avg} g_i^{-1} h_j - 1\right) \qquad \text{..... (2.7)}$$

Average orientations of both crystals are defined in experimental section of this chapter. The advantage of using such an orientation mapping is that the spatial distribution of orientation gradients within a grain can be easily visualized. It can be seen that the regions of high deviation angle relate to an accumulation of dislocation content away from the position of average orientation, as seen in Figure 2.8(b). Alternatively, the high deviation angle might relate to high dislocation content at the cell boundaries.

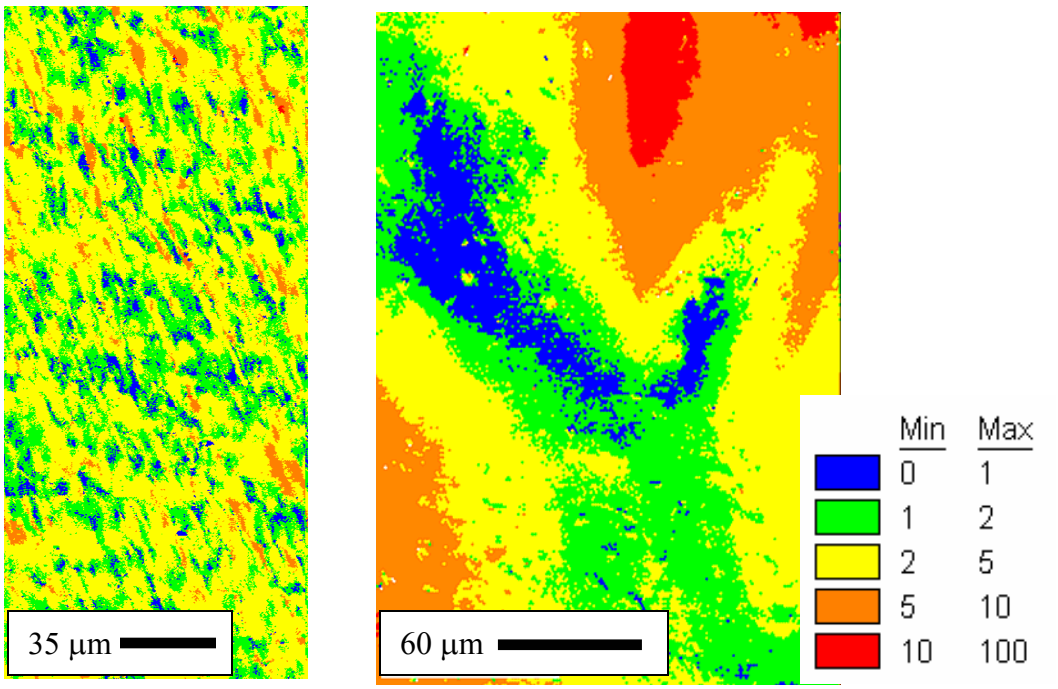

Figure 2.9: Maps of the structures shown in Figure 2.5 with shading according to deviation angle from the average orientation (in degrees) of the crystallites.

2.6.4 Axis of Deviation

A vector defining the axis of rotation, $\boldsymbol{n}(\boldsymbol{x})$, is plotted on a color coded grid defined over the unit triangle of the stereographic projection. Since complete orientation information is obtained from individual measurements, the misorientation values, including both $\Delta\omega(\boldsymbol{x})$ and $\boldsymbol{n}(\boldsymbol{x})$ can be directly obtained from each measurement position. Figure 2.10 shows the axis of rotation for the measured misorientation of the orientation images shown in Figure 2.5. Regions of relatively small $\Delta\omega(\boldsymbol{x})$ have a somewhat indeterminate $\boldsymbol{n}(\boldsymbol{x})$ because of the angular resolution of the EBSD measurement. Regions of larger angle misorientation show that not only the angle varies continuously, but also the axis of

rotation varies in a continuous manner in the high strain rate specimen shown at the right in Figures 2.9 and 2.10.

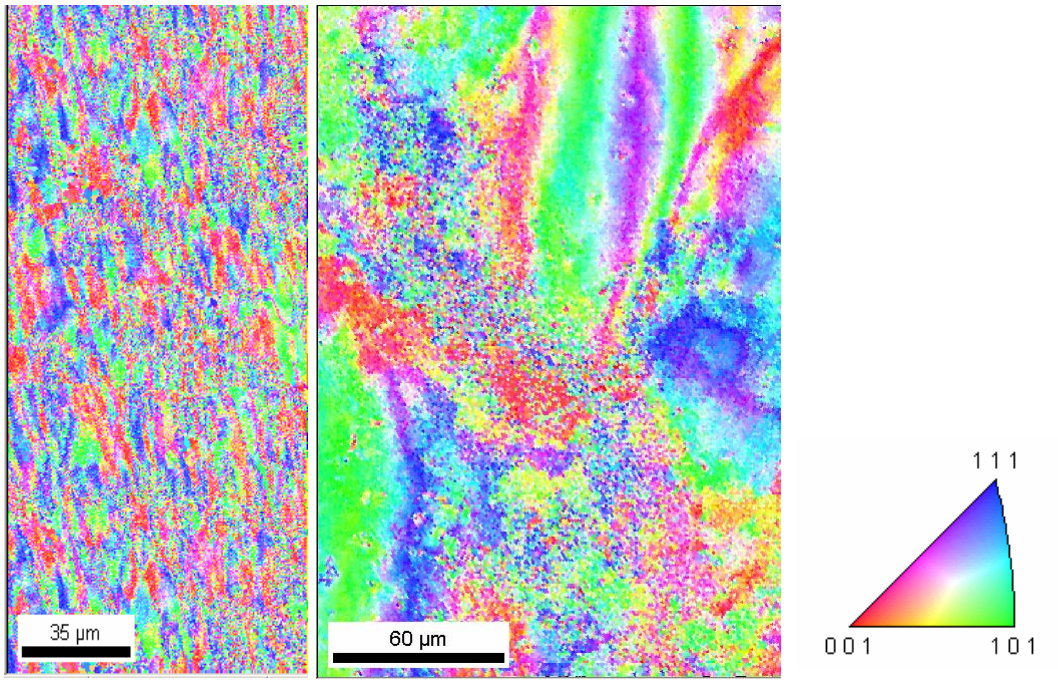

Figure 2.10: Maps of both single crystals with shading according to the axis of rotation describing the misorientation from the average orientation of the crystallites. Blue color in above images indicate that crystal lattice at that point is misoriented from an average orientation along [1 1 1] axis.

2.6.5 Orientation Difference Vector

Representation of misorientation data in Rodrigues space is sometimes adopted by researchers because the symmetry of the crystallite is reflected in the asymmetric region of Rodrigues space. The Rodrigues vector, $\boldsymbol{R}$, is defined as $\boldsymbol{R} = \boldsymbol{n}\tan\left(\omega/2\right)$, where $\boldsymbol{n}$ is the axis of rotation and ω is the rotation angle defining the lattice [14]. Figure 2.11a shows the asymmetric region of Rodrigues space for cubic crystals where [r_1 r_2 r_3] defines

components of the Rodrigues vector. Let $\boldsymbol{R}_{ave}$ defines the average orientation of the crystallites (given by an equation similar to Equation 2.7) in Rodrigues space such that the sum of misorientation between $\boldsymbol{R}_{ave}$ and all the orientations is minimized. Typically the misorientations are mapped into a fundamental zone that is an asymmetric domain shown graphically in Figure 2.11b.

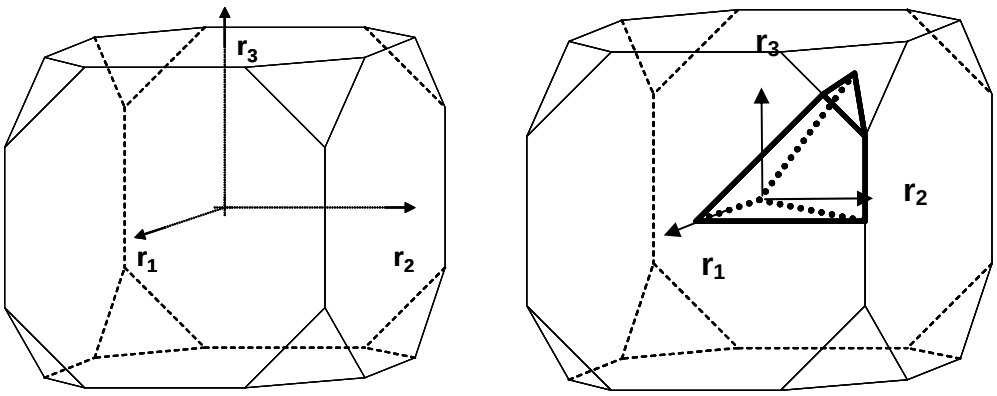

Figure 2.11: Schematics showing (a) asymmetric region of Rodrigues space for cubic crystals (b) fundamental region of Rodrigues space for misorientations between cubic crystallites

The result of two successive rotations $\boldsymbol{R}_1$ and $\boldsymbol{R}_2$, is given by

$$\boldsymbol{R}_2 \circ \boldsymbol{R}_1 = \frac{\boldsymbol{R}_1 + \boldsymbol{R}_2 - \boldsymbol{R}_1 \times \boldsymbol{R}_2}{1 - \boldsymbol{R}_1 \cdot \boldsymbol{R}_2}, \qquad \ldots\ldots\ldots\ldots\ldots\ldots\ldots\ldots\ldots\ldots \quad (2.8)$$

so the rotation $\delta\boldsymbol{R}$ from $\boldsymbol{R}_{ave}$ to $\boldsymbol{R}(\boldsymbol{x})$ assumed to be near one another in orientation space, is obtained from $\boldsymbol{R}(x) = \delta\boldsymbol{R} \circ \boldsymbol{R}_{ave}$ or

$$\delta\boldsymbol{R} = \boldsymbol{R}(x) \circ \left(-\boldsymbol{R}_{ave}\right). \qquad \ldots\ldots\ldots\ldots\ldots\ldots\ldots\ldots\ldots\ldots \quad (2.9)$$

Using $\boldsymbol{R}_{ave}$ and $\boldsymbol{R}(\boldsymbol{x})$ in the form given by the above equation leads to the result, where $\delta\boldsymbol{R}$ is a difference vector with a direction that can lie anywhere in space, but aligns with the misorientation axis as defined in Rodrigues space. This vector differs from the misorientation Rodrigues vector in that it is not mapped into the asymmetric domain, but maintains the proper relationship with the average orientation of the grain. If the deviation vector is now operated upon by the average grain orientation, so that the axes defining the Rodrigues space are aligned with those defining the crystallite lattice, the deviation vector is defined in the specimen coordinate frame (Figure 2.12). These are represented in a plane of the sample coordinate frame as indicated by the RD and TD labels (reference direction and transverse direction).

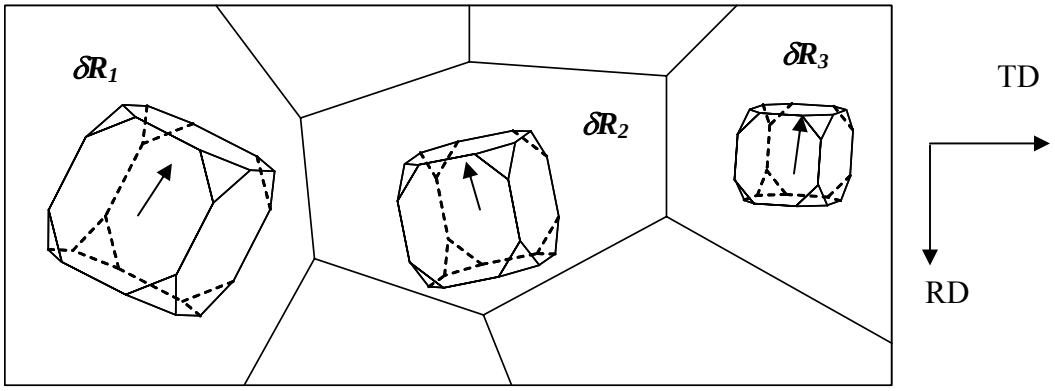

Figure 2.12: Schematic showing the Rodrigues difference vector plotted for different grains in the sample coordinate frame (given by TD and RD).

An example of the information that can be graphically presented is shown in Figure 2.13. This image contains a portion of the single crystal deformed in channel die to 15% height reduction. It is apparent that orientations within the cells are uniformly rotated from the grain average orientation about a given axis, and that neighboring cells are rotated about

different axes from the average orientation. The magnitude of the flow field should correspond to the total dislocation density required to rotate the lattice at each point from the average orientation.

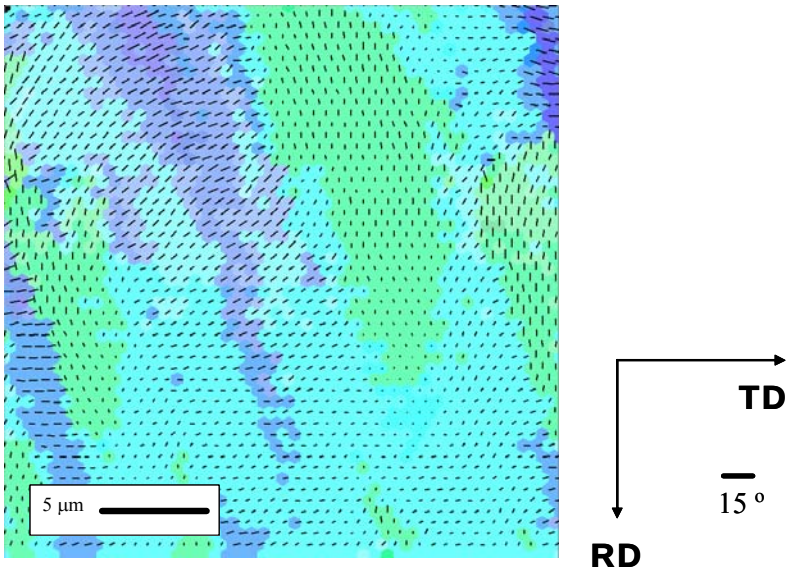

Figure 2.13: Misorientation flow field from average orientation generated using difference vector ***(δR(x))*** in a small region of 15% deformed single crystal sample shown in Figure 2.5(a).

2.6.5 Divergence & Gradient of Orientation Difference Vector

Additional quantitative information about the local orientation gradient can also be obtained by calculating the divergence of the orientation difference vector. Divergence of a vector function ***F(x,y,z)*** is a scalar function of position and is given by Equation 2.10. To understand the physical significance of divergence, consider a small region of space (with volume *V*) in which some 'matter' is moving. If we assume that 'matter' is neither created nor destroyed within this volume, then calculation of divergence will help us to

know the rate at which the amount of matter in volume *V* is changing. So the negative value of divergence indicates net flow out of *V* meaning the amount of matter in *V* is decreasing. In our case, divergence of the difference vector at any point (*x*,*y*) in the sample yields a scalar quantity that indicates the degree of rotation of the crystal lattice at any given point with respect to its neighborhood,

$$DivF = \frac{\partial F_x}{\partial x} + \frac{\partial F_y}{\partial y} + \frac{\partial F_z}{\partial z} \qquad \text{..... (2.10)}$$

A divergence of zero at any given point would indicate that the crystal lattice at that point and its near-neighboring points are deviated from an average orientation by the same magnitude about a common axis. A negative value of divergence at any point will indicate that the crystal lattice at that point is closer to the average orientation than its neighboring points. If the positive values of divergences are continuously increasing as a function of distance, it can be said that the lattice is continuously moving away from an average orientation in that particular direction. Figure 2.14 shows the divergence field for both deformed crystallites investigated. One disadvantage of using the divergence map is that any rotation about the *z*-axis of the difference vector is ignored with only *x* and *y* components of the vector considered. This disadvantage can be overcome by calculating the gradient field in lieu of the divergence of the difference vector.

The gradient of a scalar function *F(x,y,z)* (given by Equation 2.11) is a vector in the direction in which *F* undergoes the greatest rate of increase and whose magnitude is equal to the rate of increase in that direction.

$$gradF = i\frac{\partial Fx}{\partial x} + j\frac{\partial Fy}{\partial y} + k\frac{\partial Fz}{\partial z} \qquad \text{..... (2.11)}$$

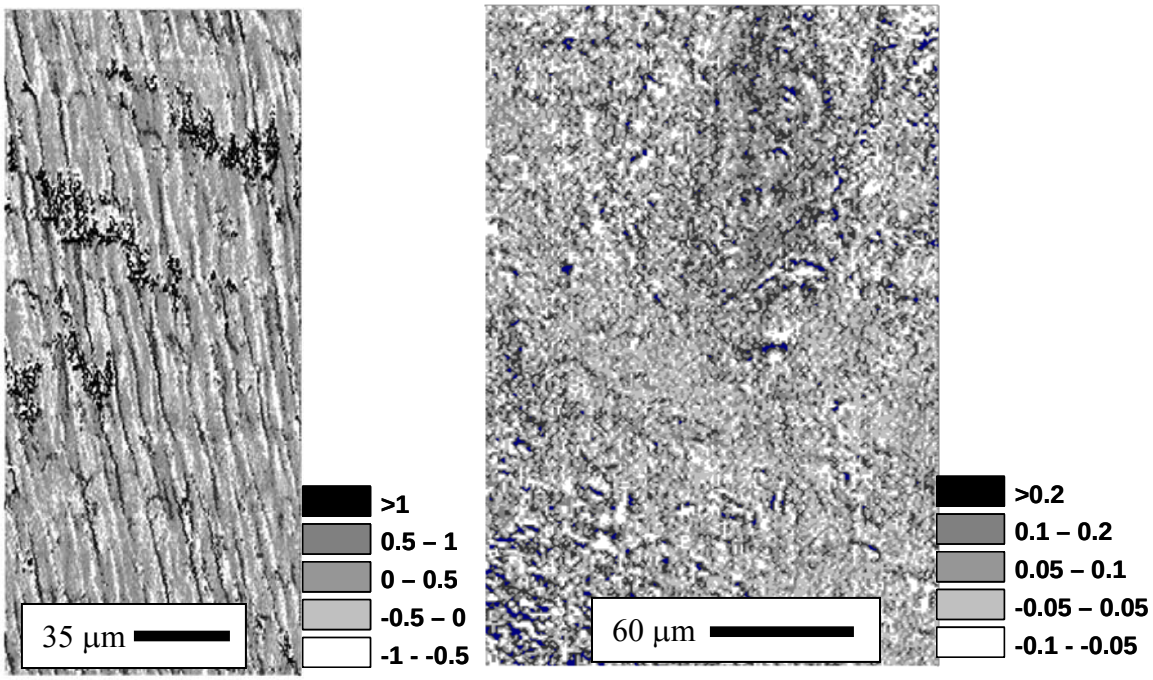

Figure 2.14: Plots containing the distribution of divergence (units are degrees/micron) of orientation difference vector calculated for the crystals shown in Figure 2.5.

The magnitude of the difference vector represents the angle of rotation (in degrees) of the crystal lattice at any point from the average orientation. The gradient of the magnitude of the difference vector yields a vector which points in the direction of greatest change in orientation of the crystal lattice at any given point with respect to the neighboring points. The magnitude of this gradient vector will always be positive and will indicate maximum deviation in orientation at any given point compared to neighboring points. A higher magnitude of the gradient vector at any point suggests that the deviation in orientation from an average orientation at that point is larger as compared to its neighboring points. Figure 2.15 contains orientation gradient maps showing the distribution of the gradient vector magnitudes for both crystallites used in the present investigation.

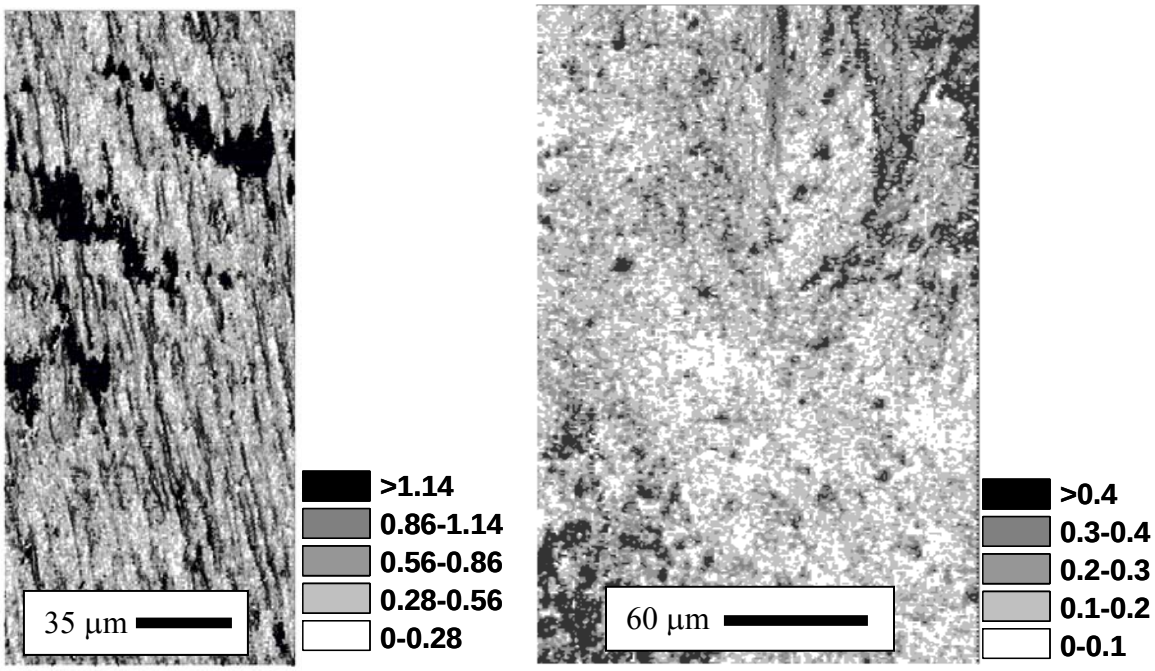

Figure 2.15: Magnitude of the gradient calculated from the magnitude of the difference vectors for both samples.

2.7 Summary

From the lattice curvature measurement it is possible to represent the local orientation gradient observed during deformation by a number of different parameters. In the current chapter an attempt has been made to estimate the density of geometrically necessary dislocations based on lattice curvature information at each point within the scanned region of the sample. Also the spatial information about local orientation gradient is retained using mapping procedures based on scalar measures of geometrically necessary dislocation density, and introduces various mappings based upon the orientation difference vector field. Specific advantages of each of the characterization procedures are discussed in Chapter 5. Since characterization of orientation is done in 2 dimensions, all

the plots presented in the current paper assume that there is zero lattice curvature normal to the plane of observation. Using modern 3-D microstructural analysis it is possible to obtain orientation information on parallel serial sections and a more accurate measure of GND density can be made.

2.8 References

[1]. Taylor, G. I., *Proc. R. Soc. London* 145A, (1934) 362.

[2]. Orowan, E., *Z. Phys*. 89, (1934) 605.

[3]. Polanyi, M., *Z. Phys*., 89, (1934) 660.

[4]. Callister, W. D. Jr., *Materials Science and Engineering: An Introduction* (John Wiley, New York 1999).

[5]. Hull, D., *Introduction to Dislocations*, (Pergamon Press, London, UK, 1965).

[6]. Taylor, G.I., *J. Inst. Met*. 62, (1938), 307.

[7]. Adams, B. L., Wright, S. I., Kunze, K., *Met. Trans*.24A, (1993) 819.

[8]. Wright, S.I., *Electron Backscatter Diffraction in Materials Science*, ed. A.J. Schwartz, M. Kumar, and B.L. Adams (Kluwer Academic/Plenum Publishers, New York 2000).

[9]. Nye, J.F., *Acta Metall.* 1, (1953) 153.

[10]. Ashby, M.F., *Phil. Mag*. 21, (1970) 399.

[11]. Arsenlis, A. and Parks, D.M., *Acta Mat*. 47, (1999) 1597.

[12]. El-Dasher, B.S., Adams, B.L., Rollett, A.D., *Scripta Mat*. 48, (2003) 141.

[13]. Field, D.P., Wright, S.I., Trivedi, P., *Mat. Sci. Forum* 426-432, (2003) 3739.

[14]. Frank, F.C., *Metall. Trans*. 19A, (1991) 403.

CHAPTER – 3

MICROSTRUCTURE EVOLUTION DURING SMALL STRAIN DEFORMATION OF Al ALLOYS

This section focuses upon the small strain regime and compares the measured microstructural evolution of 3003, 5005, and 6022 aluminum alloys during deformation. Room temperature tensile deformation experiments were performed on industrially manufactured specimens of each alloy and the evolving microstructure was compared with the mechanical response. The dislocation structure evolution was characterized using transmission electron microscopy and orientation imaging of deformed specimens. It was observed that structural evolution is a function of lattice orientation and the character of neighboring grains. In general, the dislocation cell size and misorientation angle between dislocation cells evolves systematically with deformation at relatively small strain levels. In addition, the influence of precipitate morphologies on the evolution of dislocation structure was particularly investigated during small strain deformation of 6022 Al alloy. It was found that needle shaped (β") precipitates produce a higher increase in density of geometrically necessary dislocations than overaged (β-Mg_2Si) precipitates.

3.1 Background

To date, interest in thermomechanical processing has been mainly focused on large strain plastic deformation. Recently, however, the small strain behavior has received attention,

because some regions in the hot formed workpiece may undergo very little deformation during certain stages of processing [1]. Such is the case for large section rolling or forging, where localized regions of the sections may receive very little or no deformation in certain passes. Mechanical equations of state are available for aluminum alloys for large strain plasticity but these equations cannot be extrapolated with confidence to small plastic strains [2]. Also constitutive models used in process modeling and optimization of Al are not generically applicable at small strains as the models were typically developed empirically or phenomenologically using data from large strain experiments and may not incorporate phenomena observed at small strains. It is clear that there is a need to understand fully the whole deformation behavior, including transient stress–strain curves, and the microstructural processes taking place at small strains in thermomechanical processing. Also a fundamental understanding of the constitutive response of polycrystalline metals in the small to intermediate strain regime is essential to the development of physically based deformation models that are predictive rather than interpolative in nature.

The secret to the physics of the mechanisms responsible for material response at smaller strains is likely held in understanding dislocation motion and the evolution of dislocation structures. Measures of forest and mobile dislocation densities, subcell size and morphology, cell wall thickness and density, and misorientation angles have all been used as physical measures of the dislocation structure by various modelers [3-6]. Most common among such relationships is

$$\sigma - \sigma_o = \alpha_1 \mu b \rho^{1/2} \qquad \text{..... (3.1)}$$

where $\boldsymbol{\sigma_o}$ is the backstress, α_1 is constant, and $\boldsymbol{\mu}$, $\boldsymbol{b}$, and ρ are the shear modulus, Burger's vector and a measure of dislocation density, respectively. Also commonly referenced is the relationship between stress and dislocation cell size (or mean free path for dislocation motion):

$$\sigma - \sigma_o = \alpha_2 \mu \left(\frac{b}{\lambda} \right)^m \qquad \text{..... (3.2)}$$

where λ is the average dislocation cell size and α_2, and m are constants.

Assuming that dislocation structure evolution controls the constitutive response of a material, it is reasonable to quantify the observed post-mortem dislocation structures as a function of deformation and to use such measures as structural variables in a physically based constitutive model. A previous study examining dislocation structure evolution in the small strain regime for commercially pure Al concluded that grain orientation and neighboring grain interactions play major roles in dictating the character of dislocation structures that develop [7]. Figure 3.1 shows the orientation image of pure Al deformed to 15% strain during channel die compression. It can be easily visualized that grains of certain orientation develop a regular cell structure, while others do not. A proper statistical description of the microstructure is therefore paramount to reliable modeling of microstructural evolution including crystallite lattice rotation and dislocation motion. Direct observations of dislocation structures by transmission electron microscopy (TEM) aid in understanding physical processes, but do not provide a statistically relevant description of the microstructure. This is particularly true when the microstructural statistics must describe neighboring grains, such as in the orientation correlation function [8]. A statistically reliable description of dislocation cell morphology may be obtained

by orientation imaging (OIM) techniques, albeit with no information about individual dislocations [9].

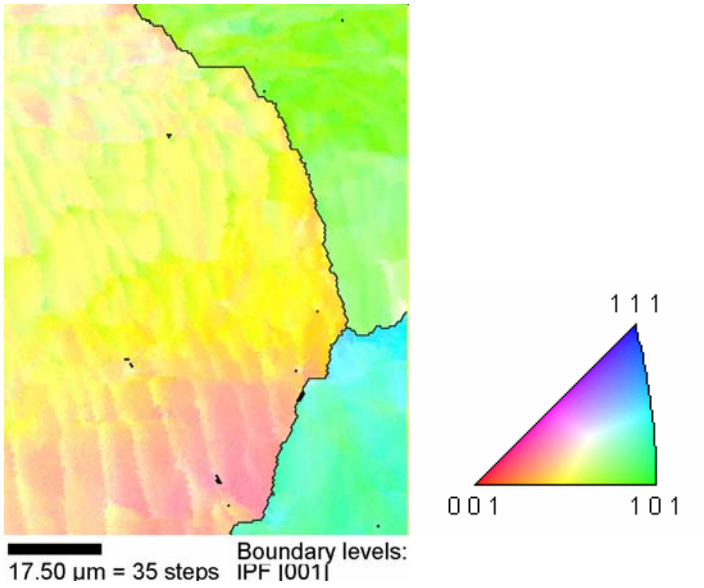

Figure 3.1: Orientation image of pure Al deformed to 15% strain showing regular cell structure for grain of certain orientation. The orientation color key is shown at right.

It is widely known that the addition of solid solution alloying elements such as Mg and Mn to commercially pure Al changes the mechanical properties to increase the strength and alter the ductility. It is also generally accepted that these strength increases with alloying additions can be explained by a textbook solid solution strengthening argument of the added elements creating further obstacles for dislocations. Additional considerations of precipitate morphology must be considered for proper characterization of heat-treatable alloys. Some effort has been made in the past couple of decades to understand alloying effects upon dislocation structure evolution in the moderate to large strain regime relevant to industrial processes such as rolling, extrusion and forging [10-

12]. The present work concentrates upon the strain regime up to about 10 percent strain for specific 3003, 5005, and 6022 Al alloys and focuses upon a comparison of microstructural evolution in the three alloys.

3.2 Experimental Plan

Three commercially available Al alloys were selected for the study; 3003 (nominally, 0.12 Cu, 1.2 Mn), 5005 (0.8 Mg), and 6022 (0.6 Mg, 1.2 Si). The 5005 and 6022 Al alloys were chosen to have similar amounts of Mg with 6022 being roughly the same composition as 5005 with the exception of the additional Si that results in significant β phase (Mg_2Si) precipitation. Each of these was obtained as hot-rolled plate that was fabricated by standard industrial practice prior to deformation. The 6022 Al alloy was naturally aged for a minimum of 3 months prior to deformation, which is believed to have negligible influence on the microstructure of the alloy.

Room temperature tensile tests were performed on standard dog-bone specimens (cross-section 18.75 mm x 6.25 mm) of each of these alloys to final strains of 2% and 10%. Specimens were machined such that the tensile direction of the specimens was aligned with the rolling direction of the original plate. The strengths obtained from the deformation experiments for each alloy are consistent with those found in various aluminum properties data books. Namely, the yield strengths were similar for all three alloys with 5005 exhibiting the highest hardening rate, followed by 6022 and 3003. The specimens were characterized by bright field imaging and selected area diffraction in the

TEM. Orientation imaging was also used to obtain information on the character of the dislocations and cell structures that evolved during deformation.

3.3 Results

As indicated above, this investigation focused upon small strains. In this small strain regime, the overall character of the dislocation substructure did not appreciably evolve, but an increase in dislocation density was observed as well as a reduction in subcell size and an increase in misorientation angle of the subcell structure. To quantify these structures, four general measures of dislocation content were determined; dislocation cell diameter, grain orientation spread, grain average misorientation, and fraction of low angle grain boundaries in the distribution. The cell diameter was estimated by measuring the area of the cells as seen in TEM and orientation images, and reducing the values to a diameter using the assumption of an equiaxed structure. This measurement gives an indication of mean free path for dislocation motion and is reasonable when no significant cell shape anisotropy exists in the structure. During plastic deformation initially uniform grains do not rotate as a unit but subdivide into regions with a range of different orientations. This phenomena leads to the formation of in-grain orientation spread. Studies show that the formation of grain orientation spread is strongly dependent on the initial orientation of the undeformed grain and is less dependent on the character of neighboring grains [13]. The grain boundaries in this study were defined using a criterion of 5 degrees misorientation between neighboring orientation measurements. This allows for a much larger total misorientation between points that lie in the same "grain" but that are not adjacent to one another. Grain orientation spread is a measure

giving the algebraic average of the misorientation angle between all points (whether adjacent or otherwise) within a given grain. Grain average misorientation is a second measure that gives the algebraic average of the misorientation between all points and their nearest neighbor measurement points. While both measures are given by algebraic averages of misorientations within a grain, the grain orientation spread differs from the grain average misorientation in that only nearest neighbor measurements are considered in the grain average misorientation. The grain average misorientation will be low for structures with no geometrically necessary dislocations that accommodate lattice rotation. It will also be low for structures consisting of subcell boundaries with dislocation free subcells. The grain orientation spread, on the other hand, could be very high for a well-recovered structure consisting of subcell boundaries with few forest dislocations. The final measure documented is the number of low angle grain boundaries that develop during deformation. This is indicative of both subcell formation by dislocation activity and forest dislocations, and can be directly measured by looking for misorientations on the order of 1-5 degrees (less than our definition of a grain boundary).

Deformation of a grain is dependent on the current dislocation content, crystal lattice orientation, grain size and shape, second phase particle content, and on the orientations and the topology of neighboring grains. Crystal lattice orientation has a primary influence on the evolution of dislocation sub-structure. Hence in order to study the effect of crystal lattice orientation on the dislocation structure evolution in the present investigation, the data were separated into cube oriented grains {001}(i.e. grains with <001> in the tensile direction), and those with {110} or {111} planes aligned normal to

the tensile direction. These grains were analyzed separately for subcell size, grain orientation spread and other features. The cube grains were the only orientations for which a large enough ensemble of grains was consistently present in the distribution, but general observations can be made for the {110} and {111} grains as well.

3.3.1. Characterization of Starting Material

Initial microstructural characterization of each alloy reveals a partially recrystallized microstructure consisting of a mixture of recrystallized grains and recovered grains. This is evidenced by the existence of grains with significant dislocation cell structure with minimal amounts of forest dislocations and pileups, indicating a well-recovered microstructure. A fully recrystallized structure would have all evidence of dislocation cells removed by the growth of the recrystallization nuclei. Figure 3.2 contains the starting microstructures of AA5005 and AA6022. It can be seen from Figure 3.2.a that some of the grains in AA5005 contain significant dislocation structure as evidenced from the subgrain structure and low angle boundaries within grains. The microstructure of AA6022 shows a higher fraction of recrystallized or well-recovered grains during annealing (Figure 3.2.b). AA3003 is the most well-recovered/recrystallized starting structure, with a slightly smaller amount of initial substructure in comparison to the other alloys investigated. Orientation imaging over several square millimeters of the specimens reveals local inhomogeneity in the crystallite orientation distribution as a general rule with clusters of various texture components. Figure 3.2 shows an example of a local texture gradient in a cross-section image (ST view) of AA5005. It is apparent that grains at the surface of the sheet (top of image) have few cube oriented grains, while the

cube orientation is dominant at the center of sheet, about 3 mm away. Bands of predominantly cube oriented grains are observed throughout the structure.

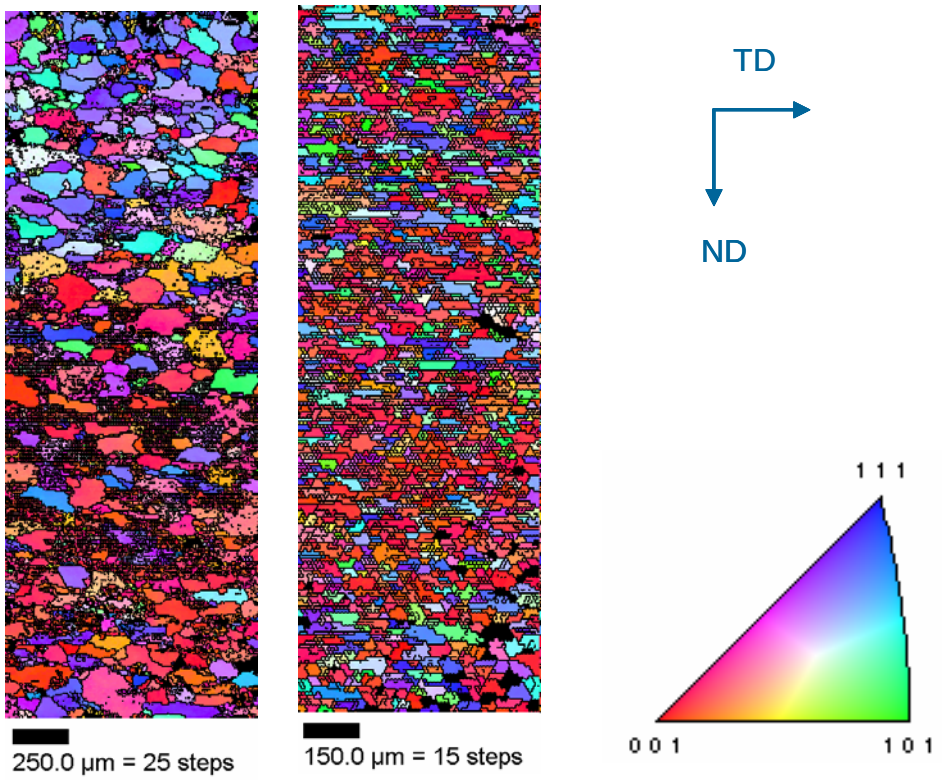

Figure 3.2: (a) Local orientation gradient and partially recrystallized structure in the cross-section of AA5005 over the length of a few millimeters. (b) Orientation image of AA6022 before deformation. The orientation color key shows poles aligned with RD of the sample. Each black line in the images represents a misorientation angle of 1º or higher.

Figure 3.3 contains {111} pole figures showing the starting textures of each alloy. AA3003 consists of a moderate Cube texture with a minor component of Goss texture ({110} <001>). Both of these components are characteristic of recrystallized Al plate.

AA6022 is similar, with the dominant texture being Cube, and having minor components in the distribution along the β fiber, such as Brass ({110} <112>) and S ({123} <412>), characteristic of rolled FCC metal. In contrast, the initial texture of the 5005 Al alloy shows a retained rolling texture with Brass being the major texture component and Cube being a relatively minor component in the distribution.

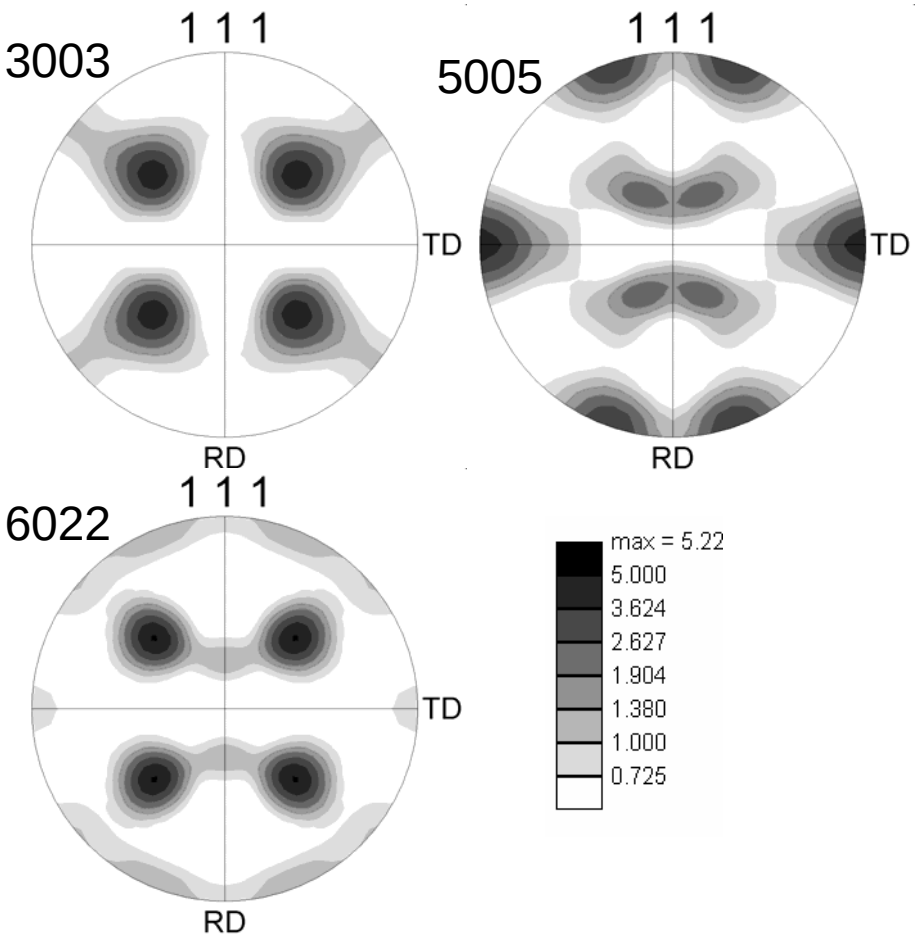

Figure 3.3: {111} pole figures showing crystallographic textures of each alloy.

The average grain sizes as observed from orientation imaging of the plan sections of 6022, 5005 and 3003 alloys were 30 μm, 55 μm and 4 μm respectively. The much

smaller grain size for the 3003 Al alloy can be attributed to the pinning effect of the fine Mn rich precipitates and the differences in industrial processing of the alloys.

3.3.2. Characterization of Deformed AA3003

Figure 3.4 contains TEM bright field images of 3003 Al alloy deformed to strains of 2% and 10%. The images are from a grain having a {110} plane aligned normal to the tensile axis. It is apparent that there is no significant change in the average size and volume fraction of the precipitate particles. It follows that evolution of particle distribution as a function of deformation does not need to be addressed in modeling the room temperature behavior of this alloy at small strains. The average size of the precipitates measured from the TEM bright field images was around 125 nm for samples deformed at 2% and 10%. The precipitates are typically distributed uniformly within the grains and are often observed along the cell boundaries.

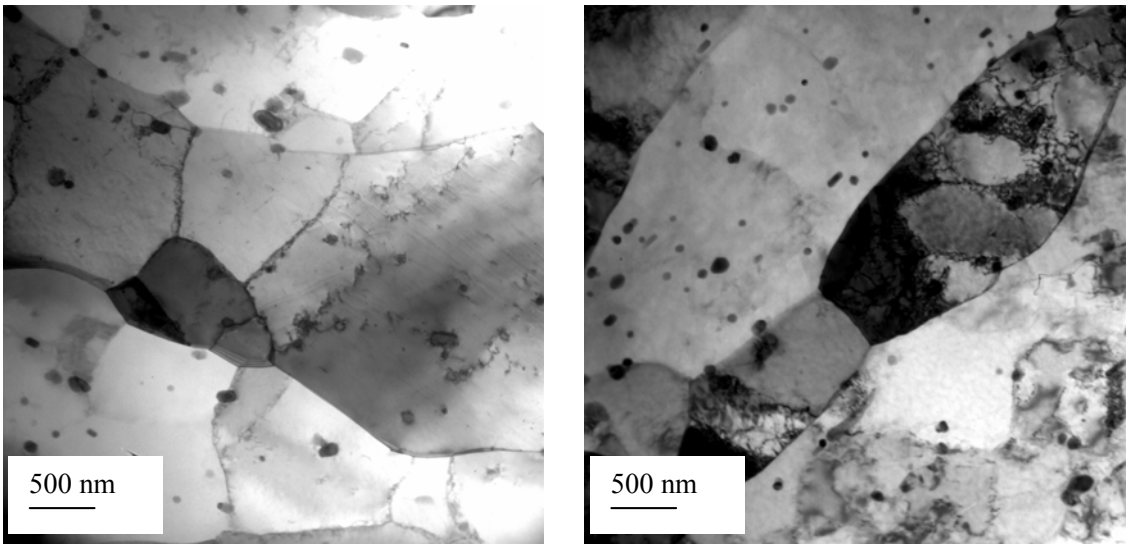

Figure 3.4: TEM bright field images of 3003 Al alloy (a) deformed at 2% (b) deformed at 10% showing no significant change in density of sub-structure after 10% deformation.

Measurement of dislocation substructure using OIM analysis showed that average subcell diameter in AA3003 was 1 μm for 0%, 2% and 10% deformations. The fraction of low angle grain boundaries was 29% for 0% deformed sample, which increased to 46% after 10% deformation. As mentioned previously, the subcell structure in alloy 3003 was the most recovered of the alloys investigated, being generally free from regions of significant dislocation tangles. The dark grain with significant dislocation substructure in Figure 3.4 is an exception. While several such grains exist, they are not as common as those observed in Al alloys 5005 or 6022. The subcell structure evolution to 10% strain was seen in the grain orientation spread evolving a modest amount from 2.1 to 2.2 degrees. The effect was more significant for the cube oriented grains. These grains saw an increase in the grain average misorientation from 1.4 to 1.9 degrees as seen on the plan view sections of specimens with 0 and 10% deformation respectively. The grain average misorientation and grain orientation spread values for all alloys and sections analyzed are given in Table 3.1. Since the grain average misorientation is step size dependent and the grain sizes vary so dramatically among these alloys, this value does not represent the substructure well and is reported here only for completeness.

The average grain size decreased from 4 to 3.5 μm during deformation to 10 percent. This is likely a result of dislocation structure forming to create subcells of 5 degrees misorientation within the original grains, thereby reducing the grain size as determined by orientation imaging. A similar reduction was observed in the other alloys discussed in this study.

Table 3.1: Change in average grain orientation spread, grain average misorientation and fraction of low angle grain boundaries with deformation for 5005, 6022 and 3003 Al alloys calculated using OIM analysis.

Property	View	Deformation	AA5005		AA6022		AA3003	
			All Data	Cube Grains	All Data	Cube Grains	All Data	Cube Grains
Avg. Grain Orientation Spread (degrees)	Cross section	0%	2.4	2.4	1.4	1.0	2.1	1.3
		10%	2.7	2.8	1.9	2.4	1.7	1.1
	Plan view	0%	2.2	N/A	1.4	1.2	2.1	1.4
		10%	2.4	N/A	2.9	2.5	2.2	1.9
Grain Avg. Misorientation (degrees)	Cross section	0%	1.7	0.8	1.1	0.57	1.4	1.0
		10%	1.4	1.0	1.24	1.55	1.3	1.0
	Plan view	0%	1.6	N/A	1.0	0.7	1.4	1.1
		10%	1.5	N/A	1.8	1.3	1.7	1.7
Fraction of low angle boundaries	Plan view	0%	0.69		0.53		0.47	
		2%	0.77		0.51		0.38	
		10%	0.85		0.60		0.68	

3.3.3. Characterization of Deformed AA5005

Figure 3.5 contains TEM bright field images of AA5005 deformed at 2% and 10%. The images are from a grain having a {110} plane aligned normal to the tensile axis for 2% deformed sample and {100} plane aligned normal to tensile axis for 10% deformed

sample. TEM analysis indicates that the alloy is almost precipitate free, suggesting that the Mg is primarily in solid solution, as expected for this alloy. A substantial increase in the density of dislocation sub-structure is seen in the TEM images after 10% deformation. These dislocation structures form loosely defined cells with a substantially reduced mean free path for dislocation motion.

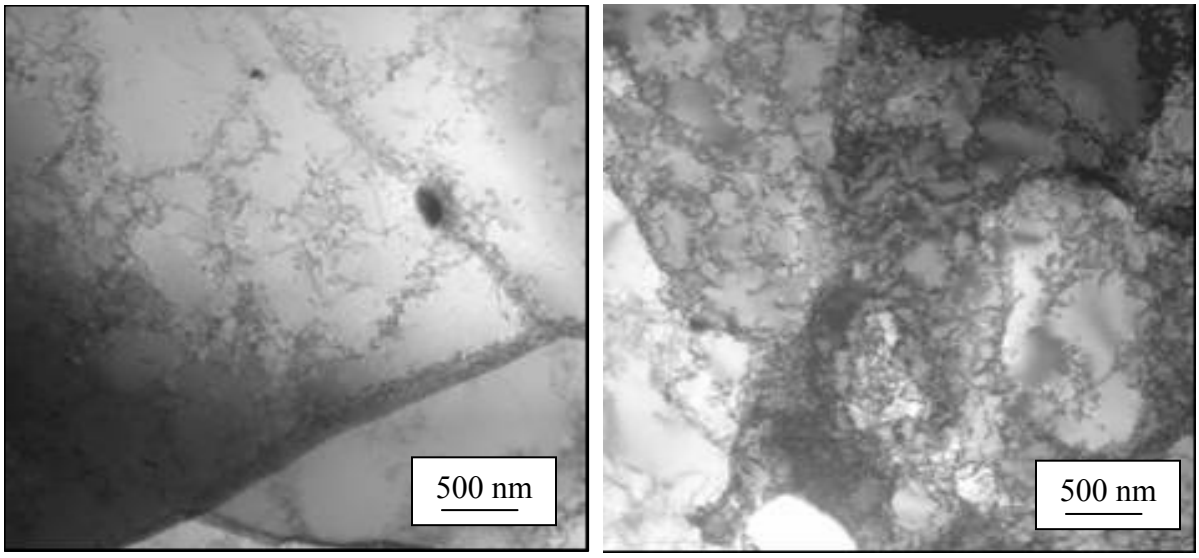

Figure 3.5: TEM bright field images of 5005 Al alloy (a) deformed at 2% (b) deformed at 10% showing increase in density of substructure after 10% deformation.

The average subcell diameter measured using OIM in alloy 5005 was 1.6 μm for 0%, 2% and 10% deformation. OIM analysis indicate that the average grain orientation spread evolves from 2.4-2.7 degrees through 10% tensile deformation as observed on the cross sections and from 2.2-2.4 as observed on the plan view sections. The cube grains followed the same general trend with an insufficient number being present in the distribution to report for the plan view sections. This structure varies markedly from that shown in Figure 3.4 for the 3003 alloy.

3.3.4. Characterization of Deformed AA 6022

Figure 3.6 shows TEM bright field images for 6022 Al alloy deformed to 2% and 10% strain. These images show the apparent uniform distribution of coarse precipitate particles both at the cell boundaries as well as within the cells. The precipitate particles are almost equiaxed with an average size of 0.37 μm measured manually using TEM image. Analysis of the 10% deformed sample of AA6022 showed a greater volume fraction of precipitate particles in the cross-section of the sample than in the plan section.

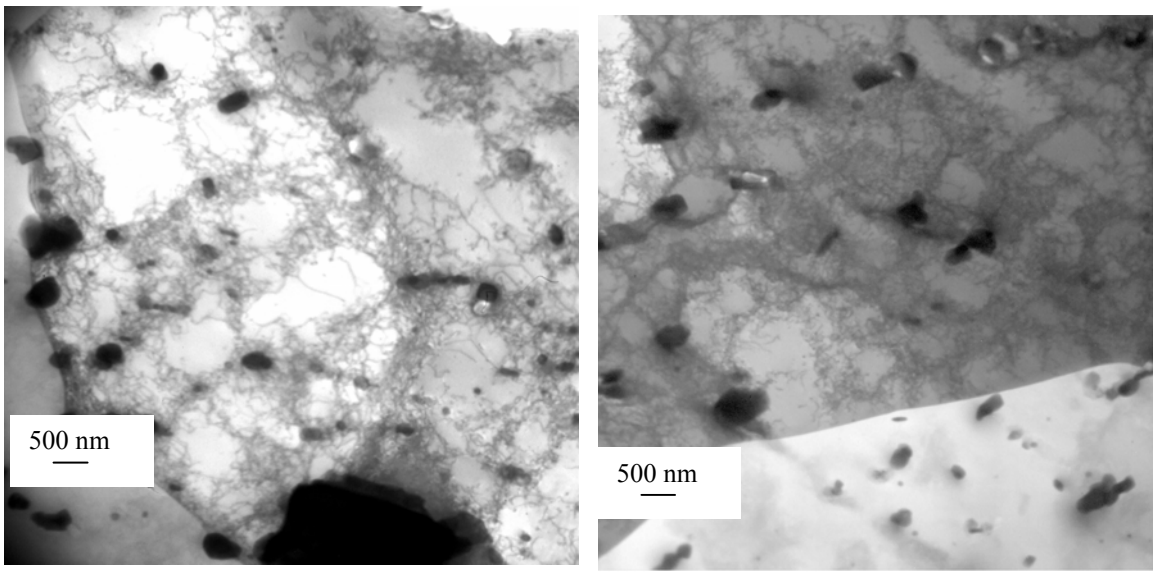

Figure 3.6: TEM bright field image of {110} grains in 6022 Al alloy deformed to (a) 2% strain, and (b) 10% strain, showing uniform distribution of precipitate particles.

In the plan view of orientation image of AA6022, almost all grains possessed significant dislocation sub-structure after 10% deformation. The density of substructure at 0% and 2% strain remained almost the same as indicated by the measures documented. Grains of {111} and {110} orientation were nearly substructure free subsequent to deformation, both in the cross-section and the plan view section of the samples. The average subcell

diameter measured using OIM in alloy 6022 was 2 μm for 0%, 2% and 10% deformation. The fraction of low angle grain boundaries was 24% for 0% deformed sample and it increased to 46% after 10% deformation. The average grain orientation spread increased substantially after 10% deformation from 1.4-2.9 degrees as seen in the plan view section. Cube grains evolved in concert with those measured in the overall distribution (1.2-2.5 degrees).

3.4 Discussion

Table 3.1 indicates the change in grain orientation spread as a function of deformation and alloy compositions. Grain orientation spread increased with deformation for the 6022 and 5005 Al alloys, but showed minimal evolution for AA3003. As the material deforms plastically the dislocations generated during deformation produce cell boundaries of high misorientation or the grains develop long range orientation gradients. Either case may increase the orientation spread within a grain. The more rapid sub-structure evolution for the 6022 Al alloy, evidenced by the greatest increase in grain orientation spread, is a function of the efficiency of the precipitates in generating and pinning dislocations. Differing grain sizes did not adversely influence the results according to our data, and initial dislocation content can be dismissed as a significant biasing factor because the recrystallized cube oriented grains from each alloy followed the same overall trend.

A large increase in the density of dislocation sub-structure was observed both in the cross-sections and the plan view sections for 10% deformed samples of 5005, 6022 and 3003 Al alloys. Figure 3.7 contains the orientation images indicating the change in the

density of dislocation sub-structure in the plan section for 0% and 10% deformed samples of 5005, 6022 and 3003 alloys. These images are created by drawing lines where the misorientation angle between neighboring measurements is greater than 1 degree.

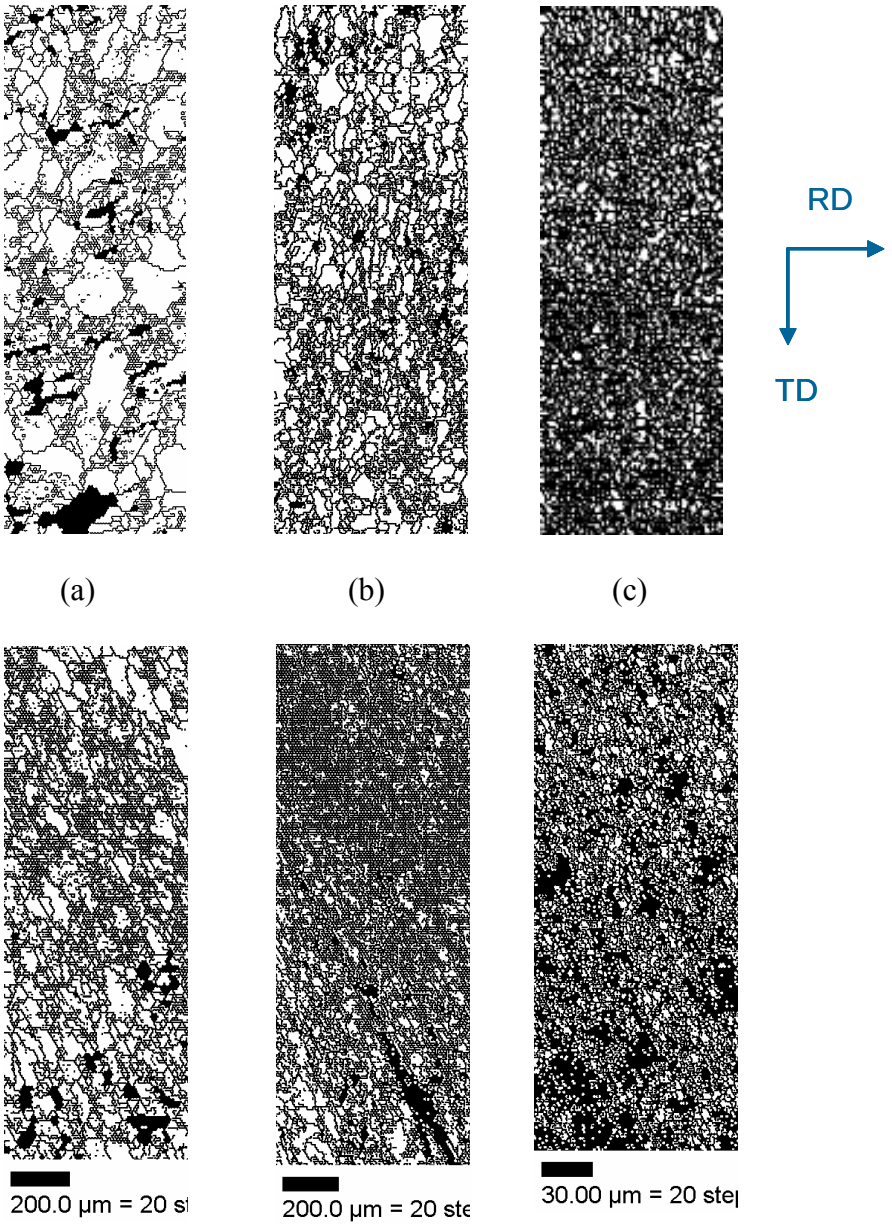

Figure 3.7: OIM images showing change in the density of substructure from 0 (top row) to 10 percent (bottom row) tensile strain in plan view of (a) 5005, (b) 6022 (c) 3003 Al alloys (scale bars are consistent for each alloy). Tensile axis is parallel to RD of sample.

The density of dislocation sub-structure was similar for 0% and 2% deformed samples (see Table 3.1 that gives the fraction of low angle grain boundaries). The increase in density of dislocation sub-structure was more in AA6022 than in 5005 and 3003 Al alloys which is in accordance with the results obtained for grain orientation spread and grain average misorientation in the respective alloys (Table 3.1). The 6022 Al alloy contained a higher concentration of Mg, which is believed to have greater influence on the substructure evolution with deformation.

It can be seen from Table 3.1 that the fraction of low angle grain boundaries increased with deformation for all three alloys investigated. Alloys 5005 and 3003 showed a large increase in number fraction of low angle grain boundaries after 10% deformation. This is believed to be due to the effectiveness of solute atoms in pinning dislocations in AA5005 and due to the presence of fine precipitates in AA3003. A relatively small change in the fraction of low angle grain boundaries after 10% deformation for 6022 Al alloy could be due to the presence of much coarser particles than that observed in 3003 Al alloy. However the statistical reliability of the measurement of low angle grain boundaries obtained using OIM analysis is a function of the area of the sample examined in relation to the grain size. As discussed previously there exists significant inhomogeneity in the texture and microstructure of the alloys. Since grains with cube orientation consistently possessed the highest density of dislocation substructure the presence of such grains in the analysis regions would result in a higher number of low angle grain boundaries. The cube orientation in FCC metals has a strong tendency to undergo orientation subdivision both in polycrystals as well as in single crystals [13-15]. The fraction of low angle grain

boundaries is also dependent upon the sample surface preparation and step size used for OIM measurements. All these factors contribute to statistical uncertainty in the values of the fraction of low angle grain boundaries reported in Table 3.1. In order to study the effect of grain size on the grain orientation spread and grain average misorientation values, the data were partitioned for various grain sizes. It was observed for all alloys that grain orientation spread and grain average misorientation values did not have significant dependence on grain size. This differs from the result of Delannay et al. [16], who showed that for large deformations there was a systematic increase in misorientation within a crystallite as grain size increased.

3.4.1 Effect of Grain Orientation

Figure 3.8 shows inhomogeneous distribution of dislocation structures among grains of different orientation of 5005 Al alloy before and after deformation. Inhomogeneous distribution of dislocation structure can be visualized from grain orientation spread map and geometrically necessary dislocation density map. Black regions in the GOS map are the regions of least substructure while white regions correspond to highest degree of substructure within a grain. Substructure evolution with deformation for grains with {100}, {111} and {110} orientations was studied for all the 3 alloys. In alloy 5005 for 0%, 2% and 10% deformed samples, grains with {111} orientation were found to be almost free from dislocation sub-structure, whereas grains with cube (100) orientations had the highest density of sub-structure. It can also be seen from Table 3.1 that the grains with cube orientation suffered the highest increase in orientation spread. Similar results were also obtained using TEM analysis, in which {111} grains were found to be free

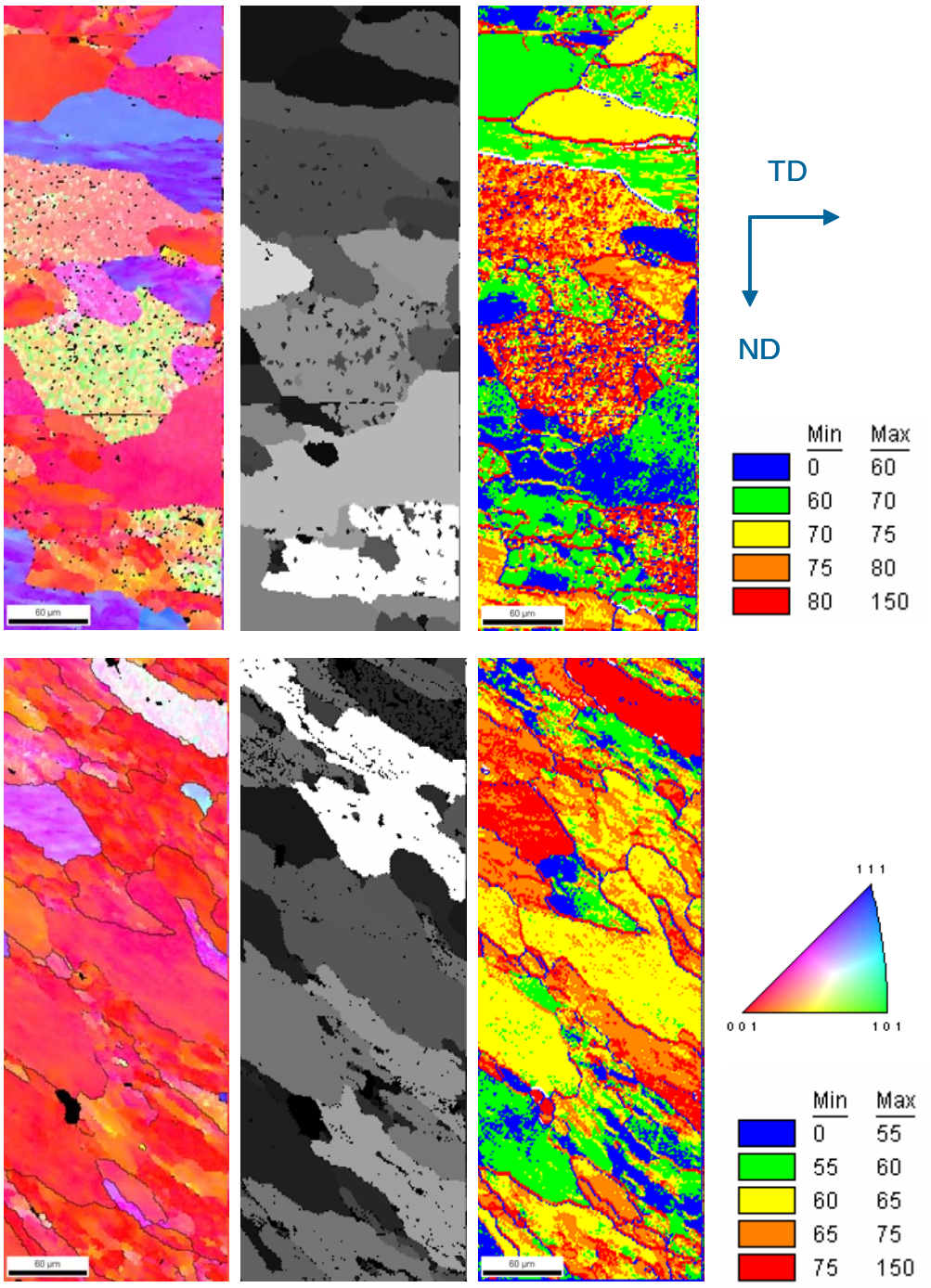

Figure 3.8: (a) OIM images of undeformed (top) and deformed (bottom) 5005 Al alloy showing inhomogeneous distribution of dislocation structures among grains of different orientation through (b) GOS map and (c) GND density distribution ($x10^{14}/m^2$)map. The orientation color key at the right indicates poles aligned with RD of the sample.

from dislocation sub-structure. The average sub-cell size was about 2 μm for 0%, 2% and 10% deformed samples, which is in agreement with the TEM analysis. The average aspect ratio of subgrains was close to 1 indicating the equiaxed morphology of cells, which can also be seen from the TEM micrographs (Figure 3.5).

Figure 3.9(a) contains an orientation image of AA5005 after partial recrystallization. A point to point and point to origin misorientation profile was plotted for grains having {111} and cube orientation. The grain with cube orientation (Figure 3.10(a)) had misorientations of up to 3.5^{o} where as the grain with {111} orientation (Figure 3.10(b)) had misorientations of only 1.5^{o}. Even though there was no significant substructure observed in either grain, it can be seen from the plot in Figure 3.9 that the grain with cube orientation had generally higher misorientation angles indicating higher dislocation content. Figure 3.9(b) is the OIM image of 5005 alloy deformed to 10%. An inhomogeneous distribution of dislocation substructure was observed among grains with cube orientation in 5005 deformed samples, since there were some cube oriented grains with dense dislocation sub-structure whereas others were substructure free (Figure 3.9(b)).

A similar misorientation profile was generated (Figure 3.11) for the cube grain having significant dislocation substructure. The higher misorientation angles of the cube grain after 10% deformation is due to the formation of cell boundaries as seen by peaks in the point to point misorientation trace. The point to origin misorientation was as high as 13º and point misorientation reached 10º. Dillamore and Katoh [14] demonstrated that near-

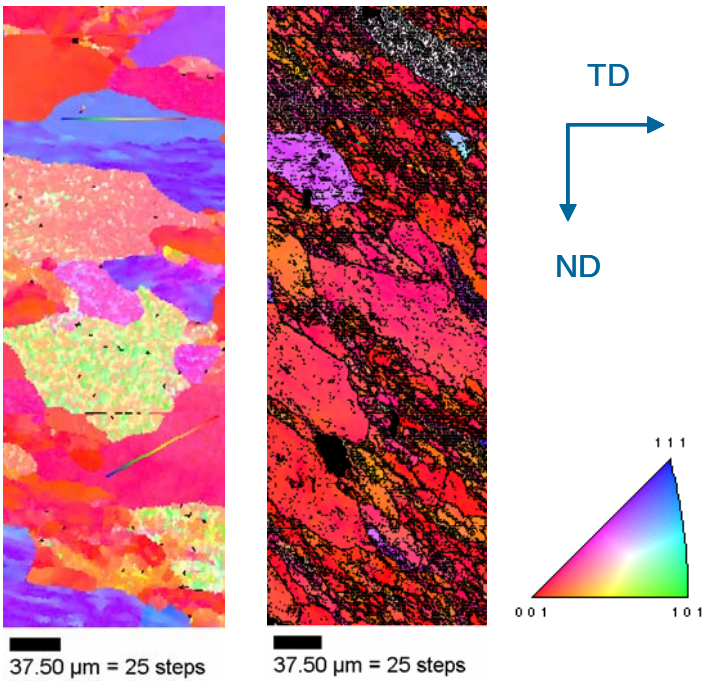

Figure 3.9: OIM images of 5005 Al alloy (a) deformed at 0% showing no significant sub-structure (b) deformed at 10% showing inhomogeneous distribution of dislocation sub-structure among grains with cube orientation (substructure as identified by boundaries drawn at misorientation angles of 1 degree or greater).

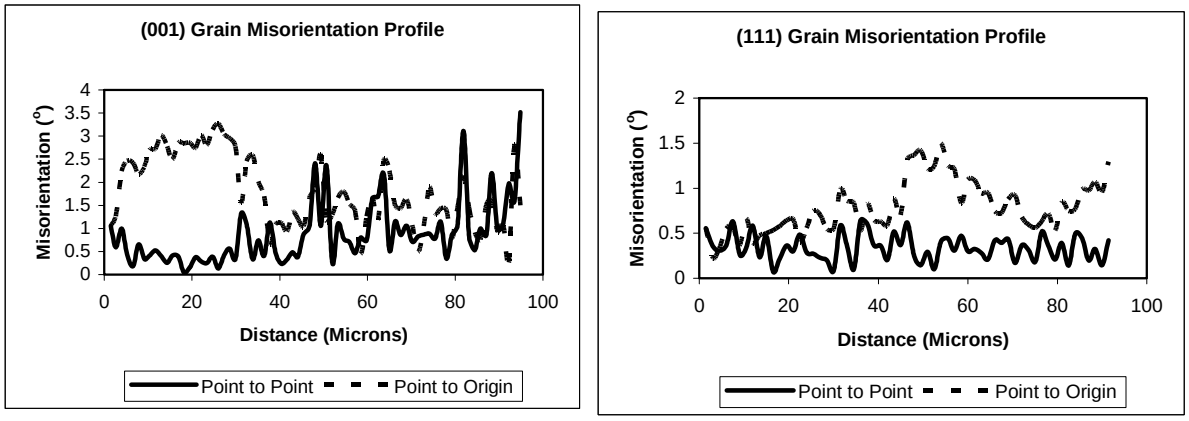

Figure 3.10: Point to Point and Point to Origin misorientation profile for 5005 Al alloy deformed to 0% (a) Grain with Cube orientation (b) Grain with {111} Orientation. The misorientation chart was drawn from the lines shown in Figure 3.9 (a).

cube orientations form substantial lattice curvatures during rolling because they lie in a "divergent" region of Euler space. Several regions of the grain rotate towards distinct stable texture components, but the grain centre maintains the cube orientation throughout deformation.

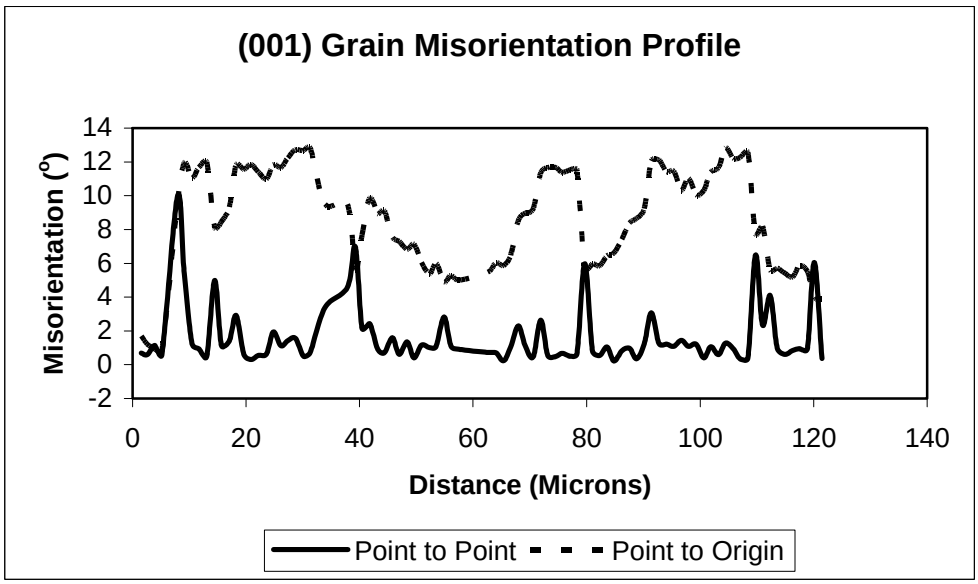

Figure 3.11: Point to Point and Point to Origin misorientation profile for 5005 Al alloy deformed to 10% for a grain with Cube orientation.

The existence of a higher dislocation content in {100} grains and the heterogeneous distribution of substructure in grains of similar orientation can also be explained by a simple discussion based upon the well-known Taylor factor [17]. The Taylor factor, *M*, gives an indication of resistance to deformation as a function of lattice orientation. This can be derived from the principle of virtual work as:

$$M = \frac{\sum \gamma_i}{\varepsilon} = \frac{\sigma}{\tau_{crss}} \quad \text{..... (3.3)}$$

where γ_i is the amount of slip on slip system i (assuming 5 simultaneously active slip systems), and τ_{crss} is the critical resolved shear stress (assumed constant for all slip systems). A larger Taylor factor indicates that a greater amount of local slip is required for unit strain, and a higher value of tensile stress is required to achieve the critical resolved shear stress on the simultaneously operating slip systems. Therefore a grain with a high Taylor factor can be considered a geometrically "hard" grain and those with relatively lower Taylor factors are "soft" grains. For crystallite lattice directions aligned with the tensile axis, the following Taylor factors are obtained: (<100> – 2.45, <110> – 3.11, <111> – 3.67).

In general, the cube oriented grains are those in which the dislocation substructure is most rapidly evolving. These orientations have one of the lowest Taylor factors and will be the first to deform. It is likely that for these materials, the majority of the deformation can be accounted for by structure evolution within the {100} oriented grains. The {111} grains, on the other hand, possess less substructure after 10% strain, and likely had little dislocation activity during deformation because of their inherent geometric resistance to deformation. This type of analysis also explains why one observes such a large scatter in the data.

In order to predict the deformation behavior of polycrystals, the statistical distribution of crystallite lattice orientation in the materials should be included in Equations (3.1) and (3.2). No attempt has been made to include such description in the current analysis, however a general form of the equations can be written as follows:

$$\sigma - \sigma_o = \alpha_1(\dot{\varepsilon},T)\mu(T)b\left[\frac{1}{8\pi^2}\oint_{g\in SO(3)} f(g)\,\rho_t(g)dg\right]^{1/2} \quad \text{..... (3.4)}$$

$$\sigma - \sigma_o = \alpha_2(\dot{\varepsilon},T)\mu(T)b^m\left[\frac{1}{8\pi^2}\oint_{g\in SO(3)}\left(\frac{f(g)}{\lambda(g)}\right)dg\right]^m \quad \text{..... (3.5)}$$

f(g) is the normalized crystallite orientation distribution function (ODF) which serves as a weighting factor for the integration of $\rho(g)$ and $\lambda(g)$, respectively the dislocation density and cell size (or mean free path for dislocation motion) as functions of orientation, $\boldsymbol{g}$. The integrations are performed over the special orthogonal group of three dimensional rotations, *SO*(3), and normalized by the factor immediately preceding the integral. α_1 and α_2 are assumed to be functions of strain rate and temperature. Orientation dependence of $\boldsymbol{\mu}$ is neglected, as it does not appreciably affect the result for aluminum alloys.

3.4.2 Effect of Neighboring Grains

An inhomogeneous distribution of dislocation sub-structure among grains of cube orientation could be due to the effect of neighboring grains. When clusters of {100} grains exist, these are readily deformed. On the other hand, if a {100} grain is surrounded by "hard" grains, they will shield the softer grain from deformation. This is shown schematically in Figure 3.12 where the light colored grains represent soft grains in an ideal structure and gray indicates geometrically hard crystallites. At "A" there is little chance for the soft grain to deform since it is shielded by the harder grains, while at "B" the cluster of hard grains will resist deformation, causing the surrounding matrix to absorb the majority of the dislocation activity.

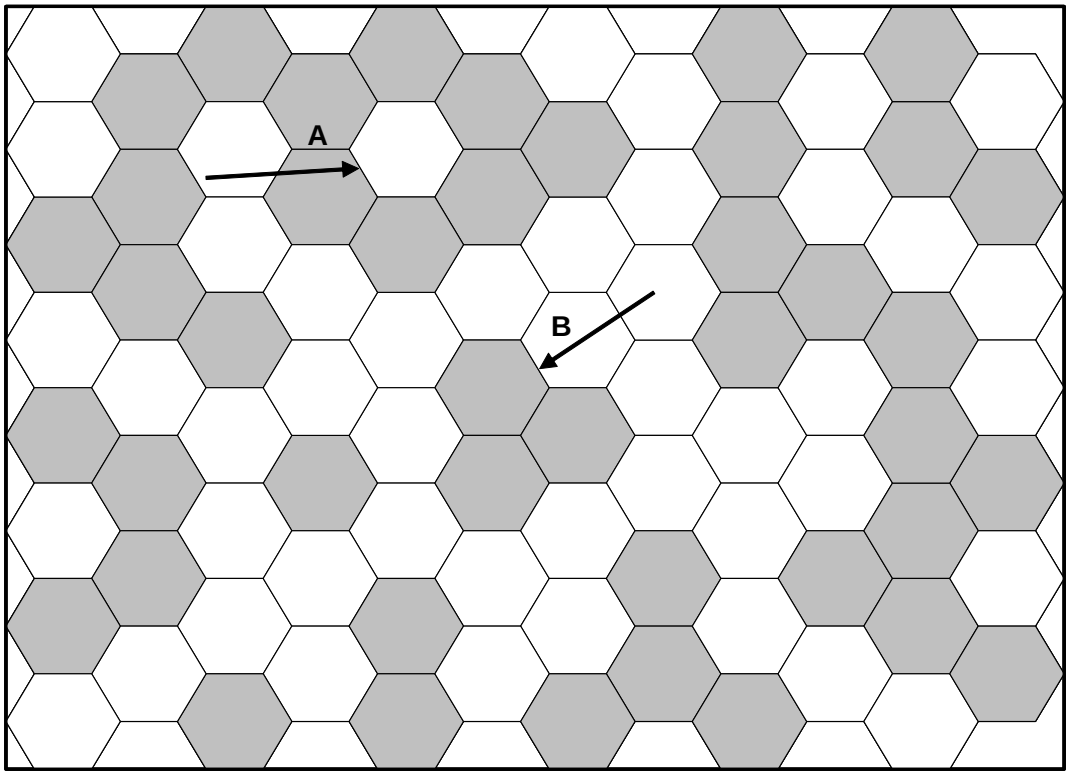

Figure 3.12: A schematic showing effect of orientation of neighboring grains on the deformation behavior of a given grain. Light colored grains are low Taylor factor "soft" and gray grains are geometrically "hard" grains.

In order to quantify the effect of neighboring orientations on the evolution of dislocation structures in a polycrystal, investigations using single crystals should be performed using identical deformation. Statistical analysis can then be performed to determine whether the scatter in the data is much greater in polycrystalline materials than for single crystal deformations. Assuming non-local effects are important, Equations (3.4) and (3.5) can be modified to include higher order statistics:

$$\sigma - \sigma_o = \alpha_1(\dot{\varepsilon},T)\mu(T)b\left[\iiint_{g,\vec{r},g'} h\left(g(p),g'(p'),\vec{r}\right)\rho_t\left(g(p),g'(p'),\vec{r}\right)dgd\vec{r}dg'\right]^{1/2} \quad \ldots\ldots (3.6)$$

$$\sigma - \sigma_o = \alpha_2(\dot{\varepsilon},T)\mu(T)b^m\left[\iiint_{g,\vec{r},g'}\left(\frac{h(g(p),g'(p'),\vec{r})}{\lambda(g(p),g'(p'),\vec{r})}\right)dgd\vec{r}dg'\right]^m \quad \ldots\ldots\ldots\ldots (3.7)$$

where vector $\vec{r} = (p - p')$ and $h(g(p),g'(p'),\vec{r})$ is the 2-point probability density function that gives probability density that two measuring points *p* and *p'* are separated by the vector ***r*** and the orientations in these points are ***g***, ***g'*** respectively.

3.5 Influence of Precipitate Morphology

The overall slip and fracture behavior of age-hardenable Al alloys depend greatly on the microstructure and in particular the deformation characteristics of the strengthening precipitates in the alloy [18]. There are two ways a particle can interact with dislocation and provide strengthening. Large incoherent particles can create dislocations to form loop around them while small coherent particles can be sheared by dislocations. Shearable, coherent, and ordered precipitates promote planar slip whereas non-shearable, incoherent, and bypassed precipitates encourage wavy glide [19]. Planar slip is considered inhomogeneous plastic deformation that is concentrated on few slip systems as a result of the local work softening on the operative slip plane. This work softening is due to the reduced cross-section of the sheared precipitates, which decreases the strengthening effectiveness on that specific slip plane. Planar slip continues until an obstacle such as a high-angle grain boundary inhibits further dislocation movement and activates adjacent slip systems to accommodate the applied stress. Wavy glide is considered homogeneous deformation that operates on many slip systems simultaneously. Below is the study performed to investigate the influence of precipitate morphologies on dislocation structure evolution:

3.5.1 Experimental Plan

Hot rolled plate of precipitation hardenable AA6022 (Al-0.55%Mg-1.1%wt Si) was solutionized at 550ºC for 3 hours and then quenched in water. The specimens were aged at 175ºC in salt bath furnace for 500 mins and 5500 mins to produce materials with different precipitate morphologies. Characterization of precipitates was done using TEM prior to deformation. EBSD analysis on the aged samples showed the presence of very large grains (~2mm diameter) of <110> orientation in the microstructure. It is assumed that the deformation behavior of these grains is dominant over the deformation behavior of small grains and thus these large grains were subjected to EBSD analysis. The other existing orientations in the EBSD scan were excluded from the data. After ageing, specimens were deformed to 10% at room temperature using channel die compression. Microstructure evolution was investigated in the large grains of <110> orientation in the deformed samples using EBSD with a step size of 3 microns.

3.5.2 Results & Discussion

Figure 3.13 shows the bright field TEM images of specimens aged for 500min and 5500min. The ageing kinetics and precipitation sequence of this alloy has been investigated and the results show that the precipitates in Figure 3.13a and b are β″ and β+Si+Q respectively [20]. The β″ precipitates are needle shaped and are aligned in $<100>_{Al}$ direction of matrix. Si precipitates with various morphologies are seen with β-Mg_2Si platelets and Q lath shaped precipitates in Figure 3.13b.

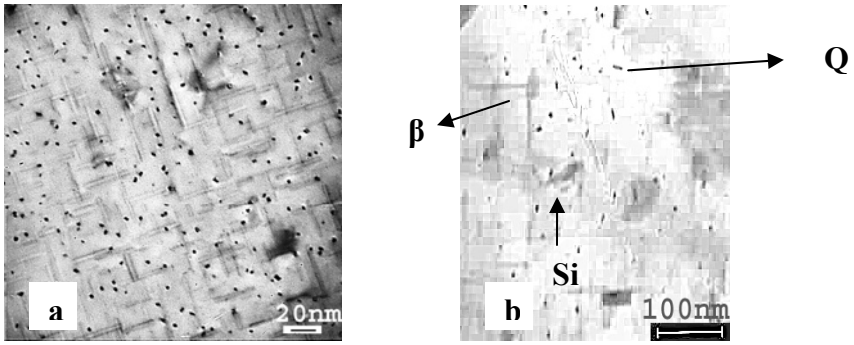

Figure 3.13: TEM micrographs showing different precipitates in AA6022 samples aged at 175ºC for (a) 500min and (b) 5500min.

Large grains of (110) orientations observed in both the samples was used to quantify GND density before and after deformation. Figure 3.14 shows the distribution of GND density measured for the grains of (110) orientation for both the aged samples after 10% deformation. Initial GND density in both the samples was approximately same, however after deformation it was observed that the total GND density in the sample aged up to the peak of hardness (~500min) is 25% higher than the overaged (~5500min) sample. The reason can be explained by the fact that the needle shaped precipitates are the strongest barrier to the motion of dislocations and therefore more dislocations are expected to pile up around these precipitates. Thus the lattice rotation associated with these precipitates would be higher. In contrast, the overaged precipitates are large and the space between them is wide, therefore the dislocations can overcome them more easily and the lattice rotation would be less for this type of structure.

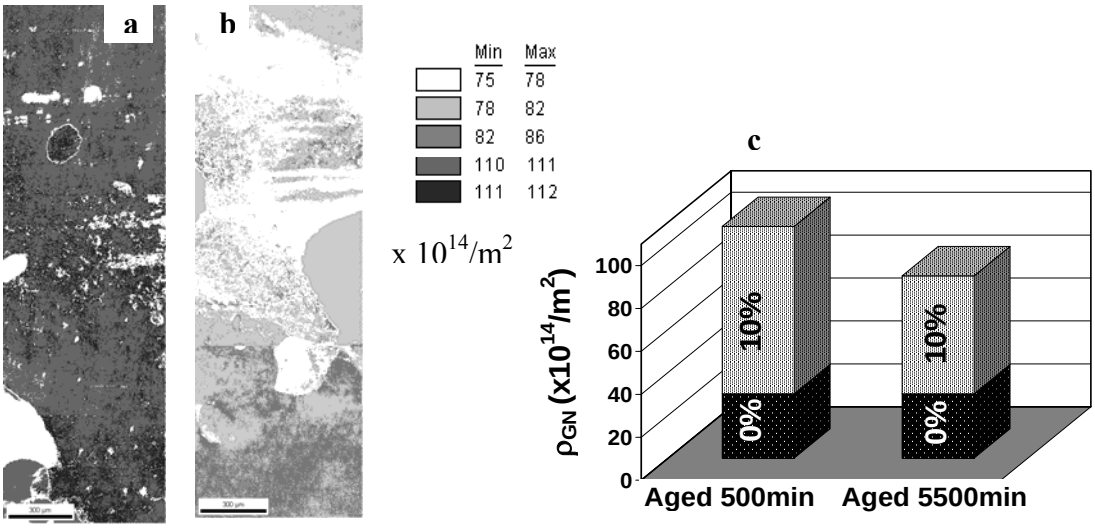

Figure 3.14: GND density distribution plot for the samples aged for (a) 500min (b) 5500min and then deformed 10% (c) plot showing difference in GND density evolution after 10% deformation of samples aged for different times.

3.6 Conclusions

In general, orientation imaging analysis of the deformed samples showed an increase in the density of dislocation substructure and fraction of low angle grain boundaries with deformation for the 3 alloys studied in the present investigation. AA6022 showed highest increase in grain orientation spread and grain average misorientation during deformation. Mn in alloy 3003 significantly increased the fraction of low angle grain boundaries with deformation but maintained a similar value of grain orientation spread. Mg remained in solid solution in alloy 5005 and had an intermediate effect in increasing the fraction of low angle grain boundaries, grain average misorientation and grain orientation spread compared with alloys 6022 and 3003. It was also observed that the grains with near {111} orientation were primarily substructure free, whereas grains with cube orientation developed significant dislocation substructure in all alloys at each deformation level

investigated. An inhomogeneous distribution of dislocation substructure observed among grains with cube orientation is attributed to the effect of neighboring grains. A separate study on the influence of precipitate morphologies on GND density evolution showed that strong coherent particles cause a more dramatic in GND density with deformation than overaged incoherent particles.

3.7 References

[1]. Carmona, R., Zhu, Q., Sellars, C.M., Benyon, J.H., in *Proceedings of 21st Risø Intl. Symp. on Matls. Sci.,* Roskilde, (ed. N. Hansen, et al. Denmark), (2000) 283.

[2]. Shi, H., McLaren, A.J., Sellars, C.M., Shahani, R., Bolingbroke, R., *Mater. Sci. Technol*. 13, (1997) 210.

[3]. Mecking, H. and Kocks, U.F., *Acta Metall*. 29, (1981) 1865.

[4]. Barlat, F., Glazov, M.V., Brem, J.C., Lege, D.J., *Int. J. Plasticity* 18, (2002) 919.

[5]. Raj, S.V. and Pharr, G.M., *Mat. Sci. Eng*. 81, (1986) 217.

[6]. Horstemeyer, H.F., Baskes, M.I., Godfrey, A., Hughes, D.A., *Int. J. Plasticity* 18, (2002) 203.

[7]. Field, D.P. and Weiland, H., *Mat. Sci. Forum* 157-162, (1994) 1181.

[8]. Adams, B.L., Morris, P.R., Wang, T.T., Willden, K.S., Wright, S.I., *Acta Mat*. 35, (1987) 2935.

[9]. Field, D.P., Weiland, H., Baggethun, P., in *The Integration of Material, Process and Product Design*, (eds. Zabaras, N., Becker, R., Lalli, L., Ghosh, S. A.A. Balkema, Rotterdam, Brookfield, VT), (1999) 27.

[10]. Hughes, D.A., *Acta Mat.* 41, (1993) 1421.

[11]. Bay, B., Hansen, N., Duhlmann-Wilsdorf, D., *Mat. Sci. Eng*. A113, (1989) 385.

[12]. Garmestani, H., Kalidindi, S. R. Williams, L., Bacaltchuk, C. M., Fountain, C., Lee, E. W., Es-Said, O. S., *Int. J. Plasticity* 18, (2002) 1373.

[13]. Raabe, D., Zhao, Z., Mao, W., *Acta Mat*. 50 (2002), 4379.

[14]. Dillamore, I. L. and Katoh, H., *Met. Sci*. 8, (1974) 73.

[15]. Akef, A. and Driver, J. H., *Mat. Sci. Engg* A132, (1991) 245.

[16]. Delannay, L., Mishin, O.V., Juul Jensen, D., Van Houtte, P., *Acta Mat*. 49, (2001) 2441.

[17]. Taylor, G. I., *J. Inst. Metals* 61, (1938) 307.

[18]. Martin, J.W., *Micromechanisms in Particle-hardened Alloys*. Cambridge University Press, Cambridge (1979).

[19]. Hornbogen, E., *Z. Metallk* 66, (1975) 511.

[20]. Yassar, R. S., Field, D.P., Weiland, H., *Mater. Sci. Eng*. In press, (2005).

CHAPTER – 4

MICROSTRUCTURE EVOLUTION AND OBSERVED STRESS RESPONSE DURING HOT DEFORMATION OF 5005 & 6022 Al ALLOYS

The mechanical response of material is strongly dependent on the details of the starting microstructure. The objective of this chapter is to experimentally and statistically analyze the effect of physically measurable features of the starting microstructure on the yield stress of 6022 Al alloy. In this study, two commercially used AA5005 and AA6022 Al alloys were deformed at various combinations of processing parameters (such as strain, strain rate and temperature) to produce samples with a variety of microstructures. Quantitative parameters obtained from microstructural characterization and stress analysis were performed by a multiple regression analysis technique to determine the relative influence of various microstructural parameters on the observed stress response. The geometrically necessary dislocation (GND) density was determined to be the most important measured parameter affecting the yield stress. Experimental and statistical analysis showed a linear relationship between yield stress and square root of GND density. A statistical formulation was used to develop the yield strength model for 6022 Al alloy as a function of microstructural parameters.

4.1 Background

A proper understanding of the relationships that connect processing conditions, microstructural evolution and mechanical properties is important for any materials

scientist to improve productivity and product quality. Optimization of fabrication processes requires a profound understanding of the microstructure evolution at various length scales. There are many different scenarios in which microstructural prediction is particularly valuable such as:

a. where microstructure is critical in controlling final properties (e.g. toughness of steel welds) or subsequent material processability (e.g. earing in drawing of sheet metal);
b. where process optimization requires knowledge of microstructural limits (e.g., maximum welding or extrusion speeds);
c. where microstructure captures the coupling through multi-stage processes, giving opportunities for alloy and process development (e.g., effect of homogenization on precipitation after extrusion, or the effect of prior forming and heat treatment on weldability).

Many aspects of microstructure modeling and microstructure-property relationships have been studied, however the understanding is still incomplete especially in the area of size dependent material behavior. There are many experimental observations which indicate that, under certain specific conditions, the specimen size may significantly affect deformation and failure of the engineering materials and a length scale is required for their interpretation. Experimental observations indicate that material hardening increases as the size of material decreases. This dependence of mechanical response on size could not be explained by the classical continuum mechanics since no length scale enters the constitutive description. However, gradient plasticity theory has been successful in

addressing the size effect problem. Thus GNDs has received lot of attention recently, however no specific attempt has been made to relate the experimentally measured GNDs to the stress response. The present study is an effort to incorporate experimentally determined density of geometrically necessary dislocations (GNDs) into a statistically formulated model of deformation response. GNDs are defined as dislocations needed to accommodate the difference in crystal lattice rotation produced by different slip system activity from point to point within a given grain [1-4]. It is possible to get an estimate of GND density from spatially specific orientation measurements such as those obtained from automated EBSD analysis. Some other microstructural parameters that describe misorientation within a grain are grain orientation spread (GOS) and grain average misorientation (GAM). GOS is a measure giving the algebraic average of the misorientation angle between all points (whether adjacent or otherwise) within a given grain. GAM is a second measure that gives the algebraic average of the misorientation between all points and their nearest neighbor measurement points. Even though all of the above 3 microstructural parameters (GND density, GOS and GAM) provides a scalar number that describes the misorientation within a grain, computation of GND density provides additional information about the spatial distribution of densities of individual dislocation types that are required to support lattice curvature during deformation. Orientation spread within a grain arises, when stressed, because of differential rotation of crystallite regions (both in terms of angle and direction) within a grain. Development of in-grain orientation spread affects the mean free path of dislocation and therefore alters the stress required for deformation. Other microstructural features measured were grain size, inter-particle spacing, volume fraction of precipitates, and radius of precipitates.

Following are the major areas of investigation in the following discussion:

i. Investigate the effect of GND and other microstructural parameters on the observed stress response.

ii. Compare the experimentally observed microstructural evolution during annealing and deformation of 5005 and 6022 Al alloys.

iii. Develop a model based on statistical formulation that predicts the yield stress of 6022 alloy as a function of experimentally measured microstructural parameters.

4.2 Experimental Plan

Flat samples with dimensions of (25 x 10 x 4) mm^3 were cut from hot rolled plates of 5005 and 6022 Al alloys and annealed at 520^oC for 30 mins. Three samples (to form each batch for hot deformation) were placed on top of one another and deformed using channel die compression such that the direction of material flow is parallel to the direction of rolling (Figure 4.1). Various combinations of processing parameters (i.e. temperature of 250^oC, 350^oC and 450^oC, strain of 10%, 20% and 30%, and strain rate of 0.01, 0.1, 1 s^{-1}) were applied during hot deformation to generate a variety of microstructures. Table 4.1 shows the deformation conditions used for 5005 and 6022 alloys. Microstructural analysis of the hot deformed samples was done along the long transverse cross-section (so that there is a minimum of orientation gradient along the third direction) using a scanning electron microscope (SEM) equipped with EBSD. Texture analysis was performed using EBSD scans with a step size of 10 μm and the dislocation structure analysis was done using a step size of 0.2 μm. Backscatter electron imaging, which provides compositional contrast, was used to detect precipitates in AA6022. Image

analysis software was used to characterize precipitates in AA6022 in terms of inter-particle spacing, area fraction and radius of precipitates. Three miniature sized dog-bone

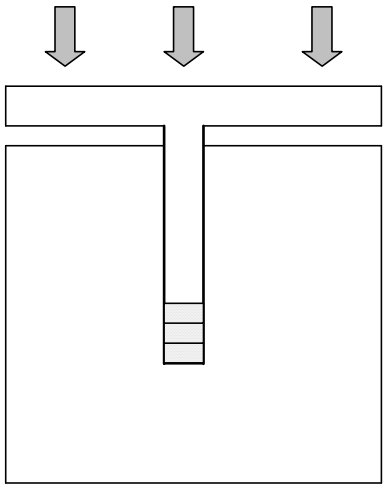

Figure 4.1: Schematic showing the process of channel die deformation used in this study.

Table 4.1: Different combinations of processing parameters used in the study.

Temperature (^{o}C)	Strain	Strain Rate (s^{-1})
450	25%	0.01
450	38%	0.01
450	40%	0.1
450	24%	1
450	37%	1
250	16%	0.01
250	41%	0.01
250	15%	1
250	44%	0.1
250	44%	1
350	10%	0.01
350	22%	0.01
350	23%	1
350	11%	1

samples (gage length – 10 mm and thickness – 2mm) were prepared from each batch of hot deformed samples and room temperature tensile testing was performed to failure with a constant crosshead speed of 0.005 in/sec. Statistical regression analysis was performed

using MINITAB-14.0 (a commercial statistical and graphical analysis software package from Minitab Inc.) with an input of parameters from microstructural characterization and stress analysis.

4.3 Results and Discussion

The major focus of this study is to quantitatively understand the influence of experimentally determined GND density on the observed stress response during deformation. We chose two commercially used Al alloys 5005 and 6022 for this study with a chemical composition shown in Table 4.2. It is known that in AA5005, Mg forms a substitutional solid solution with Al, whereas in AA6022 precipitates of Mg_2Si form in an Al matrix. In the following part of the paper, the first 3 sections are devoted to the comparison of experimentally observed microstructural evolution and stress-strain behavior of 5005 and 6022 alloys and the last two sections are devoted to the development of a yield strength model for 6022 alloy. The GND density is determined to be the major microstructural parameter, sufficient enough to represent all characteristics of dislocation structures, affecting the yield strength.

Table 4.2: Chemical compositions (in wt. %) of 5005 and 6022 Al alloys.

Alloy	Mg	Cu	Si
5005	0.7-1.1	0.05	0.3
6022	0.55	0.056	1.1

4.3.1 Characterization of Starting Material

Figure 4.2 contains boundary images of hot rolled 5005 and 6022 alloys obtained from EBSD; each line in both images represent misorientation of 1° or higher. Dense dislocation cell structure is observed in all the grains, irrespective of their crystal lattice orientation. The density of dislocation cell structure appears to be same for both the alloys. It can be seen from Figure 4.2 that no recrystallization occurred during hot deformation, since all the grains possessed dislocation cell structure. The number fraction of grain boundaries with misorientation of 1-5^{o} was approximately 48-57%; 5-10° was 25-27%; and 10° and higher was 18-24% for both the alloys. This indicates that significant number of dislocation cells contained high angle grain boundaries with misorientation greater than 5°. Higher misorientation across the cell boundaries occurs during hot deformation primarily by recovery processes that increase the dislocation content at the boundaries. Most of the grains possessed an aspect ratio of 0.63 for both alloys indicating preferential elongation in the direction of rolling, which is expected during deformation. The average grain sizes measured in the plan section of the samples were 38 μm and 35 μm for 5005 and 6022 alloys respectively. The average grain orientation spreads were 3.97 for 5005 alloy and 2.95 for 6022 alloy and the grain average misorientations were 2.37 for 5005 alloy and 1.97 for 6022 alloy.

Both alloys were annealed at 520^{o}C for 30 mins to recrystallize the microstructure and reduce the total dislocation content. Figure 4.3 shows orientation images of 5005 and 6022 Al alloys after recrystallization. It can be seen that all the grains are almost free

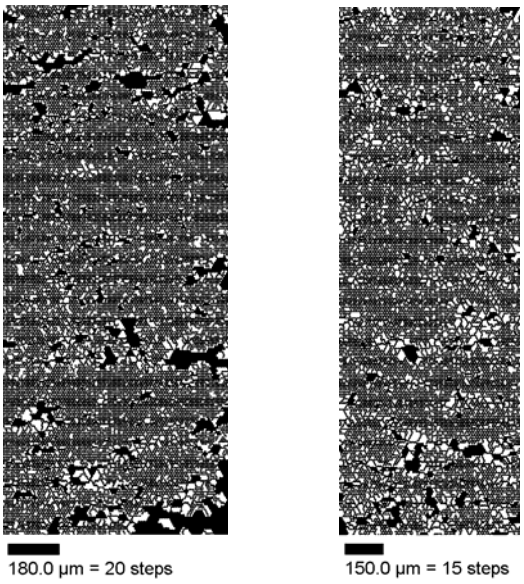

Figure 4.2: Boundary maps showing well recovered microstructure after hot deformation for (a) 5005 and (b) 6022 Al alloys. Each line in the images represent misorientation of 1^{o} or higher.

from dislocation substructure. The average grain orientation spread reduced to 0.91 and grain average misorientation reduced to 0.84 after annealing. During recrystallization small, strain free grains are nucleated and grow in the deformed matrix. As these grains grow and consume the matrix, the dislocations in the matrix are absorbed and essentially get annihilated at the boundaries of the newly formed grains. When the new grains impinge upon one another, the process of recrystallization is complete. The kinetics of recrystallization are very dependent on a large number of external variables, the most important of which are probably the amount of pre-strain, the purity of the material and the orientation difference between recrystallized grain and the matrix into which it is growing. An inhomogeneous grain size observed in 5005 alloy is believed to be due to

extra annealing of the material above recrystallization treatment leading to a grain growth of few grains.

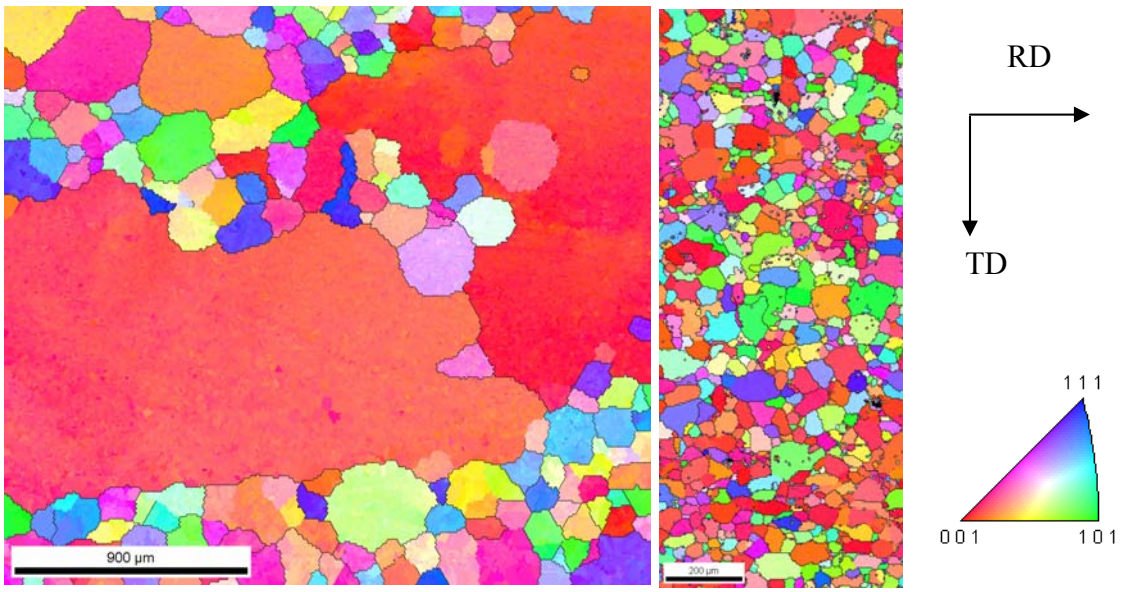

Figure 4.3: Orientation images of (a) 5005 and (b) 6002 Al alloys after recrystallization treatment. The orientation color key indicates poles aligned with ND of the sample.

4.3.2 Effect of Processing Parameters

Industrial processing of metals and alloys requires application of a wide range of processing parameters such as strain, strain rate and temperature, which influence the microstructure evolution and the kinetics of deformation. Various approaches have been used in the past in the area of microstructural modeling with the length scales ranging from atomistic, to slip system activity, to grain structure and continuum level. It is important to have statistically reliable and experimentally verifiable information about the microstructural evolution and stress response as a function of processing parameters to validate such models. Such understanding is important to define mechanisms driving microstructural evolution during thermo-mechanical processing and can be applied to

develop processes that produce materials with a microstructure just good enough for a desired application. This section discusses the effect of processing parameters on the stress response and texture evolution of both alloys.

Figure 4.4 contains a plot of the Zener-Holloman parameter (temperature modified strain rate$\left(Z = \dot{\varepsilon} \exp\left(\frac{U}{RT} \right) \right)$) versus flow stress obtained during channel die deformation for both alloys [5]. In the above equation $\dot{\varepsilon}$ is applied strain rate, R is the gas constant, T is the absolute temperature and the activation energies, U (obtained from commonly selected values for Al alloys) used for the calculation were 156 kJ/mole and 140 kJ/mole for 6022 and 5005 Al alloys respectively. In accordance with earlier experimental observations and theoretical understanding, it can be seen from Figure 4.3, that higher flow stress is observed for samples deformed at high Z (i.e. low T and high $\dot{\varepsilon}$). Also the plot describes the effect of alloy chemistry on the deformation behavior of the two alloys at high temperatures. Trivedi et al. [6] studied the room temperature small strain (up to 10%) deformation behavior of AA5005 and AA6022 and observed that AA6022 generated a higher increase in dislocation structure (and correspondingly flow stress) with strain than AA5005. However a reverse effect is observed from Figure 4.3 during hot deformation in the sense that, at low values of Z (i.e. at low $\dot{\varepsilon}$ and/or high T) AA5005 showed higher flow stress than AA6022. This suggests that under the current experimental conditions, solid solution hardening observed in AA5005, is more effective in resisting deformation, especially for samples deformed at low Z values (i.e. at high T

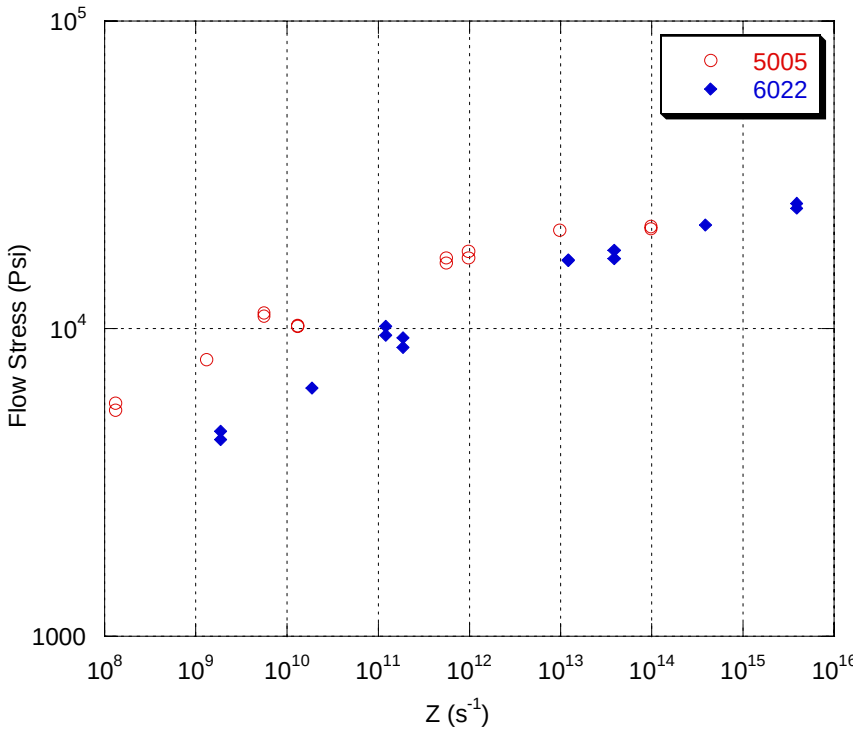

Figure 4.4: Plot showing flow stress obtained during channel die compression as a function of Z for both 5005 and 6022 Al alloys.

and low $\dot{\varepsilon}$), than precipitation hardening in AA6022. The difference in stress-strain behavior during channel die compression between the two alloys can be due to the difference in starting microstructure and/or their alloy content. Since both alloys were fully annealed before hot deformation, AA6022 has a distribution of coarse overaged equilibrium particles, which are easily bypassed by dislocations and hence do not significantly, contribute to strengthening. Solute atoms in AA5005 are in solid solution even during high temperature deformation and therefore possess higher ability of resisting deformation at higher temperatures.

Figure 4.5 contains the (001) pole figures showing predominantly cube texture of AA6022 after hot deformation at various processing parameters. In contrast AA5005 showed (Figure 4.6) an ND rotated cube texture under similar deformation conditions due to the presence of large grains having a rotated cube orientation in all the samples. Since both the alloys were subjected to similar deformation conditions, the difference in texture evolution is due to the difference in alloy content of the two alloys.

4.3.3 Effect of Microstructure

This section is devoted to the influence of starting microstructure (specifically density of GND) on the different stress responses observed during tensile testing.

Texture evolution after channel die deformation was similar under all deformation conditions for both alloys – predominantly cube for 6022 alloy and predominantly rotated cube for 5005 alloy. Therefore the effect of texture on stress response during subsequent tensile deformation was neglected. Figure 4.7 shows a plot of change in the flow stress for both alloys as a function of deformation conditions. Change in flow stress was calculated as percentage difference in stress (at a particular value of strain) obtained after room temperature tensile deformation compared to stress obtained after high temperature channel die deformation. A relatively higher increase in flow stress was observed in AA6022 especially for samples previously deformed at low Z values. This is because samples deformed at low Z showed relatively higher density of GNDs in the final microstructure and therefore contributed to higher flow stress during subsequent tensile deformation.

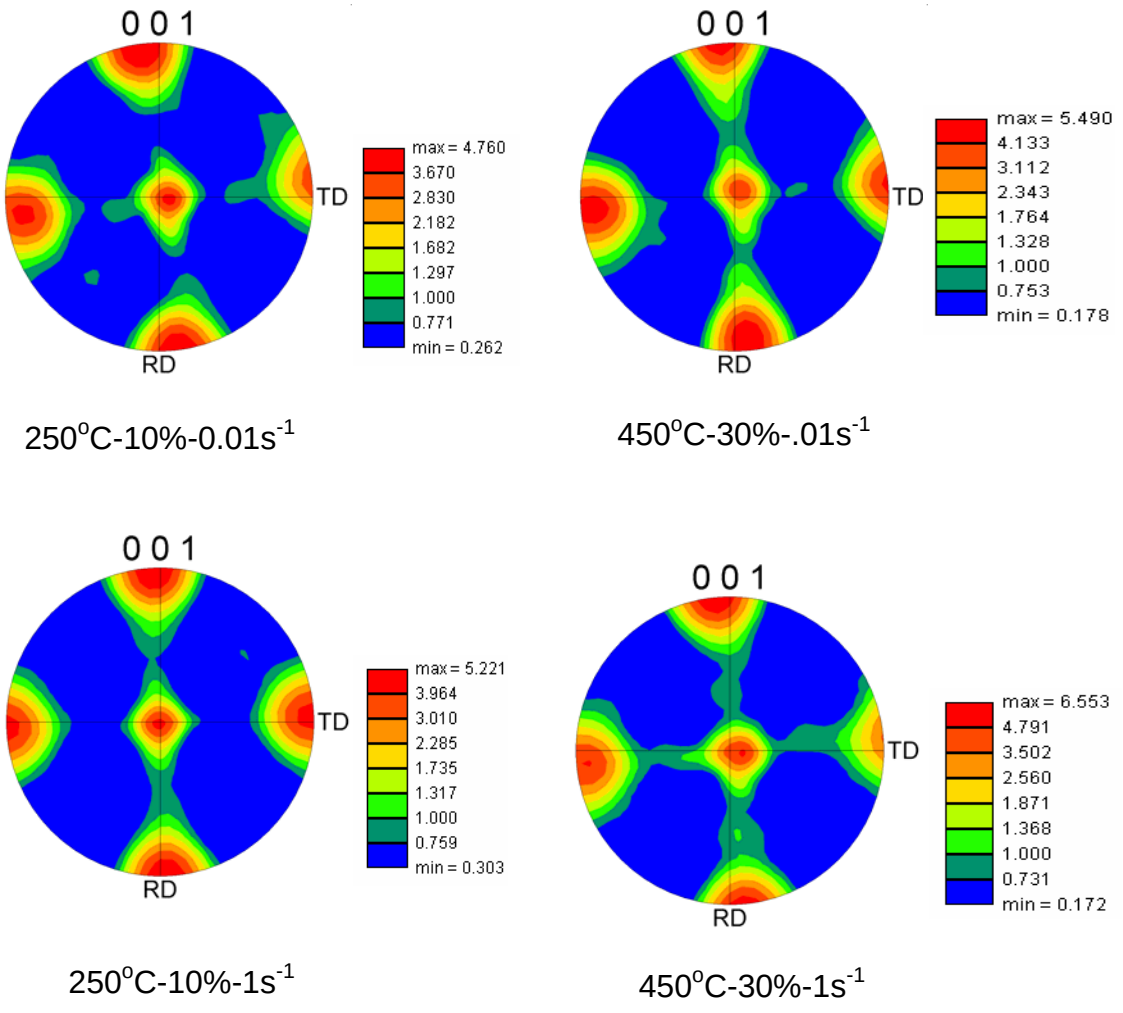

Figure 4.5: (001) texture pole figures of 6022 Al alloy showing predominantly cube texture for samples deformed under various processing conditions.

Figure 4.8 shows the variation in the 0.2% yield stress, obtained during room temperature tensile testing, with square root of GND density for 6022 alloy. Details about the calculation of GND density is described in Chapter 2. It can be seen that with increasing GND density the stress required for plastic deformation for both alloys increases. Such a

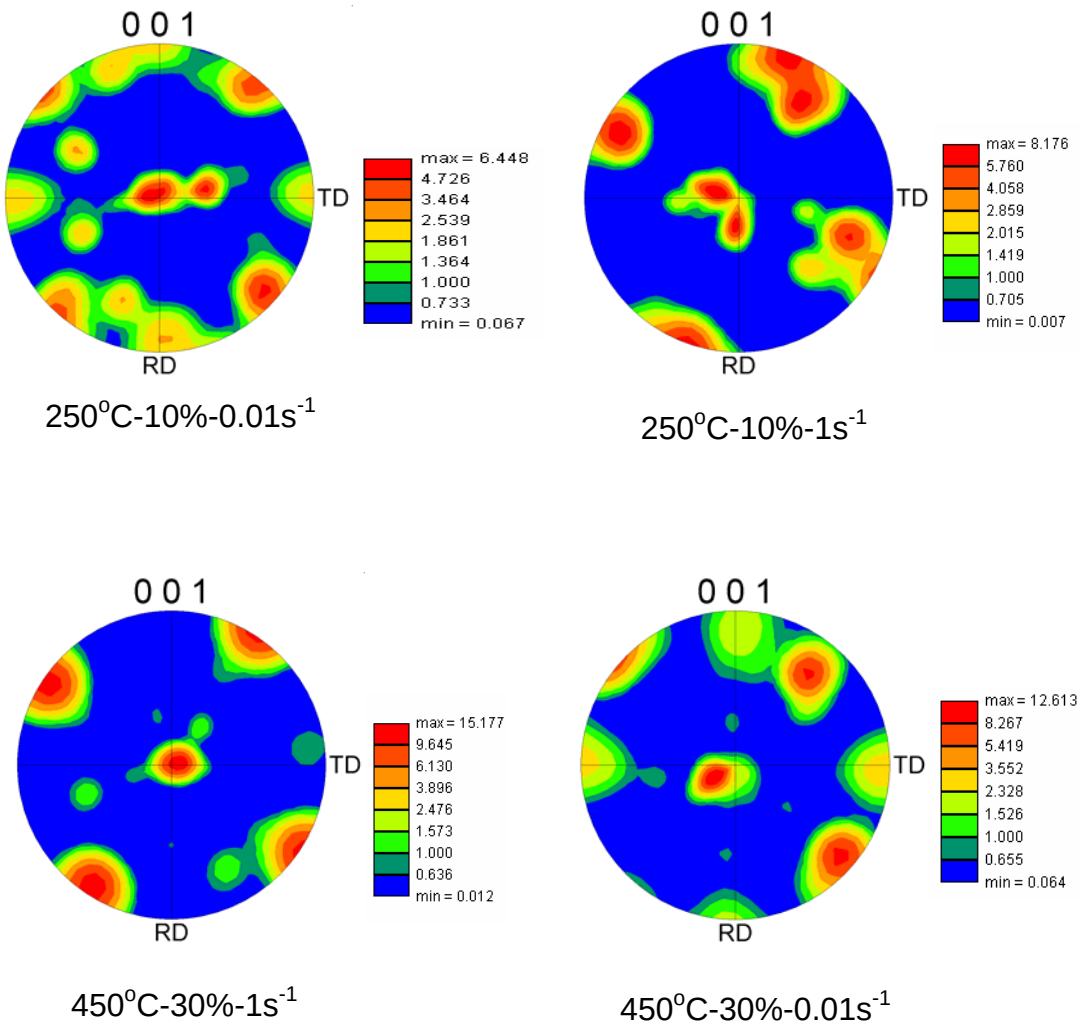

Figure 4.6: (001) texture pole figures in 5005 Al alloy showing predominantly rotated cube texture for samples deformed under various processing conditions.

direct relationship between dislocation density and flow stress has been suggested by various modelers [7] with an equation of the type

$$\sigma = \sigma_0 + \alpha G b M \sqrt{\rho_f} \qquad \ldots\ldots\ldots\ldots\ldots\ldots\ldots\ldots\ldots\ldots (4.1)$$

where σ is the macroscopic stress response, σ_0 is the friction stress, M is the Taylor Factor, G is the shear modulus, α is constant and ρ_f is the density of forest dislocations.

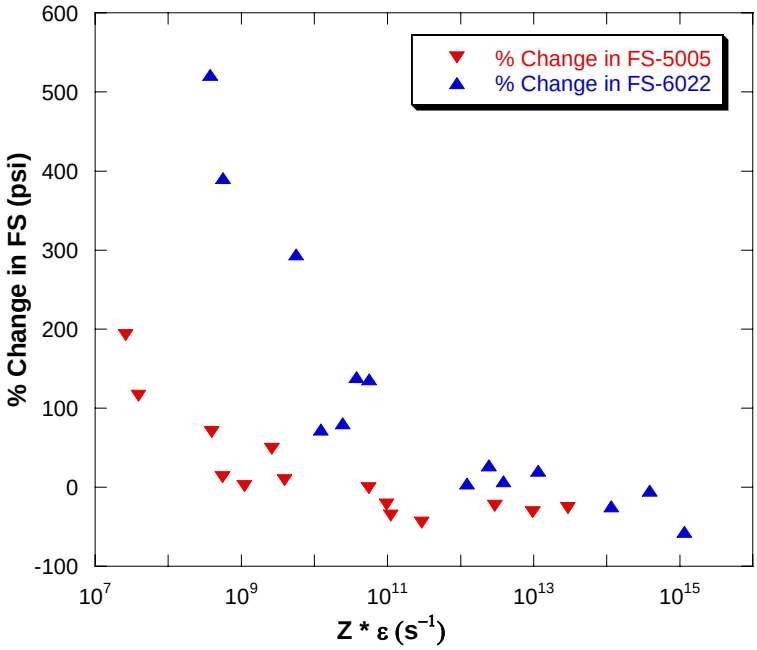

Figure 4.7: Plot showing variation in % change in flow stress versus deformation conditions (described by Z * strain) for 5005 and 6022 Al alloys.

Forest dislocations in the above equation include both GNDs and statistically stored dislocations (SSDs), formed by statistical mutual trapping of dislocations such as dislocation dipoles. In the current analysis we have ignored the effect of statistically stored dislocations on the stress response because of difficulties associated with determining the content of SSDs. It is known that at high temperatures Al alloys tend to form well-organized cell structures separated by dislocation cell walls creating small misorientations across them. Dislocations along those cell walls develop lattice curvature and contribute to GNDs. In the current experimental conditions most of the

microstructure consists of those cell walls (and consequently the microstructure should be dominated by GNDs) and therefore it may be reasonable to ignore the effect of SSDs on the stress response. In the present study it is assumed that SSDs and GNDs scale similarly, so measuring one or the other will yield the desired relationships. The effect of GNDs on the stress response is evident in Figure 4.9, which shows the stress-strain curves obtained during RT deformation for 6022 alloy plotted as a function of GND density.

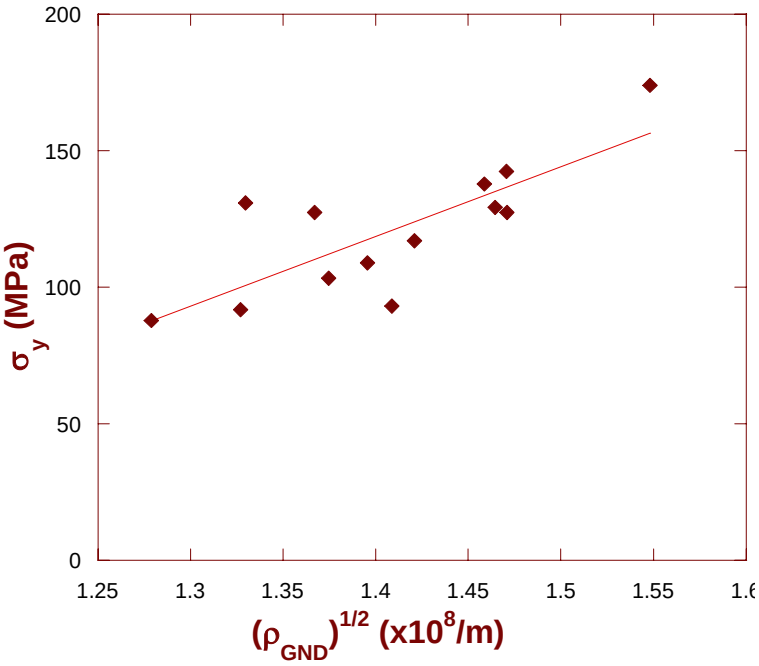

Figure 4.8: Plot showing variation in 0.2% yield stress (MPa) obtained during tensile testing with square root of GND density (x10^8/m) for 6022 Al alloy.

During the process of plastic deformation, dislocations have to overcome both short-range and long-range obstacles. For FCC metals, the primary short-range barriers are other dislocations which intersect the slip plane and impede the motion of gliding

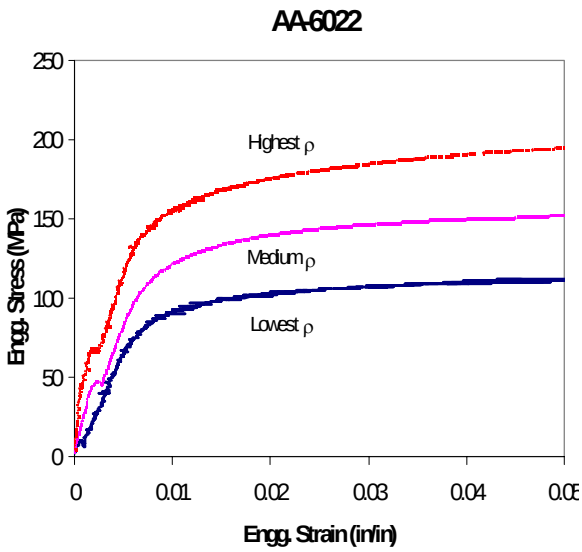

Figure 4.9: Stress-Strain curve of AA6022 for samples containing different GND densities in the starting microstructure.

dislocations. The evolution of SSDs during crystallographic slip increases the number of short-range interactions and accordingly results in isotropic hardening of the metal. Furthermore, the absolute GND densities equally well contribute to this short-range effect. The resistance to crystallographic slip due to short-range obstacles can be overcome by thermal activation, whereas effect of the long-range obstacles is essentially independent of the temperature, and can be overcome with the aid of the applied resolved shear stress. It is believed that the GNDs are responsible for the long-range contribution and they originate from any macroscopically inhomogeneous plastic deformation after removal of external loads.

Influence of GNDs on stress response was particularly studied by Hansen and Juul-Jensen [8] and they suggested that strengthening due to GND follows a Hall-Petch type equation:

$$\sigma_{GNB} = K_1\sqrt{Gb / D_{GNB}} \qquad \text{..... (4.2)}$$

where K_1 is constant and D_{GNB} is the spacing between geometrically necessary boundaries (GNBs). Figure 4.10 is the TEM image showing geometrically necessary boundaries and incidental dislocation boundaries (IDB) in deformed Ni [9].

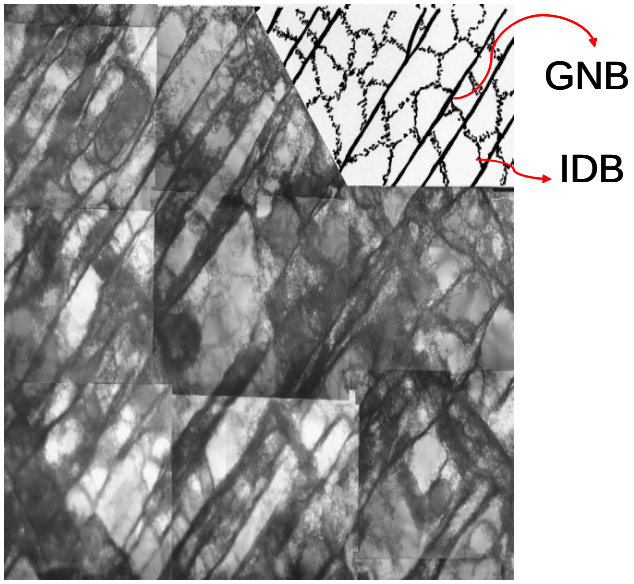

Figure 4.10: TEM image of deformed Ni showing geometrically necessary boundaries and incidental dislocation boundaries.

TEM investigation showed that GNBs are produced by GNDs at medium to high strain and that they have preferred crystallographic orientation. With increasing strain, misorientation across GNBs increases and the spacing between them decreases due to accumulation of GNDs. It is also experimentally verified that these boundaries can have

large misorientations across them (10-15^{o}) and are capable of restricting glide. Such observations clearly explain the effect of GND density on the stress response observed in the current analysis (Figures 4.8 and 4.9).

4.4 The Model

Many experimental studies on metals and alloys suggest that the macroscopic flow strength of the material is given by

$$\sigma = \sigma_0 + \sigma_d \qquad \text{..... (4.3)}$$

where σ_0 is the friction stress and σ_d is the strength contribution due to dislocation structure. In the case of precipitation hardening systems (such as in AA6022 in the present analysis) or solid solution hardening systems (such as AA5005), there should be an additional term describing their effect in Equation 4.3. A linear addition of strength contribution due to the matrix, precipitates and solid solution has been suggested by various modelers [10-12]. Depending on the type of systems (precipitation hardening or solid solution hardening), the flow stress relationship then becomes

$$\sigma = \sigma_0 + \sigma_d + \sigma_p(\sigma_{ss}) \qquad \text{..... (4.4)}$$

where σ_p and σ_{ss} are the strength contribution due to precipitates and solid solution respectively. It is known based on a large number of experimental data of metals and alloys that the strengthening due to dislocation structure is related to the dislocation density by the relation

$$\sigma_d = \alpha(\dot{\varepsilon},T)MGb\sqrt{\rho_T} \qquad \text{..... (4.5)}$$

where α is a material parameter, G is the shear modulus, b is the Burger's vector and ρ_T is the total dislocation density [7]. As mentioned earlier the total dislocations can be

divided into two different categories: statistically stored dislocations (SSDs) and geometrically necessary dislocations (GNDs) and so Equation (4.5) becomes

$$\sigma_d = \alpha(\dot{\varepsilon}, T) MGb\sqrt{\rho_{SSD} + \rho_{GND}} \qquad \ldots\ldots\ldots\ldots\ldots\ldots\ldots\ldots (4.6)$$

Also, based on current experimental observations, SSDs and GNDs scale similarly and therefore assuming that the effects of SSDs and GNDs are proportional, we get

$$\rho_{SSD} + \rho_{GND} = \rho_{GND}(p+1) \qquad \ldots\ldots\ldots\ldots\ldots\ldots\ldots\ldots (4.7)$$

where p is a proportionality constant. Including $\sqrt{(p+1)}$ in the material constant α, Equation (4.6) becomes

$$\sigma_d = \alpha MGb\sqrt{\rho_{GND}} \qquad \ldots\ldots\ldots\ldots\ldots\ldots\ldots\ldots (4.8)$$

To describe the effect of precipitates ***(σ_p)*** we are considering the model proposed by Deschamps and Brechet [13] such that the strengthening due to particles follows the relationship

$$\sigma_p = \frac{M\overline{F}}{bL} \qquad \ldots\ldots\ldots\ldots\ldots\ldots\ldots\ldots (4.9)$$

where $\overline{F}$ is the mean obstacle strength and L is the average inter-particle spacing. The above equation assumes homogeneous distribution of particles such that dislocations have to pass through all the obstacles to cause deformation. Depending on the initial characteristics of the precipitates, $\overline{F}$ and L will evolve with aging time and processing conditions. For coherent fine particles, the obstacle strength $\overline{F}$ is dependent on particle radius and for coarse and overaged particles, obstacle strength $\overline{F}$ is constant. Deschamps and Brechet further developed Equation (4.9) for the case of all precipitates being bypassed by the dislocations (which is the case in AA6022 in the current work) such that

$$\sigma_p = \frac{kMGbf_v^{1/2}}{\overline{R}} \qquad \text{..... (4.10)}$$

where k is constant (usually 0.6-0.7), $\boldsymbol{G}$ is the shear modulus, f_v is the volume fraction of precipitate particles, and $\overline{R}$ is the mean radius of precipitates. Incorporating the effect of dislocation and precipitate structures into Equation (4.4), we get

$$\sigma = \sigma_0 + \alpha MGb\sqrt{\rho_{GND}} + \frac{kMGbf_v^{1/2}}{\overline{R}} \qquad \text{..... (4.11)}$$

4.4.1. Regression Analysis

Microstructures of materials can be described by various structural parameters and each variable can potentially have a dominating effect on certain properties exhibited by the material. Therefore the selection of a microstructural variable of importance should depend on the desired property (response variable). One of the ways to extract the information about which microstructural features are dominant is by using statistical analysis. In the current paper we use multiple regression analysis to investigate the effect of various experimentally measured microstructural parameters on the response variable. Regression analysis is a method that can be used to quantify the relationship between two or more predictor variables (X) and a response variable (Y) by fitting a line or plane through all the points such that the fitted line or plane minimizes the sum of the squared deviations of the points from the fitted values [14]. The level of significance of a particular predictor variable on a response variable is determined from *P* value obtained from regression analysis. *P* value is an indication of how likely the coefficients of predictor variables are real. A *P* value of .05 means that there is a 5% chance that the relationship emerged randomly and a 95% chance that the relationship is real. It is

generally accepted practice to consider variables with a *P* value of less than .1 as significant. The response variable chosen was 0.2% yield strength determined from room temperature tensile testing.

Various microstructural parameters measured were grain size, grain orientation spread, grain average misorientation, density of geometrically necessary dislocations, and some of the precipitates characteristics such as average inter-particle spacing, area fraction of precipitates, and mean radius of precipitates. A similar parametric study in single crystal Ni was performed by Horstemeyer [15] using the analysis of variance (ANOVA) technique with an input of data from MD simulation. He divided various parameters such as crystal orientation, strain rate, temperature, deformation path, x, y, and z dimensions into different levels in the analysis. In the current paper processing parameters such as strain rate and temperature were not included in the analysis because stress parameters (forming response variable in the regression analysis) were obtained from room temperature and constant strain rate experiments. In the current regression analysis we included the actual values of quantitative parameters that describe different microstructural features rather than dividing them into various levels to allow more degrees of freedom (and obtain least error mean square).

4.4.2. Application to AA6022

When all the microstructural parameters such as grain size, density of GND, grain orientation spread, grain average misorientation, average inter-particle spacing, average particle radius and area fraction of precipitates were incorporated in the regression

analysis, large '*P*' values were obtained for all the parameters (Plot 4.11a). This indicates that such combinations of microstructural parameters fed into the analysis are ineffective in describing the stress response due to existing correlations between them. The matrix of correlation between various microstructural features was determined and it was observed that there exists a relatively strong correlation between density of GND and GOS, GOS and GAM, density of GND and inter-particle spacing. Various combinations of microstructural parameters were fed into the regression analysis to determine major parameters that influence yield strength. The regression equation that best defines the relation and the one that gave minimum '*P*' values for corresponding microstructural parameters was

$$\sigma_y(MPa) = -111 + 0.000001\sqrt{\rho_{GND}} + 0.000045\frac{\sqrt{f_v}}{\overline{R}} \quad \text{……...…… (4.12)}$$

It is interesting to note that the regression equation obtained for the yield stress (Equation 4.12), by choosing the parameters that give minimum '*P*' values, is similar to the one proposed by Deschamps et al. in Equation (4.11). '*P*' values obtained during the

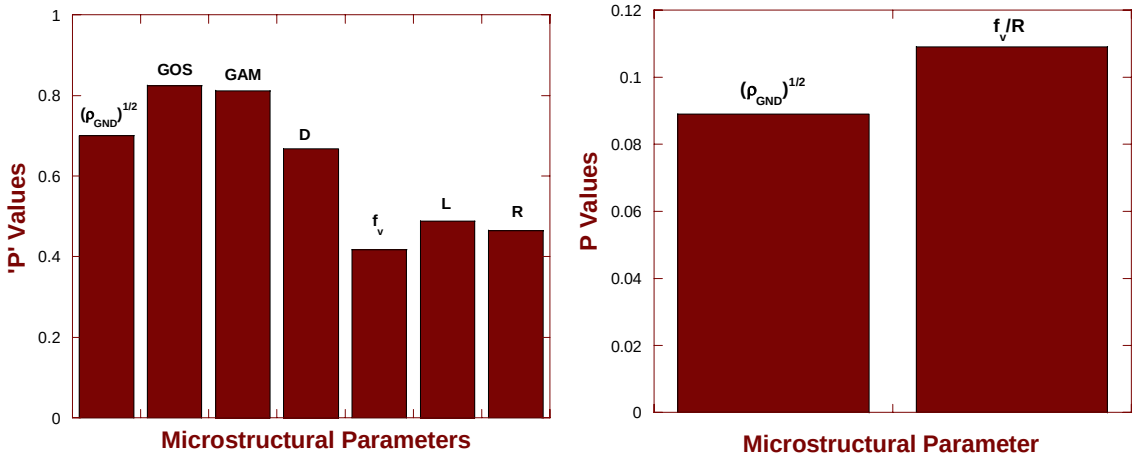

Figure 4.11: Summary of regression analysis showing influence of microstructural parameters on the yield stress of 6022 Al alloy.

regression analysis (Plot 4.11b) suggest that the GND density explains more variation in the yield strength than the characteristics of particles. This in fact is believable and precipitates do not significantly affect the yield stress because precipitates in AA6022 are overaged and so dislocations can bypass them easily. The strength contribution due to precipitates is directly related with volume fraction of precipitates suggesting that with increase in volume fraction of precipitates in the matrix, the number of obstacles to dislocation motion also increases, which eventually increases the stress required for plastic deformation. In the current analysis the strength contribution due to dislocation structures is considered to be only due to the GND density and we have ignored the effect of other dislocation structures such as cell-size, cell-shape, SSDs, cell-wall misorientation etc. However it can be seen from the statistical analysis that under the current experimental conditions, GND density alone could satisfactorily represent the overall strength contribution due to dislocation structures. We attempted to use dislocation cell-size, to represent D_{GNB} (in Equation 4.2) in the regression analysis. Cell-size was measured using EBSD analysis by changing the grain definition to 0.5^{o} misorientation and substituted for GND density in the regression analysis. A large '*P*' value was obtained for cell-size in the regression analysis indicating that the cell-size was not a major parameter influencing the yield stress of the alloy. This could be because of fairly constant cell sizes, in the range of 2.0-3.0 μm, obtained in all hot deformed samples. It is possible to obtain such an equilibrium cell-size during hot deformation and so the effect of applied stress during deformation will increase misorientation across cell-walls due to accumulation of dislocations, keeping cell-size relatively constant.

4.4.3. Determination of Coefficients

If we consider the average Taylor Factor as 2.73 (calculated for grains with cube orientation since the texture of 6022 alloy is predominantly cube), shear modulus ***(G)*** of 6022 alloy as 26 GPa and magnitude of Burger's vector as 2.86 x 10^{-10} m, the material constant α is determined to be 0.05. The material constant α is a function of strain rate and temperature and when strengthening of materials is due to pure dislocation-dislocation interaction (without considering the effect of precipitates), the value of α is proposed to be 0.3 [7]. As expected, we obtained a lower value of α because of additional strength contribution due to dislocation-precipitate interactions included in the current analysis. Various yield strength models (regions of small strain) developed for Al alloys used M value as 2, and they suggested that since the material is in early stages of plastic deformation, grains are not fully constrained and so the homogeneous stress hypothesis can be applied [13, 16]. Thus, reducing the value of M to 2.0 will further increase the value of the material constant α to ≈ 0.1.

4.5 Conclusions

The current work supports the trend of increasing interest in the scientific community towards quantifying the GND density in deformed samples and incorporating it into a physically based model. In general, the yield strength model developed for 6022 alloy is similar to the model proposed by Deschamps and Brechet [13]. Statistical analysis and experimental observations showed a linear relationship between yield stress and square root of GND density. It was observed that GND density alone can sufficiently represent

the strength contribution due to dislocation structures and samples with higher GND density observed higher flow stress.

4.6 References

[1]. Nye, J.F., *Acta Metall*. 1, (1953) 153

[2]. Ashby, M.F., *Phil. Mag*. 21, (1970) 399.

[3]. Bay, B., Hansen, N., Hughes, D.A., Kuhlman-Wilsdorf, D. *Acta Metall*. 40, (1992) 205.

[4]. Arsenlis, A. and Parks, D.M., *Acta Mat*. 47, (1999) 1597.

[5]. Zener, C., Holloman, J. H., *J. Appl. Phys*. 15, (1944) 22.

[6]. Trivedi, P.B., Field, D.P., Weiland, H., *Int. J. Plasticity* 20, (2004) 459.

[7]. Mecking, H. and Kocks, U.F., *Acta Metall*. 29, (1981) 1865.

[8]. Hansen, N., Juul Jensen, D., *Acta Mat*. 40, (1992) 3265.

[9]. Hughes, D.A., Hansen, N., Bammann, D.J., *Scripta Mat*. 48 (2003), 147.

[10]. Ardell, A.J., *Metall. Trans*. 16A, (1985) 2131.

[11]. Lloyd D.J., In: *Proceedings of the 7th Int Conf on the Strength of Metals and Alloys*, I.C.S.M.A.-7, Montreal, Canada, vol. 3. Oxford: Pergamon Press; (1985) 1745.

[12]. Brown L.M. and Ham R.K., In: *Strengthening Methods in Crystals.* (Kelly A, Nicholson RB, editors New York, NY: John Wiley & Sons Inc.; 1971) 12.

[13]. Deschamps, A. and Brechet, Y., *Acta Mat*. 47, (1999) 293.

[14]. Draper, N.R. and Smith, H. *Applied Regression Analysis*, (John Wiley & Sons Inc, New York, 1981).

[15]. Horstemeyer, M.F. Baskes, M.I., Godfrey, A., Hughes, D.A., *Int. J. Plasticity* 18, (2002) 203.

[16]. Guyot, P. and Cottignies, L., *Acta Mat.* 44, (1996) 4161.

CHAPTER – 5

DISCUSSION

The ultimate goal of the project is to minimize annealing time by controlling processing parameters used during hot deformation such that final microstructure of the hot deformed material requires minimum of subsequent annealing treatment. However in order to optimize processing parameters, a better understanding of the connection between processing parameters, microstructural evolution and stress response is important. This requires systematic individual efforts in the areas of microstructure characterization, identification of important microstructural parameters and development of physically based models. This research is mainly focused on development of tools for quantitative understanding of the microstructure – property relationship. The main contribution of the present research is in the areas of improved procedures for characterization of dislocation structures, application of the developed characterization measures in a parametric study to determine major microstructural parameters affecting stress response and the use of those microstructural parameters to develop the relationship between the yield stress and the microstructure.

The development of new materials relies, to a large extent, on improved understanding of the structure-property relationship, which requires progress in microstructure characterization. Also, the determination of the degree of sensitivity of any particular microstructural parameter on properties of materials relies heavily on the accurate

analysis of microstructure. Hence, a significant portion of this research effort was directed towards development of new procedures for characterization of dislocation structures and local orientation gradient. EBSD was chosen as a major characterization technique for this study to quantify dislocation structures because bulk samples can easily be characterized at a relatively fast speed and statistically reliable information can be obtained. While it is possible to get spatially specific crystal orientation information from EBSD measurements (sometimes with a high spatial and angular resolution), it is necessary to process these data to obtain meaningful information about the local orientation gradient. The following three paragraphs summarize the usefulness and uniqueness of various new strategies developed to define and image local orientation gradients in deformed crystalline materials.

There are many instances where orientation gradients, of various magnitudes, are present in a microstructure. For example: (i) deformation-induced cellular substructures, transition bands, shear bands, particle deformation zones (PDZs), and regions in the vicinity of prior grain boundaries and (ii) orientation gradients within recrystallized, mechanically alloyed or electrodeposited materials as a result of their methods of processing. It is also known that development of microstructure such as growth of subgrains/cells or grain coarsening depends to some extent on the level of orientation gradient present in the material [1, 2].

Common measures of dislocation structures such as cell size and cell-wall misorientation could directly be obtained using OIM. The single most important quantity that describes

dislocation structures is dislocation density. In the current research, code was developed that determines the spatial distribution of geometrically necessary dislocations using the lattice curvature information from EBSD. The continuum theory of dislocations was the basis for the approach used in extracting dislocation information from the measured datasets. Nye's formulation was implemented in order to link the measured orientation gradients to the GND densities [3]. The use of this formulation necessitated the use of assumed two-dimensional materials, but for real materials orientation gradients along all three directions are important to obtain accurate information about GND densities. In Chapter 2, geometrically necessary dislocation density, orientation deviation angle, axis of deviation and metrics derived from a field of orientation difference vectors are discussed in connection with two very different microstructures. It was observed that even though both single crystals contained approximately similar values of average GND density, there is a large difference in the local orientation gradient between them. Such analysis that gives insight into local behavior of dislocation is only possible by generating spatial plots of the measured density, such as those presented in Figure 2.8. In addition, while the images of the two microstructures are distinct with all analytical strategies discussed in Chapter 2, quantitative information derived from the images is similar for the specimens using either the geometrically necessary dislocation density or the average orientation deviation angle approaches.

While GND density gives estimates of the minimum dislocation density required to maintain lattice continuity, spatial information about crystal orientation from EBSD data can also be filtered to obtain information about the deformation behavior of subgrains.

The misorientation between subgrains is an important parameter in determining the properties of a material with recovered or hot worked microstructures. The use of orientation flow fields defined by orientation difference vectors offers an imaging option that provides the user with a visual interpretation of local orientation gradients not obtained by any other imaging technique. Since the data are presented in a coordinate frame that is familiar and intuitive (the specimen coordinate frame), as opposed to the frame defined by the crystallite lattice, the user can visualize the change in lattice orientation with respect to the specimen itself. Grain fragmentation can be directly visualized in terms of relative rotation directions and magnitudes. The images containing orientation difference vectors allow the user to visualize the relative magnitudes and directions of lattice rotation for the subgrain structure. These images offer additional insight into the mechanisms of the developing microstructure. It can be seen that individual crystallites within a cell are oriented differently from neighboring cells (Figure 2.13). As with any such flow field presentation, image size is restricted to the presentation of about 10000 vectors. Images attempting to present too many measurements produce clustered figures that reduce their scientific utility. Often times it becomes necessary to analyze behavior of orientation gradient of deformed crystallites as a function of distance. The metrics of divergence and gradient that are calculated from the orientation flow fields offer additional insight into data interpretation (Figures 2.14, 2.15). Application of divergence and gradient operators to the orientation difference vector fields allows one to quantitatively describe the local orientation deviation in relation to the orientation of neighboring measurement points. Mapping of such scalar

measures gives a visual representation about the trends of deviation in crystal orientation (moving towards/away from an average orientation) as a function of distance.

The next logical step of the research effort was to apply the characterization measures described above and those directly measurable using OIM to various Al alloys and develop better understanding of the effect of alloy chemistry on the evolution of dislocation structures. The current research is focused on small strain deformation behavior because phenomenological models with good predictive capability are already available for large strain deformation [4]. Comparison of microstructural evolution during small strain deformation was done for 3 commercially used Al alloys AA3003, AA5005, and AA6022. These alloys differ by their alloy chemistry and the mechanisms by which they harden the material. Alloys AA5005 and AA3003 are non-heat treatable and thereby the hardening is achieved by the interaction between solute atoms and dislocations. Usually the strength contribution due to solid solution ***(τ_s)***, is directly related to the concentration of solute in a matrix, and is given by the relation

$$\tau_s = K_s \sqrt{c} \qquad \text{..... (5.1)}$$

where, K_s is a constant related to clustering of solute atoms in a slip plane and c is the concentration of solute atoms [5,6]. In the case of AA6022, solute atoms form second phase precipitates and therefore the strength contribution due to precipitates depends on various characteristics of precipitates such as inter-particle spacing, volume fraction, size and size distribution etc. It is apparent that there is a large inhomogeneity in the evolution of dislocation structures in a specimen with a given process history. The influence of neighboring grains on local deformation behavior gives rise to a large scatter in data of

dislocation cell structure development. Irrespective of this complication, evolution of dislocation structures is obviously dependent upon the alloy class of the material. Difference in microstructural evolution was quantified in terms of texture measurements and by measuring various characteristics of dislocation structures such as cell-size, fraction of low angle boundaries, grain orientation spread and grain average misorientation. It was observed that even though all three alloys were subjected to the same state of stress, there was a large difference in the evolution of dislocation structure even during small strain deformation. The difference in dislocation structure evolution between the three alloys observed in this study is mainly attributed to their alloy content. In general, the variables observed to influence the deformation behavior include precipitate morphologies, alloy chemistry, crystallite lattice orientation, and character of neighboring grains (including lattice orientation and dislocation content).

An inhomogeneous evolution of microstructure was observed during small strain deformation, which motivated us to develop a more quantitative study on the influence of each of the above microstructural parameters (such as precipitate morphologies, grain orientation and neighboring grains) on dislocation structure evolution. The presence of precipitates and other particles influences dislocation generation and provides pinning points for where dislocation walls and tangles form. The larger number of solute atoms, the higher the content of forest dislocations (see Figure 3.4). The presence of particles and solutes will also affect the hardening rate and perhaps the dislocation cell wall morphology if clustering exists in the particle distribution. A specific study was attempted to understand the influence of precipitate morphologies on the evolution of

GND density. The study showed that the evolution of GND density depends on the interaction between precipitates and dislocations, which in turn is governed by the precipitate morphologies of the starting microstructure. Strong coherent precipitates produced a higher increase in GND density evolution than overaged coarse particles during small strain deformation of AA6022 alloy.

Influence of grain orientation on dislocation structure evolution is clearly visualized from the construction of boundary maps and misorientation profiles as a function of deformation. It was observed that the grains with near {111} orientation were primarily substructure free, whereas grains with cube orientation developed significant dislocation substructure in all alloys at each deformation level investigated. Another example of the effect of grain orientation on dislocation structure evolution is shown in Figure 5.1, which is an orientation image of pure Al deformed at room temperature under channel die compression to a strain of 20%. It can be seen that even though both grains suffered the same macroscopic deformation there is a large difference in the pattern and content of dislocation sub-structure that is generated within a grain. There is a very well developed dislocation cell structure in one grain while the other grain is essentially dislocation cell structure free. In addition, the misorientation profile (Figure 5.2) of each grain indicates that the grain that developed dislocation cell structure has large in-grain misorientations (up to 15^{o}), while the other grain is mostly single crystal with very low misorientation between crystallites within a grain. Such information about the influence of grain orientation on the development of dislocation cell structures can be used for experimental

validation of Monte-Carlo type simulation developed to understand the phenomena of cell patterning [7].

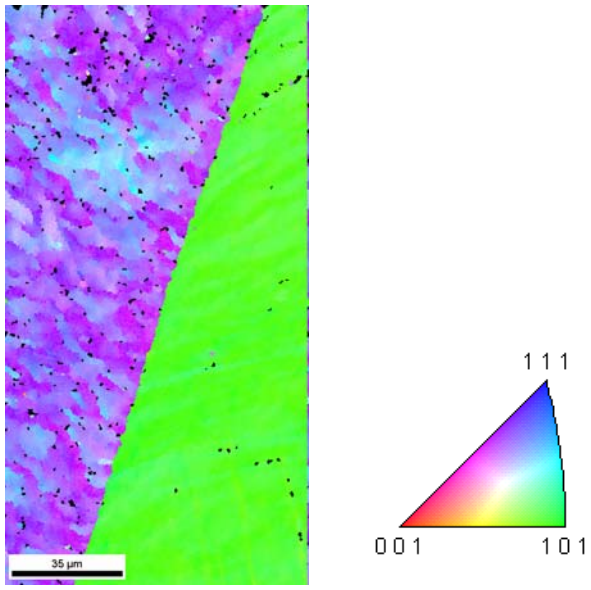

Figure 5.1: Orientation image showing different dislocation substructure in grains of different orientations generated in pure Al deformed to 20% strain.

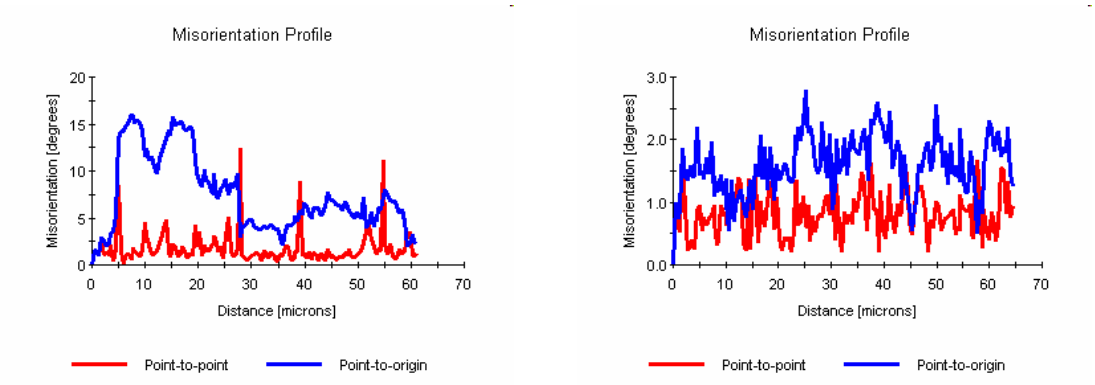

Figure 5.2: Misorientation profile indicating point to point and point to origin misorientation for two grains shown in Figure 5.1.

Development of improved characterization procedures for dislocation structures described above suggest that microstructure of material can be described by various parameters and it is necessary to identify major microstructural parameters affecting stress response. A parametric study was performed using multiple regression analysis to determine relative influence of various microstructural parameters on the yield stress of 6022 Al alloy. The analysis showed that average value of GND density was the major parameter, representing strength contribution due to entire dislocation structure, affecting the yield stress of 6022 Al alloy. It is interesting to note that while various imaging techniques described in Chapter 2 aid in understanding the local deformation behavior, a simple analysis of average GND density proved to be successful in describing observed yield stress for 6022 Al alloy under current experimental conditions. The strong dependence of the GND density on the observed stress response further motivated the interest of developing a relationship between the GND density and the yield stress of 6022 Al alloy. Statistical analysis and experimental observations showed a linear relationship between yield stress and the square root of GND density. Also the relationship developed between microstructure and yield stress was similar to the model proposed by Deschamps and Brechet [8]. Another interesting feature of the study is that only geometrically necessary dislocation density measured in 2-D plane section of the sample is used in the model and experimental analysis. Still, the relationship between dislocation density and yield stress is retained even though statistically stored dislocation density and the gradient of orientation in the third direction is ignored.

If GND density is used as one of the state variables affecting the stress response, its evolution as a function of processing parameters and starting microstructures needs to be investigated. A general form of the evolution of GND density is given by $\frac{\partial \rho_{GND}}{\partial t} = f\left(\dot{\varepsilon}, T, \rho_{GND}, S_i\right)$, where S_i includes all microstructural features that affect the evolution of GND density. A common equation used to represent evolution of dislocation density is given by $\frac{\partial \rho}{\partial \gamma} = k_1\sqrt{\rho} - k_2\rho$, where γ is the accumulated shear strain on the slip systems and k_1 is constant representing dislocation storage phenomena and k_2 is constant indicating recovery effects at high temperatures [9, 10].

We attempted to relate the evolution of GND density to various microstructural parameters that are physically measurable using EBSD. Initially it was assumed that the grain orientation strongly affects evolution of the GND density and so the evolution of GND density was studied as a function of the Taylor factor *(M)* of the grain. Figure 5.3 is a plot showing variation in average values of GND density of individual grains in the scanned region of the sample as a function of the Taylor factor of grains for 6022 alloy deformed at 450°C to a strain of 20% and 30%. The Taylor factor, (given by Equation 5.2) gives an indication of resistance to deformation as a function of lattice orientation.

$$M = \frac{\sum \gamma_i}{\varepsilon} = \frac{\sigma}{\tau_{crss}} \quad \ldots\ldots\ldots\ldots\ldots\ldots\ldots\ldots\ldots\ldots \quad (5.2)$$

where γ_i is the amount of slip on slip system i (assuming 5 simultaneously active slip systems), and τ_{crss} is the critical resolved shear stress (assumed constant for all slip systems). As discussed in Chapter 3, grains of larger Taylor factors are geometrically

hard grains and are therefore relatively difficult to deform, whereas grains of low Taylor factor are soft grains that are easy to deform. It can be easily visualized from Figure 5.3 that the evolution of GND density is not singly dependent on Taylor factor. This indicates

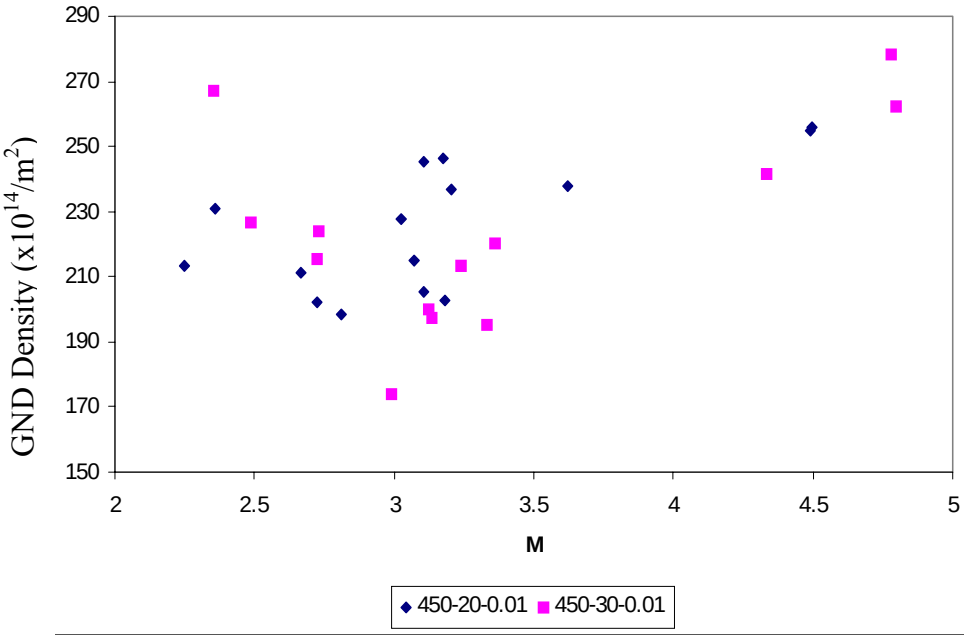

Figure 5.3: Plot showing variation in average GND density ($x10^{14}/m^2$) as a function of Taylor factor of grains of deformed 6022 Al alloy.

that a description of GND densities requires additional parameters. An attempt was made to include the weighted average of a slip transmission number of the grain with its neighbors *(N)* and weighted average of Taylor factor $(\overline{M})$of neighboring grains in thestudy of GND density evolution. The slip transmission number was calculated using Equation 5.3. Livingston and Chalmers [11] proposed that a geometrical factor, *N*, be used to evaluate the likelihood of slip transmission across a grain boundary for a pure shear. This factor is based on the slip plane directions and normals, *b* and *n*, in both grains. The operative slip system(s) have the largest value of *N*:

$$N = \left(n^i \cdot n^j\right) \cdot \left(b^i \cdot b^j\right) + \left(n^i \cdot b^j\right) \cdot \left(b^i \cdot n^j\right) \qquad \ldots\ldots\ldots\ldots\ldots\ldots (5.3)$$

In the above equation a grain with a value of N=1 indicates that a slip system of a given grain is aligned perfectly with a slip system of a neighboring grain and therefore slip transmission should be relatively easy. Another parameter used in the analysis is weighted average (weighted based on the length of grain boundary segment shared between the two grains) of Taylor factors of the neighboring grains given by Equation 5.4:

$$\overline{M} = \frac{\sum_{i}^{n} M_i * L_i}{\sum_{i}^{n} L_i} \qquad \ldots\ldots\ldots\ldots\ldots\ldots\ldots\ldots (5.4)$$

where n is the number of neighboring grains surrounding a given grain, L_i is the length of boundary segment shared between a given grain and the i^{th} grain, and M_i is the Taylor factor of the i^{th} (neighboring) grain.

Figure 5.4 is an orientation image of 6022 alloy deformed to 20% strain under channel die compression at 450^{o}C with a strain rate of 1s^{-1}. Figure 5.5 is a plot showing the variation in the average values of GND density of individual grains as a function of Taylor factor of grain *(M)*, weighted average of Taylor factor of neighboring grains $\left(\overline{M}\right)$and slip transmission number *(N)*. About 43 grains of different orientation, observed in Figure 5.4, are analyzed for variation in the average values of GND density. Grain parameters used in the above analysis are defined by 5^{o} misorientation and 5 minimum points, which means a grain is observed whenever there is a presence of at least 5 neighboring measurement points where point to point misorientation is less than 5^{o}.

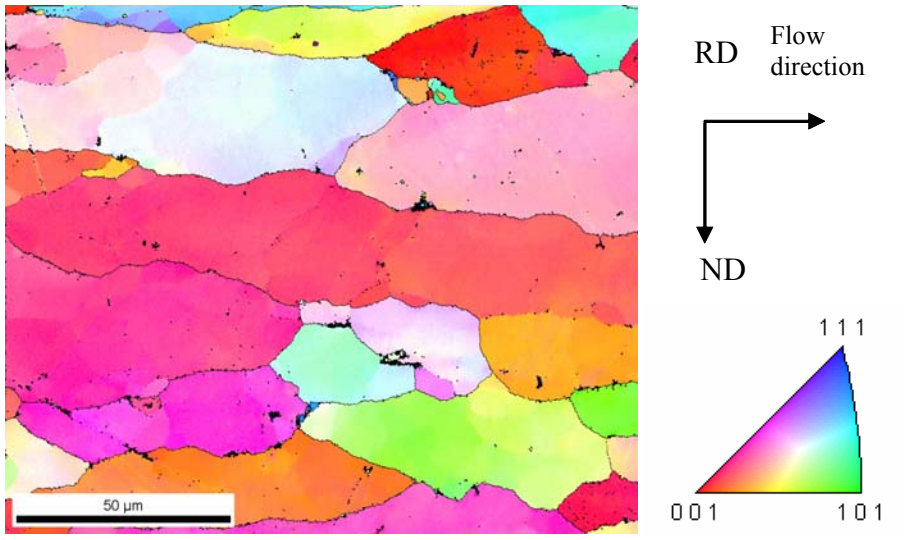

Figure 5.4: Orientation image of 6022 Al alloy deformed to 20% strain at 450°C with a strain rate of $1s^{-1}$. The orientation color key indicates poles aligned with TD of the sample.

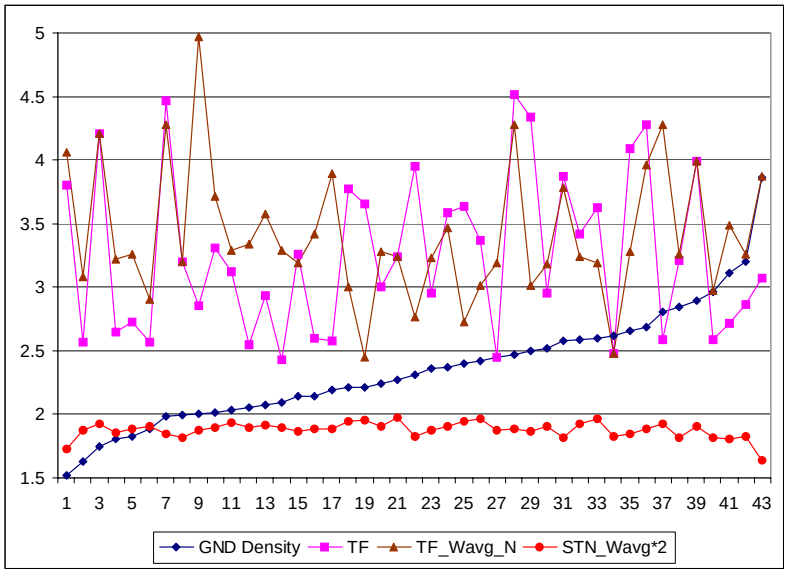

Figure 5.5: Plot showing variation in average GND density of individual grains shown in Figure 5.4 with variation in their Taylor factors, weighted average of Taylor factors of neighboring grains and slip transmission number.

The large scatter in measured parameters seen in the plot indicates that there is no direct dependency between the GND density and any of the plotted parameters. This led us to the agreement that evolution of GND density cannot be described by a simple approach used in this study. This indicates that, while algebraic average values of GND densities showed a linear relationship with yield stress, the determination of evolution of GND density is rather more complicated. Accurate determination of evolution of GND density will therefore require a more sophisticated physical approach, with the inclusion of more microstructural parameters such as precipitate morphology, or a higher order description of grain boundary characteristics etc. in the analysis.

Overall the current study claims to make contribution in the areas of dislocation structure characterization, identification of major microstructural parameters affecting mechanical response and understanding the relationship between the GND density and the yield stress. In general, a new approach to analyze local orientation gradients on relatively large areas of a sample is presented. Mapping of various scalar parameters that describe local microstructure heterogeneity is introduced to visualize deformation behavior at the subgrain scale. The observation of heterogeneous microstructure evolution during small strain deformation and its strong dependence on alloy chemistry and on the details of the starting microstructure suggest that there is a need to include physically measurable microstructural features in the constitutive model. Various parameters observed to influence the evolution of dislocation structures include precipitate morphologies, alloy chemistry, grain orientation and character and morphology of neighboring grains. The current work supports the trend of increasing interest in the scientific community towards quantifying the GND density in deformed samples and incorporating it into a physically

based model. While the linear relationship between average GND density and the yield stress was observed both experimentally and statistically in the current study for 6022 Al alloy, the model cannot be confidently extended beyond the experimental scope described. However, understanding developed from the current research efforts can aid for the development of more sophisticated model that can be used for process/alloy design.

5.1 References

[1]. Ferry, M., *Acta Mat*. 53, (2005) 773.

[2]. Ferry, M. and Humphreys, F. J. *Acta Mat*. 44, (1993) 1293.

[3]. Nye, J.F., *Acta Metall*. 1, (1953) 153.

[4]. Shi, H., McLaren, A.J., Sellars, C.M., Shahani, R., Bolingbroke, R., *Mater. Sci. Technol*. 13, (1997) 210

[5]. Nabarro F. R. N., *Theory of Crystal Dislocations*. (Oxford: University Press, 1967).

[6]. Laubusch R., *Phys Stat Sol*. 41, (1970) 659.

[7]. Cleri, F., *Comp. Phys. Comm*. In Press Uncorrected Proof.

[8]. Deschamps, A. and Brechet, Y., *Acta Mat*. 47, (1999) 293.

[9]. Mecking, H. and Kocks, U.F., *Acta Metall*. 29, (1981) 1865.

[10]. Barlat, F., Glazov, M.V., Brem, J.C., Lege, D.J., *Int. J. Plasticity* 18, (2002) 919.

[11]. Livingston, J.D. and Chalmers, B., *Acta Met*. 5, (1957) 322.

CHAPTER – 6

CONCLUSIONS

This chapter summarizes the major points of emphasis in the present dissertation, and highlights the important conclusions.

- New strategies to define and image local orientation gradient in deformed crystallites were introduced. Characterization techniques were applied to two pure Al single crystals that were deformed differently to understand the development of local orientation gradient.
    - The spatial distribution of geometrically necessary dislocation density (dislocations that are required to maintain lattice continuity) using orientation gradient information from EBSD data provided insight into the local behavior of dislocations. It was observed that even though both single crystals contained approximately similar values of average GND density, there is a large difference in the local orientation gradient between them.
    - Mapping of flow fields using orientation difference vectors helped to understand the deformation behavior at the subgrain scale. It can be seen, for a sample deformed to 15% strain, that individual crystallites within a cell are oriented differently from neighboring cells.
    - Mapping procedures based on angle of deviation, axis of deviation, divergence and gradient of orientation difference vectors were introduced to provide alternate methods of imaging local orientation gradient.

- Application of divergence and gradient operators to the orientation difference vector fields was used to quantitatively describe the local orientation deviation in relation to the orientation of neighboring measurement points. Mapping of such scalar measures provides a visual representation about the trends of deviation in crystal orientation (moving towards/away from an average orientation) as a function of distance.

- Comparison of dislocation structure evolution during small strain deformation of AA3003, AA5005 and AA6022 Al alloys was done.
  - In general, orientation imaging analysis of the deformed samples showed an increase in the density of dislocation substructure and fraction of low angle grain boundaries with deformation for the 3 alloys studied in the present investigation.
  - Quantification of dislocation structures was done by measuring dislocation cell size, fraction of low angle boundaries, grain orientation spread and grain average misorientation.
  - The difference in texture and dislocation structure evolution observed during small strain deformation of 3 alloys is attributed to their alloy content.
  - It was also observed that the grains with near {111} orientation aligned with the tensile axis were primarily substructure free, whereas grains with cube orientation developed significant dislocation substructure in all alloys at each deformation level investigated. A simple analysis based on Taylor factors could explain the effect of grain orientation on dislocation structure evolution.

- An inhomogeneous distribution of dislocation substructure observed among grains with cube orientation is attributed to the effect of neighboring grains.
- A separate study on the influence of precipitate morphologies on GND density evolution showed that strong coherent particles (capable of creating more pile ups of dislocations) cause a more dramatic increase in GND density with deformation than overaged incoherent particles (which could easily be bypassed by dislocations).

- Experimental investigation and statistical formulation was used to determine the relationship between physically measurable microstructural features and the observed stress response of 6022 Al alloy deformed at varying temperatures and strain rates.
  - A parametric study using multiple regression analysis showed that the GND density was the major microstructural parameter affecting the yield stress of 6022 Al alloy.
  - Statistical analysis and experimental observations showed a linear relationship between yield stress and square root of average GND density. It was observed that samples with higher GND density in the starting structure observed higher flow stress during subsequent deformation.
  - In general, statistical formulation was used to develop the yield strength model for 6022 Al alloy (given by Equation 4.12). The model was similar to the one proposed by Deschamps and Brechet (described in Chapter 4 by Equation 4.11). In the model, microstructural parameters affecting yield stress were determined to be dislocation density, volume fraction of precipitates and average radius of precipitates.

- An attempt was made to determine the evolution of average GND density as a function of microstructural parameters. No direct dependency between the average GND density and various measurable microstructural parameters such as Taylor factor of grains, Taylor factor of neighboring grains and slip transmission number was observed for 6022 Al alloy.

CHAPTER – 7

SUGGESTIONS FOR FUTURE WORK

The characterization strategies discussed in Chapter 2 were developed using crystal lattice orientation information from plane (2-D) sections of samples using EBSD. In particular, the calculation of GND density assumed that the orientation gradient along the third direction is zero. While the distribution of GND density will remain approximately the same for a columnar grain structure, it can vary significantly from the 2-D approximation for grains with large orientation gradients. Accurate determination of GND density is important for quantitative understanding of microstructural evolution and more importantly when incorporating it as a structural variable in a constitutive model. Nowadays there exists the capability of determining spatially specific orientation measurements in all the three dimensions, using a dual beam (ion and electron beams) equipped with EBSD or by using intense synchrotron X-ray sources, and therefore a comparison of the distribution of GND densities obtained from plane sections of the sample to one obtained from 3-D measurements is possible. Such analysis could potentially be used to develop a statistical theory that is capable of using information about GND density, for a given microstructure, from 2-D sample and provide a statistical distribution of GND densities in all the 3 directions.

Characterization of dislocation structures during small strain deformation was done as a function of alloy chemistry and grain orientation by measuring cell size, fraction of low

angle grain boundaries, grain orientation spread, grain average misorientation and GND density. The observation of inhomogeneous dislocation structure evolution offers motivation to include higher order information in a statistical description of microstructures such as:

- misorientation angle distribution within grains (subgrain misorientations)
- crystallite orientation distribution and orientation coherence functions (giving probability densities for the existence of given orientations and clustering of orientation types)
- dislocation cell size/shape distributions
- particle/precipitate pair correlation functions.

Crystal lattice orientation information obtained from EBSD data could be tailored to develop some dislocation based functions described above; however experimental determination of functions related to precipitate morphologies will require a combination of EBSD and TEM techniques.

A microstructural parametric study showed that the average GND density is the major microstructural parameter affecting the yield stress of 6022 alloy. In addition, experimental and statistical analysis showed a linear relationship between yield stress and square root of GND density. However, more experimental and theoretical analysis should be performed to validate such a relationship between the yield stress and microstructure for various Al alloys and deformation conditions.

Experimental investigation showed that precipitate morphologies of the starting microstructure affects the evolution of the GND density even during small strain deformation of 6022 Al alloy. This study motivates the use of parameters describing precipitate morphologies in the evolution of the GND density. Thus a complete understanding of dislocation – precipitate interactions can be developed by performing a similar quantitative study using TEM and EBSD as a function of deformation and alloy content.

A preliminary study on the evolution of the GND density as a function of measurable microstructural features using OIM was performed for 6022 Al alloys. A simple approach based on Taylor factors of grains, Taylor factors of neighboring grains and slip transmission number showed that these parameters are not enough to define the evolution of GND density. Thus, a rigorous theoretical analysis combined with experimental validation while adding more microstructural parameters such as precipitate morphologies, grain boundary characteristics etc. should be performed to determine the evolution of GND density accurately.